MIT/WHOI

Massachusetts Institute of Technology
Woods Hole Oceanographic Institution

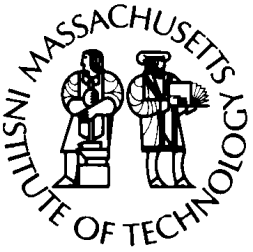

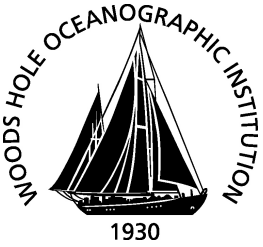

Joint Program in Oceanography/ Applied Ocean Science and Engineering

---

DOCTORAL DISSERTATION

Observing Microbial Processes at the Microscale with *In Situ* Technology

by

Bennett S. Lambert

February 2019

Observing Microbial Processes at the Microscale with *In Situ* Technology

by

Bennett S. Lambert

B.Sc., Civil and Environmental Engineering, University of Alberta (2012)

Submitted to the Joint Program in Applied Ocean Science and Engineering in partial fulfillment of the requirements for the degree of Doctor of Philosophy in Oceanographic Engineering at the

MASSACHUSETTS INSTITUTE OF TECHNOLOGY

and the

WOODS HOLE OCEANOGRAPHIC INSTITUTION

February, 2019

Signature of Author: .....

Department of Civil and Environmental Engineering
September 18, 2018

Certified by: .....

Roman Stocker
Professor, Civil, Environmental, and Geomatic Engineering
ETH Zürich
Thesis Co-Supervisor

Certified by: .....

Heidi Sosik
Senior Scientist, Biology Department
Woods Hole Oceanographic Institution
Thesis Co-Supervisor

Accepted by: .....

Henrik Schmidt
Chair, Joint Committee for Applied Ocean Science and Engineering
Massachusetts Institute of Technology
Woods Hole Oceanographic Institution

Accepted by: .....

Heidi Nepf
Professor of Civil and Environmental Engineering
Graduate Officer
Massachusetts Institute of Technology

Observing Microbial Processes at the Microscale with *In Situ* Technology

by

Bennett S. Lambert

Submitted to the Joint Program in Applied Ocean Science and Engineering on September 18, 2018 in partial fulfillment of the requirements for the Degree of Doctor of Philosophy in Oceanographic Engineering.

Abstract

Marine microbes are key drivers of biogeochemical transformations within the world's oceans. Although seawater appears uniform at scales that humans often interact with and sample, the world that marine microbes inhabit can be highly heterogeneous, with numerous biological and physical processes giving rise to resource hotspots where nutrient concentrations exceed background levels by orders of magnitude. While the impact of this microscale heterogeneity has been investigated in the laboratory with microbial isolates and theoretical models, microbial ecologists have lacked adequate tools to interrogate microscale processes directly in the natural environment. Within this thesis I introduce three new technologies that enable interrogation of microbial processes at the microscale in natural marine communities. The IFCB-Sorter acquires images and sorts individual phytoplankton cells, directly from seawater, allowing studies exploring connections between the diversity of forms present in the plankton and genetic variability at the single-cell level. The *In Situ* Chemotaxis Assay (ISCA) is a field-going microfluidic device designed to probe the distribution and role of motility behavior among microbes in aquatic environments. By creating microscale hotspots that simulate naturally occurring ones, the ISCA makes it possible to examine the role of microbial chemotaxis in resource acquisition, phytoplankton-bacteria interactions, and host-symbiont systems. Finally, the Millifluidic *In Situ* Enrichment (MISE) is an instrument that enables the study of rapid shifts in gene expression that permit microbial communities to exploit chemical hotspots in the ocean. The MISE subjects natural microbial communities to a chemical amendment and preserves their RNA in a minute-scale time series. Leveraging an array of milliliter-volume wells, the MISE allows comparison of community gene expression in response to a chemical stimulus to that of a control, enabling elucidation of the strategies employed by marine microbes to survive and thrive in fluctuating environments. Together, this suite of instruments enables culture-independent examination of microbial life at the microscale and will empower microbial ecologists to develop a more holistic understanding of how interactions at the scale of individual microbes impact processes in marine ecosystems at a global scale.

Thesis Co-Supervisor: Roman Stocker
Title: Professor
ETH Zürich

Thesis Co-Supervisor: Heidi Sosik
Title: Senior Scientist
Woods Hole Oceanographic Institution

Acknowledgements

I'd like to start off by thanking my parents and step-parents. Throughout my life, you've been incredibly supportive of my rapidly shifting interests. From that time I figured I'd give unicycling a shot, to the various sports clubs I participated in during school. I think the freedom to go out and try new things gave me the mindset I needed to close up shop and move across the continent to attend the Joint Program. Letting me disassemble old VCRs and other electronics in the garage at home was often incredibly messy and I love you all the more for putting up with me and fostering my love for all things mechanical and electronic. Beyond anything so simple as that, you instilled in me the drive, determination, and perseverance I needed to make it through some of the most enriching and difficult years of my life.

To my friends – I've been incredibly lucky to be surrounded by great people from day one. Powell River friends – thanks for always pulling for me and helping me keep perspective. Parsons friends – the early days at MIT were tough for me and I don't think I would've been able to keep a level head without you. I look forward to a day when our illustrious book club can reconvene. WHOI friends – you made the Cape all that much harder to leave every single time. Evenings at the Quahog Republic are something I've dearly missed and will continue to miss. Zürich friends – I will miss the life we've carved out for ourselves here. I've never lived in a place where I enjoy each and every season so much and that is due to you. Stocker lab friends – what a ride, eh? Moving to Europe with all of you was one of the greatest things to ever happen to me. Despite the obvious difficulties of moving to a country with a completely different culture and language, the process felt seamless. I wish each and every one of you all the best in everything to come.

To my wife Kathi – the support and love you've given me through the ups and downs of the last years has been the most essential part of my life. Words can't explain how important you are to me, so I'll just have to tell you little-by-little every day!

To all the educators and mentors I've had along the way – sometimes I stop and think about just how lucky I've been. A quick shout-out to Mr. Warner from the 3rd grade. Your creativity made math fun and your read-through of the Hobbit made me love reading at an early age. To Ania Ulrich – thanks for giving me the opportunity to work in your laboratory during my studies. That opportunity in large part is the reason I wound up here today. Heidi – being your student was an absolute joy. You're a shining example of the mentor I strive to be one day. Roman – working in your lab over the years has been incredibly fun. The excitement you maintain on a day to day level for the scientific process is something I hope to emulate and your support and guidance throughout the years has shaped the way I navigate the maze of academia on every level. Rob and Alexi – thanks for patiently teaching me things I should've probably already known and putting up with me consistently putting tools back in the wrong place. JB – you could've been just as easily put in the friends category. Working closely with you over the years has been a ton of fun and I learned pretty much everything I know about microbiology lab work from you. Vicente – thanks for all the brainstorming time and patiently explaining concepts over and over when I was slow on the uptake – if only every grad student had someone like you around! Penny and Justin – thanks for your support and kind words during committee meetings.

Finally, I'd like to thank the Gordon and Betty Moore Foundation, the National Science Foundation, and NSERC for funding portions of my research.

Table of Contents

Chapter 1: Introduction

Marine life at the microscale

Despite their minute size, marine microorganisms control key biogeochemical transformations occurring throughout the ocean (Falkowski, Fenchel, and Delong 2008). Oceanography by its nature is concerned with immense areas and volumes over which a diverse set of microbial processes play out. Quantifying the bulk rates of biogeochemical processes and large-scale biogeography of microorganisms central to these transformations is of critical importance to our understanding of these global processes. However, viewing microbial processes through such a macroscopic lens obscures the fact that these processes occur, not on human scales, but at the scale of individual microorganisms themselves.

From the human perspective, a liter of seawater often appears homogeneous, but when we zoom in to the smaller scales that microbial cells inhabit (i.e., 'the microscale' – micrometers to millimeters), the picture that reveals itself is dramatically different: the environment is often highly patchy, both in terms of the chemical landscape and the distribution of microorganisms (Stocker 2012; Fenchel 2002). These chemically-rich microenvironments have diverse origins, including zooplankton fecal pellets (Jefferson 2002), phytoplankton cells (Smriga et al. 2016), and other organic particles (Kiørboe et al. 2002; Azam and Long 2001), and represent biogeochemical hotspots where rates of chemical transformation considerably exceed bulk-scale averages (Stocker et al. 2008; Stocker 2012; Fenchel 2002; Blackburn, Azam, and Hagström 1997). Although often conceptualized as chemical patches, many of these hotspots are not purely passive features of the water column. It is becoming increasingly clear that phytoplankton cells, for example, actively participate in targeted metabolite exchange with marine microorganisms

inhabiting the region surrounding them, known as the phycosphere (Seymour et al. 2017; Durham et al. 2015; Amin et al. 2015). In addition, co-occurring phytoplankton cells may be genetically and phenotypically diverse (Kooistra et al. 2010; Koester et al. 2010; Kashtan et al. 2014; Iglesias-Rodríguez et al. 2006), further contributing to a microscale seascape that is highly dynamic from the perspective of a bacterium.

Many marine microorganisms exhibit behavioral adaptations to life in this heterogeneous environment. Motility and chemotaxis – the ability to bias swimming behavior in response to a chemical gradient – are pervasive behaviors among free-living marine microbes (Stocker 2012; Grossart, Riemann, and Azam 2001). To date, laboratory and theoretical experiments have suggested that motility and chemotaxis may be key behaviors within the marine water column (Taylor and Stocker 2012; Smriga et al. 2016; Seymour, Simó, et al. 2010; Kiørboe et al. 2002; Fenchel 2002; Blackburn, Fenchel, and Mitchell 1998; Blackburn, Azam, and Hagström 1997), allowing bacteria to encounter and remain within resource hotspots more effectively than their non-motile counterparts. In the laboratory, much of this progress can be attributed to advances in observational techniques, in particular imaging techniques coupled with microfluidics, which allows fine-scale manipulation of environmental conditions and precise observation of microbial behaviors (Rusconi, Garren, and Stocker 2014; Hol and Dekker 2014). However, despite evidence pointing to the importance of microbial behavior in the water column, we have lagged behind in efforts to interrogate microbial behavior directly in the natural environment and still know very little about the occurrence and efficacy of motility and chemotaxis in the ocean.

Resource hotspots in the water column are both short-lived and chemically diverse. Nutrient sources persist on the order of minutes (lysis events) to days (marine snow), and encounter rates between marine bacteria and hotspots can vary over orders of magnitude depending on the

composition of the microbial community and environmental conditions (Smriga et al. 2016; Seymour et al. 2017). Additionally, the chemical composition of each resource hotspot can differ greatly. Marine phytoplankton species have unique chemical signatures (Becker et al. 2014) that vary with environmental conditions (Vidoudez and Pohnert 2012) and produce a vast array of metabolites, which are hypothesized to play a central role in the interactions between phytoplankton and other marine microbes (Poulson, Sieg, and Kubanek 2009; Pohnert, Steinke, and Tollrian 2007). This begs the question – if certain marine microbes are able to find and capitalize on ephemeral hotpots, how do they tune their physiology over these short timescales to succeed in the face of the high degree of uncertainty in the timing and chemical nature of encounters?

One potential mechanism to cope with uncertainty in resource access and composition is rapid transcriptional regulation. Rapid shifts in the transcriptome have been well studied in *Escherichia coli* and other model organisms during starvation or upon exposure to stress, and are collectively known as the stringent response (Chatterji and Kumar Ojha 2001; Boutte and Crosson 2013). The stringent response is well conserved in bacteria, whereby genes encoding translational machinery and factors supporting growth and division are down-regulated, while genes related to stress are rapidly up-regulated (Boutte and Crosson 2013). Another classic example are the heat shock proteins and heat shock transcription factors, which are rapidly up-regulated upon a sudden increase in temperature (Lindquist and Craig 1988). The occurrence of these genetic circuits throughout the tree of life indicates that rapid transcriptional regulation has been an evolutionarily successful strategy to deal with sudden shifts in environmental conditions. The chemical landscape that marine microbes inhabit is wholly different compared to the origin of model organisms such as *E. coli*. Here again, though, laboratory work with model organisms

has not been accompanied by evidence from the natural environment, and we know little about the strategies adopted by microbes under natural conditions of boom and bust resource access in the ocean.

Despite significant progress in our capabilities to interrogate life at the microscale at increasing resolution in the laboratory and in numerical simulations, we still lack the capability to directly observe these processes in the natural environment. As a result, we lack information about how widespread these behaviors are in the natural environment, what environmental conditions favor them, and how microbial behavior and physiological adaptations to chemical heterogeneity ultimately impact the assembly of marine microbial communities in an environment where the encounter with resources fluctuates in a manner very dissimilar to that of our current model organisms and model studies.

Observing microbes at scales relevant to the individual

Microfluidics is now well established as a powerful technique to probe microbial processes at fine spatiotemporal scales (Hol and Dekker 2014; Rusconi, Garren, and Stocker 2014). Historically piggybacking on advances in the micro- and nanofabrication techniques employed in the semiconductor industry, microfluidics allows fine-scale control of the physical and chemical landscape that cells experience. Advances in the field have not only progressed our understanding of the nuanced physics of fluids at such minute scales, but also our ability to leverage the unique properties of fluids at low Reynolds numbers to manipulate biological systems with high precision and interrogate them under accurately controlled environmental conditions (Squires and Quake 2005). Coupled with advanced imaging techniques, microfluidics has allowed researchers to directly visualize interactions occurring within biological systems ranging from corals (Shapiro et al. 2016), to rhizosphere communities (Massalha et al. 2017), to

phytoplankton bacteria interactions (Smriga et al. 2016). In microbial ecology, this has allowed direct visualization of interactions within model microscale hotspots (Seymour, Simó, et al. 2010; Smriga et al. 2016), revealed the mechanisms of biofilm streamer formation (Drescher et al. 2013; Rusconi et al. 2011) and microbial behavior within established biofilms (Oliveira, Foster, and Durham 2016; Prindle et al. 2015), and enabled quantification of phenotypic heterogeneity within microbial populations (Ackermann 2015). Combined with numerical modeling (Rusconi, Guasto, and Stocker 2014; Smriga et al. 2016), these studies provide valuable insights into the microscale mechanisms that underpin life in the microbial world.

Microfluidic techniques have led to major inroads in the study of bacterial behavior and self-organization. In particular, the study of chemotaxis has benefited dramatically as a direct result of microfluidic chemical gradient generators (Rusconi, Garren, and Stocker 2014). Early experiments demonstrated that bacteria are capable of chemotaxis towards chemical concentrations dramatically lower than those assumed based on previous work with capillary assays, and that *E. coli* cells (and other microbes (Menolascina et al. 2017)) employ logarithmic sensing and fold-change detection in their chemotactic response (Rusconi, Garren, and Stocker 2014). These discoveries provided important mechanisms by which chemotaxis systems remain sensitive over orders of magnitude in chemical concentration. By allowing researchers to zoom in on these processes, the fine-scale control afforded by microfluidics has significantly advanced our understanding of microbial chemosensory systems and motility.

Although a powerful technology in the laboratory, microfluidic techniques have often struggled to transition to field application, due to the expertise required to fabricate and operate many devices. Additionally, a key current drawback is the general necessity to work with cultivable microbes and bulky peripherals associated with the imaging and pressure-control systems, so that

these techniques are not easily portable or applicable *in situ*. Here I develop technology based on concepts from microfluidics and millifluidics, but with the aim of deployment in the natural environment. Capitalizing on advances in rapid-prototyping, the techniques presented within this thesis are intended to be accessible to the broader scientific community. Through the use of low-cost fabrication methods with a low barrier for entry, I aim to spur adoption by non-specialist users and translate microfluidics to a field-based technology.

Thesis composition

Within this thesis, I present three novel instruments to examine aspects of microbial adaptation to life in a heterogeneous and fluctuating environment.

In Chapter 2, I describe a cell-sorter for the Imaging FlowCytobot (Olson and Sosik 2007), capable of isolating single phytoplankton cells or colonies directly from seawater (Lambert, Olson, and Sosik 2017). Within the phytoplankton a great diversity of morphologies exist, with many taxa capable of modulating cell shape or structure in response to environmental conditions (Schultz 1971; Sandgren Craig, Hall Shirley, and Barlow Steven 1996). The cryptic genetic diversity (Koester et al. 2010) and phenotypic heterogeneity present within phytoplankton populations presents an exciting opportunity to investigate the extent and function of variability in genotype and phenotype at the single cell level. Combined with imaging-in-flow cytometry, cell sorting creates a promising avenue for phytoplankton ecologists to link morphological features and their corresponding molecular fingerprint. The resulting information will yield insight into the environmental conditions and signals leading to phenotypic diversification and ultimately serve to better understand how single-cell variability impacts the dynamics and biogeography of phytoplankton populations.

In Chapter 3, I present a microfluidics-based *in situ* chemotaxis assay (ISCA) (Lambert et al. 2017). The ISCA represents a significant step forward in our ability to directly interrogate microbial behavior in the natural environment. The ISCA is a credit-card-sized microfluidic device that generates an array of chemical microplumes upon deployment in an aquatic system. Chemotactic microbes at the deployment site then hone in on the chemical gradient emanating from each well in the device and swim into the wells, where they are retained until the ISCA is retrieved. Coupling the ISCA with flow cytometry and ecogenomic techniques, information about the abundance, identity and functional capacity of chemotactic microbes can be obtained. Through the ISCA, microbial oceanographers will have direct access to the microorganisms and microbial behaviors involved in a broad range of chemical compounds and transformations.

A critical aspect of life at the microscale is the boom and bust nature of resource encounter and acquisition, with timescales of hotspot persistence that range from minutes to days (Newell, Lucas, and Linley 1981; Blackburn, Fenchel, and Mitchell 1998). In the face of extreme diversity in the composition, duration, and occurrence of nutrient patches, how do microbes tune their physiology to cope with such uncertainty? To address this question, I developed the millifluidic *in situ* enrichment (MISE) instrument, presented in Chapter 4. The MISE consists of a series of microcosms that upon deployment fill with seawater from the deployment site. The microcosms then seal and the communities within are subjected to either a chemical stimulus or filtered seawater from the deployment site as a control. Following an automated routine, the MISE preserves RNA from the community in a time series. The millifluidic design of the MISE allows rapid mixing of solutes, enabling interrogation of minute-timescale transcriptional responses that occur upon resource encounter. Combining the MISE with gene expression assays will enable microbial ecologists to examine the timescale and magnitude of transcriptional activity across

microbial communities in response to resource encounter, opening a window into the effect of microscale patchiness on resource acquisition strategies in marine systems.

While this thesis primarily focuses on experimental technology, the advances that these techniques enable will permit better parameterization of numerical models important to understand fundamental properties of the ocean microbial system, a topic in which I have developed an interest and expertise. The results of one such model are presented in Chapter 5, where I discuss the role of motility in the colonization of marine snow particles throughout the world's oceans. The oligotrophic open ocean is thought to be an environment where motility and chemotaxis are not beneficial behaviors, due to the lack of microscale resource hotspots. However, when the microbial community inhabiting particles in the open ocean is characterized, it is found to consist primarily of motile, copiotrophic bacteria. Using a simple encounter rate model, I demonstrate that motility and chemotaxis lead to disproportionate encounter rates with particles and this can explain the dominance of motile cells on particles even when their abundance in the bulk community is vanishingly small. These models provide important hypothesis generation tools and provide a framework through which we can interpret microscale phenomena and microbial behavior.

Together with advances in low-input molecular techniques, these biophysical models and purpose-built instruments allow researchers to probe previously inaccessible aspects of microbial life in the water column at scales relevant to individual microorganisms.

Chapter 2: A fluorescence-activated cell sorting subsystem for the Imaging FlowCytobot

Work presented in this chapter was published as "Lambert, B. S., Olson, R. J. and Sosik, H. M. (2017), A fluorescence-activated cell sorting subsystem for the Imaging FlowCytobot. Limnol. Oceanogr. Methods, 15: 94-102. doi:10.1002/lom3.10145".

Abstract

Recent advances in plankton ecology have brought to light the importance of variability within populations and have suggested that cell-to-cell differences may influence ecosystem-level processes such as species succession and bloom dynamics. Flow cytometric cell sorting has been used to capture individual plankton cells from natural water samples to investigate variability at the single cell level, but the crude taxonomic resolution afforded by the fluorescence and light scattering measurements of conventional flow cytometers necessitates sorting and analyzing many cells that may not be of interest. Addition of imaging to flow cytometry improves classification capability considerably: Imaging FlowCytobot, which has been deployed at the Martha's Vineyard Coastal Observatory since 2006, allows classification of many kinds of nano- and microplankton to the genus or even species level. We present in this paper a modified bench-top Imaging FlowCytobot (IFCB-Sorter) with the capability to sort both single cells and colonies of phytoplankton and microzooplankton from seawater samples. The cells (or subsets selected based on their images) can then be cultured for further manipulation or processed for analyses such as nucleic acid sequencing. The sorting is carried out in two steps: a fluorescence signal triggers imaging and diversion of the sample flow into a commercially

available “catcher tube”, and then a solenoid-based flow control system isolates each sorted cell along with 20 μL of fluid.

Introduction

Flow cytometry has contributed to our understanding of the ecology and biogeography of the world’s oceans (see reviews (Sosik, Olson, and Armbrust 2010; Olson Robert, Zettler Erik, and D. 1993; Legendre, Courties, and Troussellier 2001) and references within). Perhaps the most striking discovery that can be largely attributed to the application of flow cytometry is the existence of Prochlorococcus (Chisholm et al. 1988). Additionally, important contributions to our understanding of global distributions of marine phytoplankton have come from surveys carried out with flow cytometry as the main measurement technology (e.g., (Veldhuis and Kraay 1990; Olson Robert et al. 2003; Olson, Vaulot, and Chisholm 1985; Olson et al. 1988; Johnson et al. 2006). Flow cytometers continue to be essential in advancing understanding of spatiotemporal variability and diversity in the plankton (Mojica et al. 2015; Bonato et al. 2015; Anglès, Jordi, and Campbell 2015). Along with promoting greater understanding of ocean biogeography and biodiversity, flow cytometry is also an important tool for studies concerning the cell cycle and physiology of marine planktonic organisms (Armbrust, Chisholm, and Olson 1990; Armbrust et al. 1989).

The power of flow cytometry was extended dramatically by the introduction of cell sorting technology. (For an overview see Chapter 6 of(Shapiro 2005)) Cell sorters typically divert cells within a defined flow cytometric parameter space (i.e., defined by fluorescence and/or light scattering measurements) into a holding container; the cells within the holding container can then be analyzed further (Chisholm, Olson, and Yentsch 1988). Cell sorting has been used in combination with a variety of chemical analyses to better understand biogeochemical

cycling(Lomas, Bronk, and Engh 2011; Fawcett et al. 2011), to delve into interactions between bacteria and phytoplankton (Thompson et al. 2012; Baker and Kemp 2014), and to investigate intra-species genetic variability (Kashtan et al. 2014). With advances in single-cell genomics, transcriptomics, and cell sorting technologies, it is now possible to conduct analyses of individual sorted cells that have been isolated from cultures or environmental samples (Thrash et al. 2014; Luo et al. 2013; Kashtan et al. 2014; Baker and Kemp 2014). These studies have revealed dramatic heterogeneity at the single-cell level. With single-cell analytic techniques advancing at an impressive rate, cell-sorting flow cytometers will continue to be very valuable for isolating cells from the environment.

The introduction of imaging-in-flow represents another landmark addition to the field of flow cytometry (Sosik and Olson 2007; Sieracki, Sieracki, and Yentsch 1998; Kachel and Wietzorrek 2000). Imaging-in-flow cytometry integrated into an automated submersible instrument system enables studies of individual taxa at a greater temporal resolution than previously possible (Sosik, Olson, and Armbrust 2010; Sosik and Olson 2007). These technologies allow the investigation of numerous processes in situ including cell-cycle progression, prey ingestion, and parasite infection(Peacock, Olson, and Sosik 2014; Campbell et al. 2010; Brosnahan et al. 2014). Until now, the power of combining imaging-in-flow cytometry and fluorescence-activated cell sorting has remained untapped.

Here we bridge this gap with an Imaging FlowCytobot (Olson and Sosik 2007) (IFCB) that has been modified to operate as a bench-top instrument capable of sorting individual cells. IFCB is a submersible imaging-in-flow cytometer, which can be used to characterize planktonic cells in the size range of ~5-150 μm; it stores images of individual cells, chains, or colonies and records the chlorophyll fluorescence and side angle light scattering associated with each imaged target. The

instrument described here is in essence a fluorescence-activated cell sorting (FACS) system, but with several notable differences. Currently, FACS systems utilize fluorescence of various wavelengths and laser light scattering as selection criteria. These criteria cannot be used reliably to distinguish among different species in environmental samples. As a result, detailed investigations of community composition rely on sorting many individuals and then determining the taxonomic identity of each cell by sequencing. The IFCB-Sorter, in contrast, captures an image of a nano- or microplankton cell or colony and then sorts it into a well plate. Since the images can in many cases be used to automatically (or manually) classify the cell to genus or even species (Sosik and Olson 2007), only the sorted cells of interest need be further analyzed. Additionally, the image associated with the sorted cell can contain valuable information about the cell's condition at the time of capture. Images also make it possible to explore questions about relationships between morphology and genotype.

Materials and procedures

IFCB-Sorter

The IFCB-Sorter is a bench-top instrument that works in a manner similar to both FlowCytobot (Olson, Shalapyonok, and Sosik 2003) and Imaging FlowCytobot(Olson and Sosik 2007) in that a seawater sample is drawn into a syringe and subsequently injected into a particle-free sheath stream directed into a quartz flow cell. The main fluidics system of the IFCB-Sorter (Fig. 1) differs from that of the standard IFCB in that it utilizes a FACSCalibur sorting flow cell (BD Biosciences). The programmable syringe pump (VersaPump 6 with 48,000 step resolution) used for sample injection is configured with a 1-mL syringe (Kloehn, Inc.) (rather than the 5-mL syringe typically used in IFCB, to generate a smaller core stream). In the flow cell, the sample

stream is hydrodynamically focused such that particles pass single file through a focused 635 nm laser beam, which excites chlorophyll fluorescence in organisms that contain photosynthetic pigments. If chlorophyll fluorescence exceeds a pre-set threshold, an image is captured by concurrently triggering a 1-μs flash from a xenon lamp and frame capture from a digital camera, which is focused an appropriate distance downstream of the laser beam. Following image acquisition, the sorting flow cell module deploys a catcher tube, which momentarily diverts the sample stream containing the imaged particle into the sorting subsystem (Fig. 2).

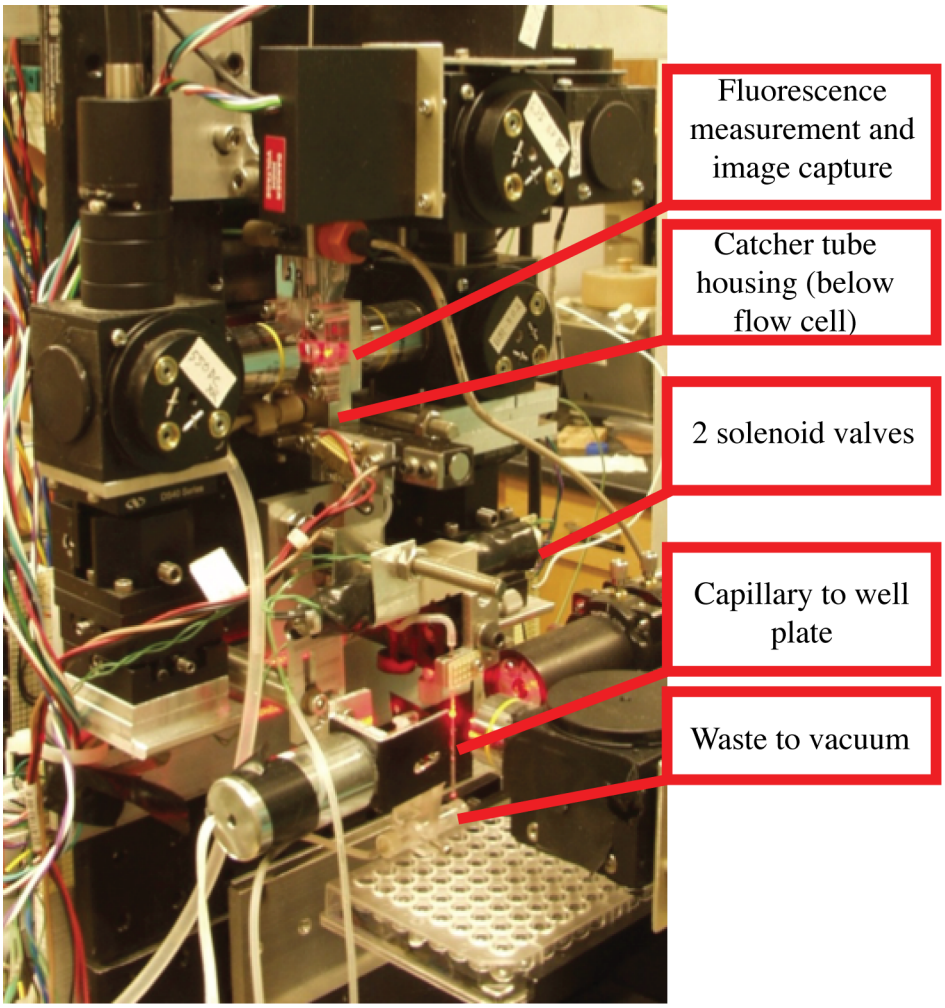

Fig. 1. IFCB-Sorter. Fluorescence measurement and image capture takes place in a BD Biosciences FACSCalibur sorting flow cell. The catcher tube is controlled by FACSCalibur circuitry (not shown), and the solenoids, capillary fluorescence detector, waste catcher (for removing the sheath flow in between sorted cells), and well plate X-Y translator are controlled by a PIC microprocessor (not shown).

The sorting subsystem includes two solenoid valves and a solenoid-operated microinjector (Biochem Fluidics, Inc.) for flow control, a fluorescence-based particle detector, a vacuum-operated waste trap, and a programmable well plate positioner. All components are mounted on an optical breadboard placed underneath the flow cell of the IFCB. The sorting subsystem is controlled by a

PIC 16F887 microcontroller (MicroEngineering Labs, Inc.), which is programmed in PICBASIC (MicroEngineering Labs, Inc.). The subsystem software consists of two main portions: i) an initialization segment, where subsystem timing parameters are set, microcontroller registers are set to establish pin function, and the comparator parameters are established (channel select, external input, logic not inverted, output is present on the COUT pin, polarity not inverted, comparator is enabled); ii) the main control loop, where the program awaits a trigger pulse from the IFCB. Once the trigger pulse is received, the catcher tube is deployed on the basis of pre-set timing parameters (see below). A sub-loop continuously polls the subsystem for a signal from the comparator, which starts the solenoid flow control sequence. Once the microinjector fires, the system resets and passes flow through the subsystem to flush the contents of the subsystem. The program then awaits the next trigger from the IFCB.

The residence time of particles in the sorting subsystem can vary due to the non-uniform velocity profile of the fluid flow and the absence of hydrodynamic focusing after capture, so a secondary fluorescence system is employed to re-locate the sorted particle before deposition (i.e., to ensure that the particle will be in the drop deposited into the well). The fluorescence detection system of the sorting subsystem is similar to that in the upstream IFCB flow cell: a 635 nm diode laser is focused with cylindrical lenses as in IFCB on a glass capillary pipet (OD 1.0 mm, ID 0.5 mm) downstream of the catcher tube, and a 10x microscope objective is placed at a right angle to the incident laser and focused on the capillary. A horizontal bar (3 mm wide) at the entrance to the objective blocks laser light reflected from the capillary. Light collected by the objective is sent to a photomultiplier tube (PMT; HC120-05MOD1, Hamamatsu Photonics, K.K.) through a 680 nm bandpass filter that separates chlorophyll signals from background laser light.

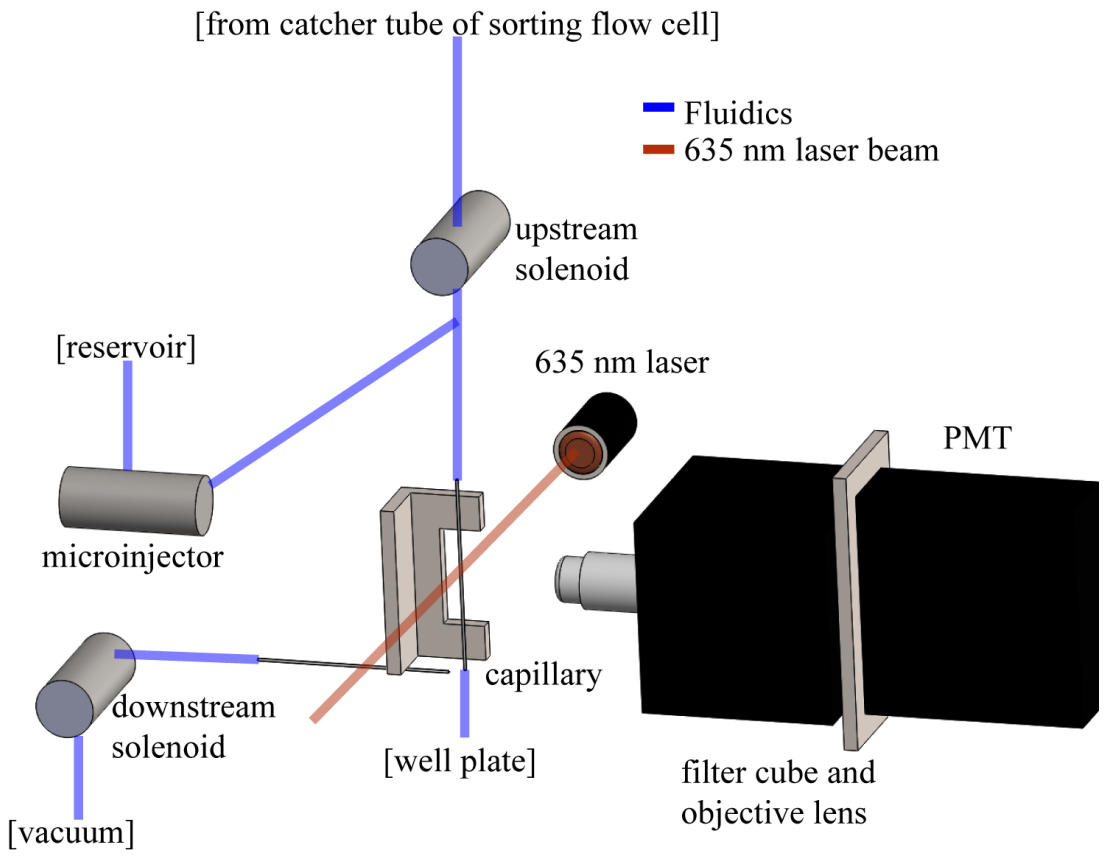

Fig. 2. The sorting subsystem of the IFCB-Sorter. A particle enters the system through the catcher tube located just after the flow cell (top) and passes through the upstream flow control solenoid. The particle then enters a capillary tube where photosynthetic pigments are excited by a 635 nm laser focused on the capillary. Emitted photons are detected by a PMT assembly and when the detected voltage exceeds a comparator threshold the solenoids are activated. The upstream solenoid stops flow in the capillary tube and the downstream solenoid stops vacuum suction. The microinjector then injects 20 µL above the capillary, ejecting the particle into a well plate.

Detection of a suitable particle by the original IFCB activates the sorting subsystem: when the signal detected by the primary PMT exceeds a comparator threshold (Fig. 3A), a deployment pulse is sent to the FACSCalibur catcher tube control board (BD Biosciences), and triggering is disabled (Fig. 3B) so that other cells passing through the IFCB observation window will be ignored while the sorted cell is being processed. The catcher tube pulse ramps from 0 to 100 V in

140 μs, plateaus, and then returns to 0 V again in 140 μs (Fig. 3C), which causes a piezo element to push the open entrance of the catcher tube briefly into the sample core stream. As the captured cell traverses the glass capillary after the catcher tube, it will pass through the subsystem laser beam and emit fluorescence, which is sensed by the subsystem PMT (Fig. 3D). The signal from this PMT is fed to a comparator in the PIC, which generates a pulse if the PMT signal is larger than a preset threshold (Fig. 3D). This pulse initiates another chain of events. First, an upstream solenoid valve (normally open) closes (Fig. 3E) to stop the flow with the sorted cell in the capillary tube. Second, a solenoid valve (normally open) that controls removal of waste by a vacuum closes (Fig. 3F); this stops suction at the end of the capillary tube. Third, the microinjector is triggered (Fig. 3G) to inject 20 μL of fluid into the capillary upstream of the cell, sending a droplet containing the cell into the well plate. Fourth, a pulse is sent to the Autoclone well plate system (Coulter Inc.) (Fig. 3H) shifting the plate to a new well. The system then returns to its base state and awaits another trigger event from the IFCB.

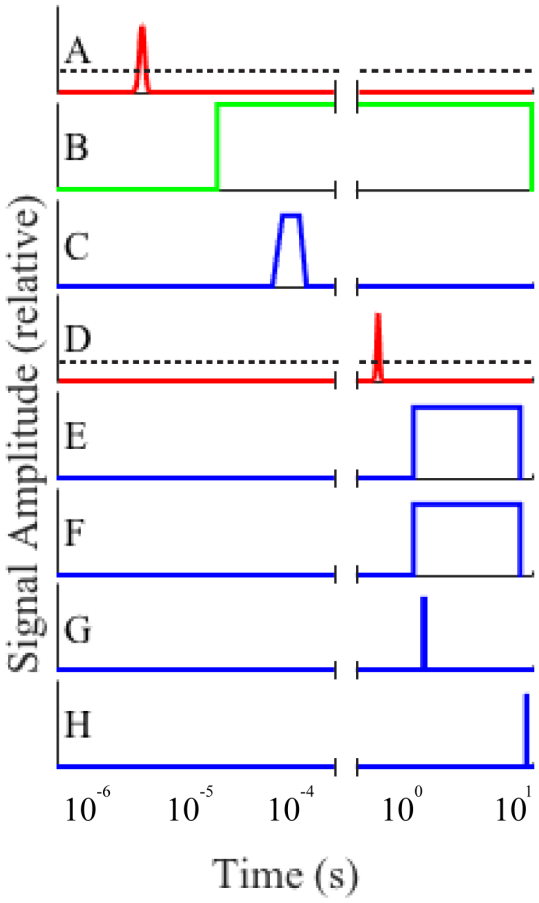

Fig. 3. IFCB-Sorter sorting subsystem signals (red) and controls (inhibition pulses in green, activation pulses in blue). (**A**) Initial signal seen by the IFCB. The comparator threshold is indicated by the dashed line; (**B**) Hold pulse to inhibit triggers until sorting is complete; (**C**) Catcher tube deployment pulse; (**D**) Sorting subsystem PMT signal and comparator threshold (dashed); (**E**) Upstream solenoid closure; (**F**) Downstream solenoid closure; (**G**) Microinjector pulse; (**H**) Pulse to advance well plate.

Optimization of timing parameters

To maximize the likelihood of successful sorts and to minimize the potential for coincidental capture of unwanted cells, it is necessary to optimize the timing of catcher tube deployment and duration. We determined capture efficiency (defined as the proportion of initial sorts subsequently sensed by the subsystem PMT) with different timing parameter values. First, we sorted phytoplankton cultures (the diatom *Ditylum brightwellii* and the dinoflagellate *Alexandrium fundyense*) and 9 µm red fluorescent beads (Thermo Fisher Scientific, Inc.) with no

delay between IFCB trigger and catcher tube deployment; by altering the duration of catcher tube deployment we were able to bound the time frame in which capture occurs. In a second experiment, we optimized the delay by varying it while holding constant the sum of delay and catcher tube deployment duration.

The phytoplankton cultures used for optimization of timing parameters were grown in f/2 media(Guillard 1975) at 18^{o}C with a 14:10 h light:dark cycle. Cells were transferred regularly to ensure they remained in the exponential growth phase. The sort efficiency was measured indirectly as the proportion of initial sorts that were sensed by the subsystem PMT.

Quantification of capture efficiency for chain-forming cells

Capture of chain-forming cells represents a significant challenge to cell sorters because their large size and complex morphology can cause unpredictable flow behavior. To quantify the capture efficiency of the IFCB-Sorter under these challenges, a culture of the chain-forming diatom *Guinardia delicatula* was used as sample. Prior to sorting, the culture was kept in f/2 media at 11^{o}C with a 14:10 h light:dark cycle.

Isolation and culture of *Alexandrium*

Cells can experience high levels of mechanical stress during the process of cell sorting, resulting in a decrease in cell viability (Rivkin, Phinney, and Yentsch 1986). The ability to sort cells that remain viable expands the range of analyses that can be performed once cells are isolated. To assess the viability of sorted cells, *Alexandrium* were cultured as described above and then sorted into a 96-well plate containing f/2 media. The well plate was then returned to the original incubator. Fluorescence readings were taken on a SpectraMax (Molecular Devices, LLC) plate reader to obtain data necessary to construct well-specific growth curves.

Isolation of cells from natural communities

Cells were sorted from seawater collected from Woods Hole Harbor. The cells were sorted onto a microscope slide and then imaged at 40X magnification. Manually identifying cells by microscopy after the final sort event allowed us to verify correspondence with the original target detected and imaged in the upstream flow cell of the main IFCB system.

Assessment

Impact of catcher tube deployment timing on capture efficiency

As described above, a pulse from the PIC microcontroller, generated when a fluorescence signal is detected, deploys the catcher tube. We determined empirically the optimal timing of pulse initiation and duration. Varying the catcher tube deployment duration with no delay showed that most captures occurred between 800 and 900 μs regardless of particle type being sorted (Fig. 4A). A second experiment, in which the delay was varied while keeping the sum of delay plus duration equal to 900 μs, showed that high capture efficiency could be maintained with a short-duration deployment pulse that included the period between 800 and 900 μs (Fig. 4B). Taken together, these results led us to choose a delay time of 700 μs and deployment pulse of 200 μs as normal operating parameters. Under these conditions, for a range of particle types from beads to cells of different size and shape, capture efficiencies are indistinguishable from the maxima achieved and the pulse duration is no longer than necessary.

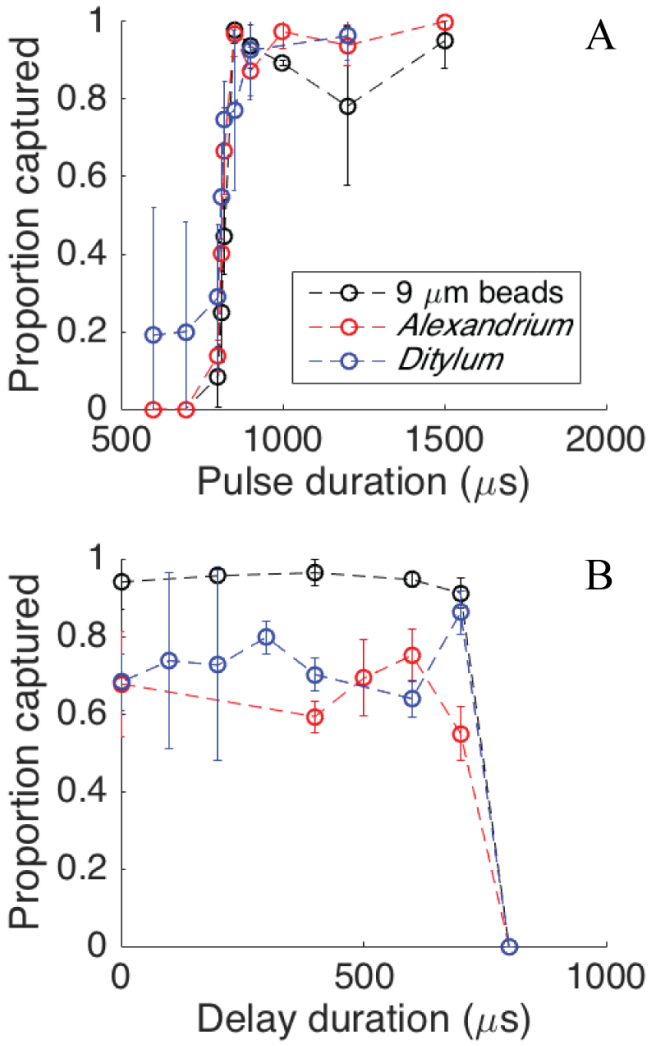

Fig. 4. (**A**) Capture efficiency with varying catcher tube deployment pulses. (**B**) Capture efficiency with differing deployment delays and total time held at 900 µs.

Re-isolation of *Alexandrium fundyense*

To demonstrate that the IFCB-Sorter can be used to isolate cells for culture and physiological experiments, individual *Alexandrium fundyense* cells were sorted into wells, which were then incubated and tracked with a plate reader. In these experiments one row of each well plate was left empty as a control to ensure that no cells were deposited through other means, such as

aerosolization. No cell growth was detected in these control wells. Of 168 sorts, 23 were viable and showed consistent growth over a 3-week post-sort period (Fig. 5). The low proportion of viable cells could be due to the health of the culture used to conduct the experiment, abrupt changes in temperature experienced by the cells during the experimental procedure, or mechanical stresses experienced during the sorting procedure. During sorting, the cells encounter several regions of high shear, including capture by the catcher tube and injection into the well-plate. These mechanical stresses are likely much lower in severity than the shear a cell experiences as it enters the flow cell of the IFCB. Notably, the rate of successful isolation in this experiment (12.3%) is considerably higher than values previously reported for isolation of dinoflagellates by manual picking or sorting with a commercial FACS system (~1-2%) (Sinigalliano et al. 2009). Our isolation rate also compares favorably with rates observed for a number of microalgae (Sieracki, Poulton, and Crosbie 2005). This comparison suggests the IFCB-Sorter provides a relatively gentle means of cell isolation.

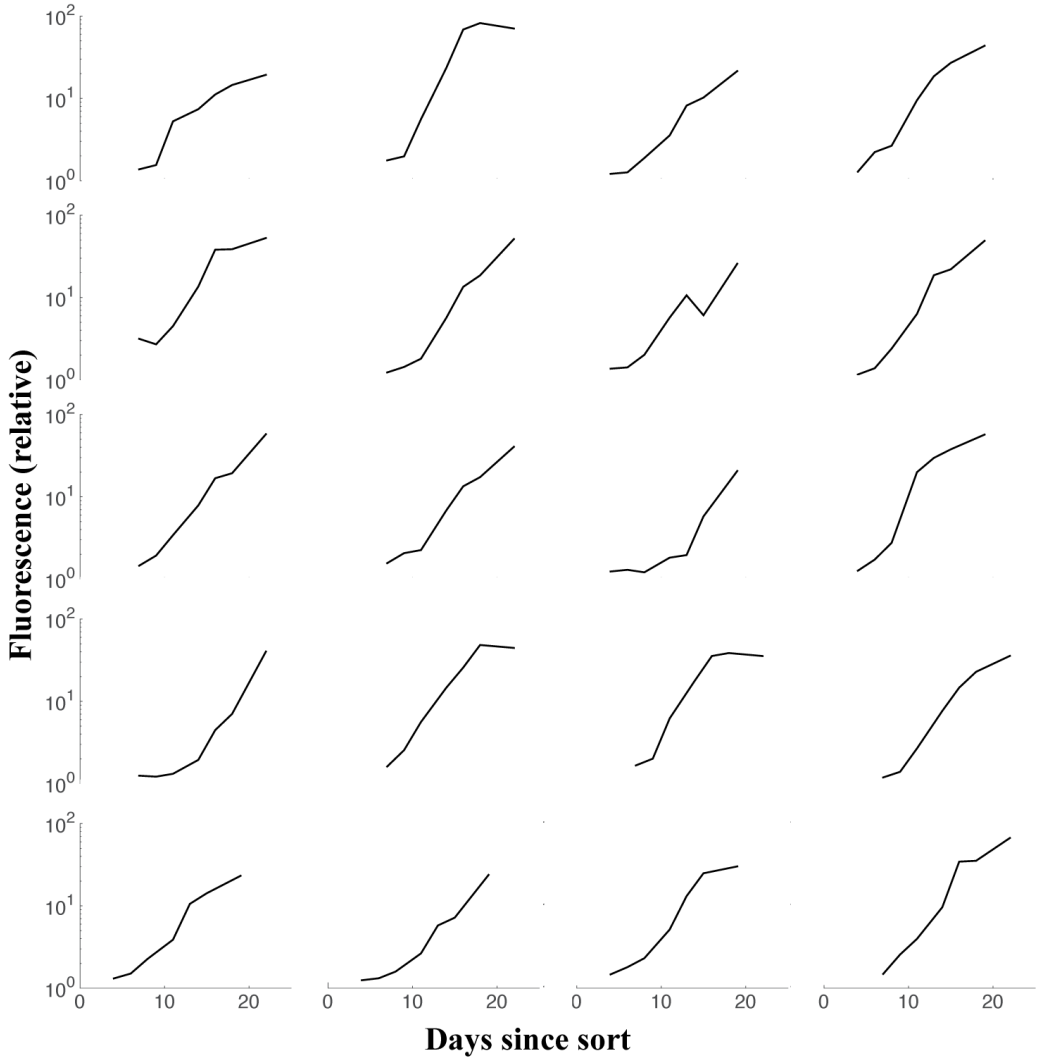

Fig. 5. Growth curves resulting from 20 individual *A. fundyense* cells sorted into wells of a 96-well plate using the IFCB-Sorter. During reisolation 23 of 168 sorted cells developed into successful subcultures.

Capture of cells from the environment

To evaluate the effectiveness of the IFCB-Sorter in isolating cells from natural samples, we used seawater collected from Woods Hole Harbor, Woods Hole, MA. During the sorting process we adjusted chlorophyll fluorescence trigger thresholds to select microplankton as the sort targets. Most triggers were ciliates, large dinoflagellates, and diatoms. Post-sort images verify both the

integrity of the sorted cells and correspondence with the initial images from IFCB (Fig. 6). During these experiments, a number of ciliates were collected on microscope slides and observed swimming very rapidly. As a result of their swimming speed these cells were very difficult to image and extended time on the microscope stage led to cell lysis, so most ciliates were not documented in post-sort images despite their prevalence and obvious post-sort viability.

It has long been recognized that analysis by flow cytometry can cause physiological damage (Rivkin, Phinney, and Yentsch 1986). While it was initially a concern that sensitive cells would be disrupted during the sorting process, our evaluation here indicates that the IFCB-Sorter can effectively sort cells traditionally thought to be fragile.

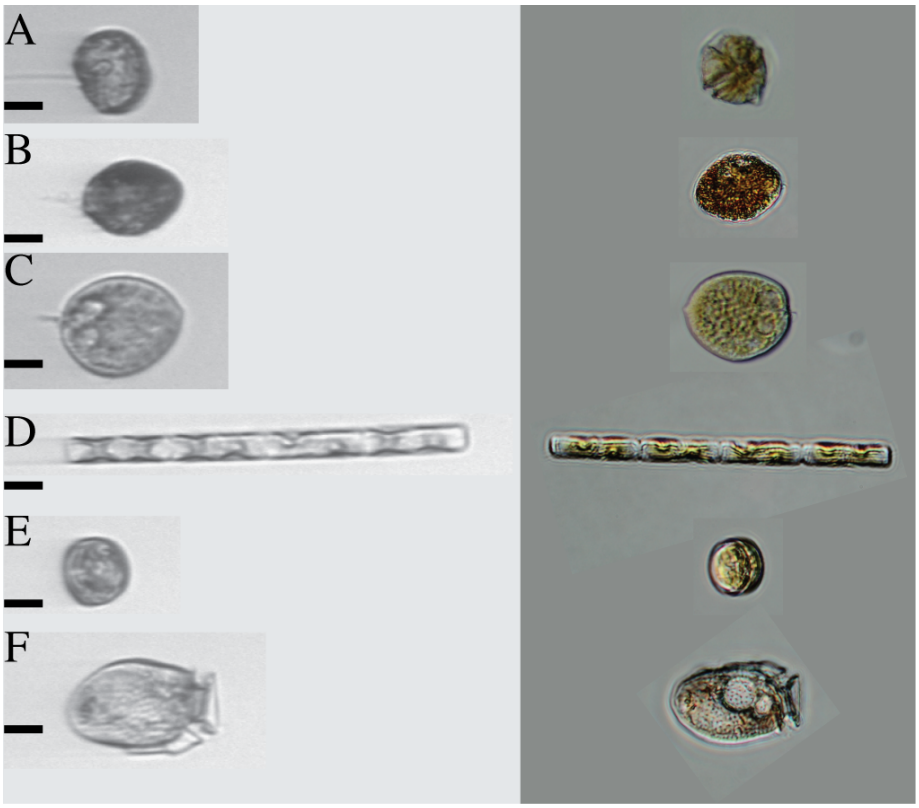

Fig. 6. Cells isolated from environmental samples. Images on the left were acquired pre-sort by the IFCB and images on the right are the same cells post-sort as seen at 40X magnification with an inverted microscope (Zeiss Axiovert S100) equipped with a Canon EOS Rebel T2i camera. Scale bar indicates 10 µm in the IFCB images. (**A**) Unidentified dinoflagellate, (**B**) unidentified cell, (**C**) *Prorocentrum* spp. (**D**) *G. delicatula*, (**E**) centric diatom, (**F**) *Dinophysis* spp.

Capture of chain-forming cells

The IFCB-Sorter is capable of capturing chain-forming cells, but with lower efficiency than the capture of cells with a simpler morphology. For example, we sorted the chain-forming diatom Guinardia delicatula with conservative timing parameters (300 µs delay, 800 µs catcher tube deployment). The result was a capture efficiency of 21.2%. This efficiency may be further decreased if complex morphological features, such as setae, are present.

Capture volume

The probability of coincidental capture of non-targeted cells is an important parameter for sorting systems and in the IFCB-Sorter it is related to the volume captured initially by the catcher tube. To calculate a worst-case estimate of that probability, we assume that during catcher tube deployment (t_d) all the volume captured is sample, and use a conservative catcher tube deployment time of 700 µs. With a sample flow rate (Q_{core}) of 0.05 mL min^{-1}, the captured volume (V_c) can be calculated from

$$V_c = Q_{core} * t_d. \quad (1)$$

With this approach, we find V_c = 5.8 x 10^{-7} mL.

The probability of coincidental capture (p) is the product of V_c and the concentration of background contaminant particles (C_{bg})

$$p = V_c * C_{bg} \quad (2)$$

Thus, for a 10% contamination probability, C_{bg} is 1.7x10^5 cells mL^{-1}. This indicates that the IFCB-Sorter should be capable of isolating microalgae with low risk of contamination by other organisms. It should be noted that the captured sample volume will be diluted by mixing with

particle-free sheath fluid during passage through the secondary sorting system, which will tend to further purify the sorted particles.

Discussion

Here we present the first sorting imaging-in-flow cytometer, with the capability to link images, flow cytometric quantities, and downstream physiological or molecular studies of single cells. From our experiments we have demonstrated a cell sorter with a low probability of coincidental capture and the capability to sort viable cells. The IFCB-Sorter can effectively sort a variety of plankton, which leads to the possibility of investigating cell-to-cell variability in traditionally difficult to capture cell types. The addition of imaging capabilities to a cell-sorting flow cytometer opens up new venues for investigation, especially for microplankton which are difficult to characterize in conventional FACS systems that only measure cell fluorescence and scattering.

The IFCB-Sorter enables new research probing relationships between morphology, genotype, and ecological role. For example, the IFCB-Sorter is capable of sorting both mixotrophic and herbivorous protozoa (depending on gut content), which are very difficult to target with traditional cell-sorting techniques. This capability provides the potential for studying linkages between phytoplankton and their grazers. One understudied group that could benefit greatly from the application of this technology is marine ciliates. Marine ciliates have long been classified according to morphotype. In recent years it has become apparent that similar morphology does not necessarily coincide with genetic similarity(Snoeyenbos-West et al. 2002). Flow cytometry has supplied crucial information about grazer dynamics in the past(Taniguchi et al. 2014; Lavin, Fredrickson, and Srienc 1990; Cucci et al. 1989) and the IFCB-Sorter, along with single-cell

genomic methods, could now allow us to investigate these predator-prey interactions in greater detail.

While the IFCB-Sorter is capable of capturing chain-forming cells, it does so with reduced efficiency compared to single cells. Chain-forming cells and those with complex features may traverse the distance between the location of image acquisition and the catcher tube at a slower rate. As a result these cells may not be captured even with conservative timing parameters. It may be possible to increase the capture efficiency by increasing the catcher tube deployment time, but this strategy conflicts with the goal of a low contamination rate. Chain-forming cells may also take longer than our observation time limit to pass through the sorting subsystem and are therefore discarded. Again it may be possible to overcome this by increasing the observation time, but this has the potential to reduce the total number of cells sorted per sample. If the aim of an experiment is to isolate chain-forming cells, the procedure could be modified and the IFCB-Sorter might then be used as an initial step in cell isolation.

Isolation of cells from the environment, along with corresponding images, offers a powerful method to investigate genetic differences in marine planktonic microorganisms, which have been observed to result in the formation of subpopulations during blooms (Koester et al. 2010). Cryptic diversity has been noted in several phytoplankton genera (Montresor et al. 2003; Kooistra et al. 2010; Iglesias-Rodríguez et al. 2006) and the IFCB-Sorter could be used to link morphology to this genetic variability and to environmental conditions. Furthermore, cells from different life cycle stages could be sorted for detailed studies of the factors regulating important processes such as sexual reproduction and cyst or resting-stage production.

Comments and Recommendations

The IFCB-Sorter is very slow (~15 seconds per sort event) compared to conventional fluorescence-activated cell sorters (up to 10,000 s^{-1}) (Shapiro 2005). The sorting rate could be increased several-fold by miniaturizing the sorting subsystem (thereby decreasing its path length). However, the main limitation to sorting speed is our secondary system for isolating the sorted cell, which requires bulk flow to the storage site followed by re-detection of the cell's position before ejection into a well. In theory sorting speed could be greatly increased by utilizing conventional droplet sorting (with electrostatic deflection of droplets after initial detection rather than a catcher tube). We chose the slower approach because sorting of our large particles of interest would require formation of very large charged droplets, which would be technically more difficult to achieve and maintain than our solenoid-based approach. In addition, compared to a contained-flow system, droplet sorting, which produces aerosols, seems less compatible with our ultimate goal of autonomous in situ operation. Our original storage strategy utilized emulsion microfluidics technology to direct sorted cells to storage chambers in a totally enclosed system, but we found that natural populations of microphytoplankton are not well suited to flow through microchannels (e.g., chain-forming or spine-bearing diatoms caused clogging of channels). Alternative storage methods such as tape reels of self-sealing wells could still enable in situ applications of our sorting approach, but are beyond the scope of this study.

As with any molecular analysis, contamination is a major concern. The ability to run IFCB-Sorter with external sheath fluid and to run regular built-in cleaning programs mitigates this issue. It is also possible to trigger sorting in the subsystem with an external trigger pulse, to serve as a negative DNA control during downstream amplification.

IFCB is commercially available through McLane Research Laboratories, Inc. While the development described here involved a prototype design, it should be feasible to alter the commercially available version of IFCB to enable cell sorting in a similar manner. This would require replacing the stock flow cell with the FACSCalibur sorting flow cell used in this study. Additionally, the instrument firmware would need to be altered to incorporate signals from the sorting subsystem.

Contributions

Bennett Lambert (B.L.), Robert Olson (R.O.), and Heidi Sosik (H.S.) designed experiments. B.L. and R.O. constructed the sorting subsystem. B.L. carried out experiments to validate IFCB-Sorter. B.L., R.O., & H.S. analyzed data. B.L., R.O., & H.S. wrote the paper.

Chapter 3: A microfluidics-based *in situ* chemotaxis assay to study the behaviour of aquatic microbial communities

Work presented in this chapter was published as "Bennett S. Lambert, Jean-Baptiste Raina, Vicente I. Fernandez, Christian Rinke, Nachshon Siboni, Francesco Rubino, Philip Hugenholtz, Gene W. Tyson, Justin R. Seymour, & Roman Stocker. A microfluidics-based in situ chemotaxis assay to study the behaviour of aquatic microbial communities. *Nature Microbiology* **2**, 1344-1349 (2017)".

Introduction

Microbial interactions influence the productivity and biogeochemistry of the ocean, yet they occur in miniscule volumes that cannot be sampled by traditional oceanographic techniques. To investigate behaviors of marine microorganisms at spatially relevant scales, we engineered an *in situ* chemotaxis assay (ISCA) based on microfluidic technology. Here we describe fabrication, testing, and first field results of the ISCA, demonstrating its value in accessing the microbial behaviors that shape marine ecosystems.

Planktonic microorganisms control the biogeochemistry and productivity of marine ecosystems (Azam 1998). This global-scale influence is governed by the rate at which individual microbes access organic substrates from the water column, which in turn is dependent upon the spatial distribution of substrates and the capacity of cells to exploit microscale nutrient hotspots (Azam and Malfatti 2007). Seawater is surprisingly heterogeneous at the scale of individual microbes (Blackburn, Fenchel, and Mitchell 1998), with nutrient hotspots on and around organic particles

(Kiørboe et al. 2002), phytoplankton cells (Smriga et al. 2016) and zooplankton fecal pellets (Jefferson 2002). These microscale features of the water column represent important biogeochemical microenvironments where microbial activity and transformation rates considerably exceed background levels (Fenchel 2002; Smriga et al. 2016). Consequently, the microbial behaviors involved in accessing, and maintaining contact with, these microenvironments can have profound implications for basin-scale chemical cycling, but have remained largely inaccessible by traditional oceanographic sampling approaches.

Chemotaxis – the ability of microbes to move in response to chemical gradients – is a pervasive microbial phenotype that allows them to exploit heterogeneous chemical landscapes. The first quantitative measurements of chemotaxis were carried out fifty years ago using the capillary assay (Adler and Dahl 1967), which relies on the molecular diffusion of a chemical cue from the tip of a capillary tube to attract bacteria. Many alternative techniques have since been developed (Ford et al. 1991), including the recent application of microfluidics to establish controlled chemical gradients and quantify microbial responses (Hol and Dekker 2014). Although chemotaxis is conventionally studied in the context of physically structured microenvironments such as biofilms, or in association with animal or plant hosts (He and Bauer 2014), there is growing evidence (albeit mostly limited to laboratory-based assays (Stocker and Seymour 2012)) that indicates its ubiquity among copiotrophic planktonic marine microbes (Blackburn, Fenchel, and Mitchell 1998; Smriga et al. 2016), which likely use it to access fleeting microscale nutrient patches in the water column (Azam 1998; Blackburn, Fenchel, and Mitchell 1998). In order to quantify and understand the importance of chemotaxis in the ocean, we need to measure this behavior *in situ*. Here we leverage the control afforded by modern microfabrication methods to

design an *in situ* chemotaxis assay (ISCA) that enables measurement of marine microbial behavior under natural conditions.

The ISCA is a robust, rapidly-producible device that bridges the gap between lab-based microfluidics and traditional oceanographic methods, by providing an *in situ* system to interrogate microbial behavior (Fig. 1). The ISCA consists of a scalable array of 110 μL wells embedded in a polydimethylsiloxane (PDMS) slab, with each well connected to the outside seawater by an port (0.8 mm diameter, 1.6 mm depth) (Fig. 1a and Supplementary Fig. 1; see Methods). The device is made of inert materials, is single-use, and is fabricated using a standard soft lithography workflow, based on a mold created using 3D printing. Each well is filled with a chemoattractant, which diffuses out of the inlet port and into the surrounding seawater during deployment, resulting in a chemical microplume extending 1-2 mm above each well (Supplementary Video 1). As in the capillary assay, microbes can respond to a specific cue by using chemotaxis to swim into the well. Following deployment, cells can be enumerated with flow cytometry to quantify the strength of chemotactic accumulation within each well and DNA sequencing approaches applied to identify responding microbial populations.

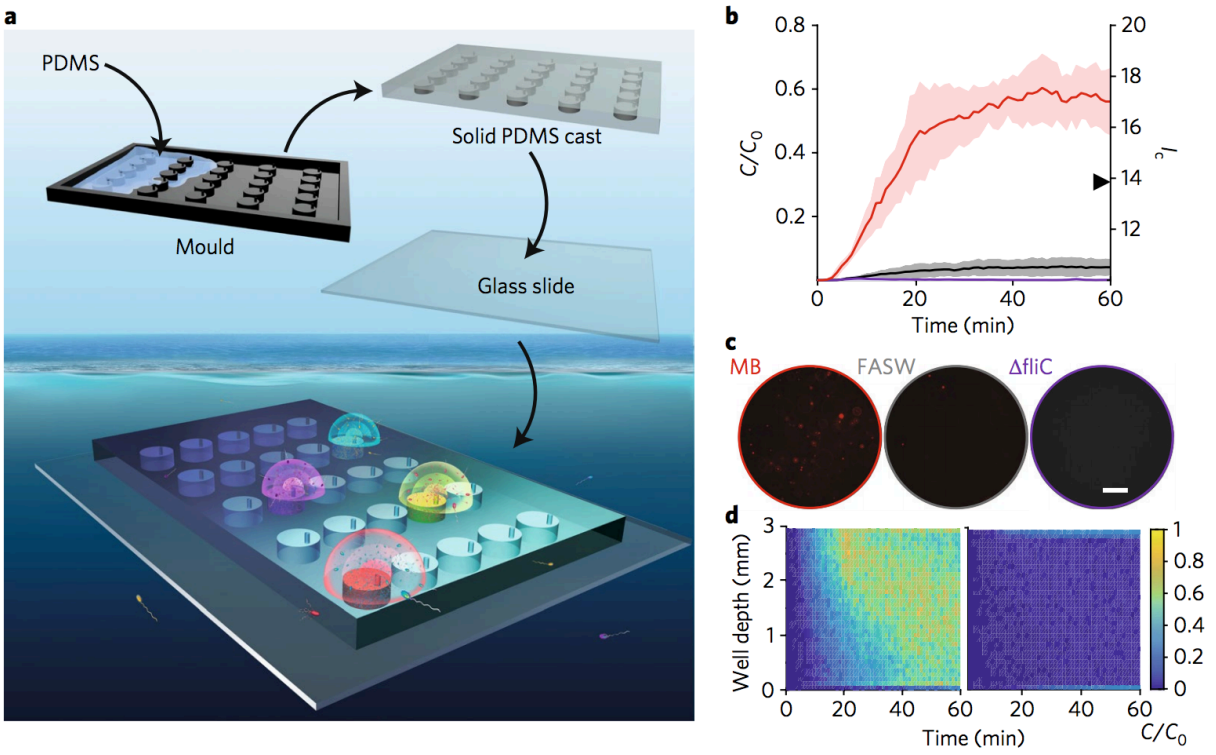

Fig. 1 | Fabrication of the in situ chemotaxis assay (ISCA) and laboratory tests. a, Polydimethylsiloxane (PDMS) is cast onto a 3D printed mould and cured overnight. The solid PDMS, containing multiple wells, is then excised and plasma-bonded onto a glass slide (100 mm × 76 mm × 1 mm). Each well has an independent connection to the external environment via a port, through which chemicals can diffuse and microorganisms enter. Upon deployment, the ISCA produces chemical microplumes that mimic transient nutrient patches. Chemotactic bacteria respond by swimming into the wells of the device and after collection can be enumerated by flow cytometry and identified by sequencing. Computer-aided design files are provided in Supplementary File 1. **b**, Accumulation of fluorescently labelled marine isolates within ISCA wells in a laboratory microcosm quantified through video microscopy. The solid line represents the mean cell concentration (n= 3) over the imaging volume normalized to that in the surrounding medium and the shaded area is one standard deviation around the mean. Red: *V. coralliilyticus* swimming into a well initially filled with 10% Marine Broth (MB). Black: *V. coralliilyticus* and filtered artificial seawater (FASW, control). Purple: *M. adhaerens* non-motile mutant control (ΔfliC) and FASW (non-motile control; almost indistinguishable from zero). The triangle on the right-hand axis indicates the chemotactic index, I_c, for *V. coralliilyticus* after 60 min, calculated as the ratio of the number of cells responding to the chemoattractant and to the FASW. **c**, Representative images taken at mid-depth of the well after 60 min. Scale bar, 100 μm; n= 3. Note the near absence of cells from the controls (FASW and ΔfliC). **d**, Average accumulation through well depth and time of fluorescently labelled *V. coralliilyticus* in response to 10% Marine Broth (left, n= 3) and in response to FASW (right, n= 3). Minor accumulation shows that random motility does not contribute significantly to the final concentration of cells in each well. The colour bar applies to both panels and indicates the concentration of cells, C, in each image, normalized to that in the surrounding medium, C_0. The resolution is 80 μm in depth and 1 min in time.

Results

Prior to field deployment, we thoroughly tested the ISCA in the laboratory by employing several chemotactic bacterial isolates, in order to assess the potentially confounding roles of random motility, ambient flow, and Brownian motion. To measure the chemotactic accumulation dynamics of bacteria within individual wells, a small ISCA (2 × 2 array of wells) was embedded within a microcosm placed on the stage of an inverted microscope (Supplementary Fig. 1). The microcosm contained fluorescently labeled *Vibrio coralliilyticus* (YB2), a copiotrophic marine bacterium and coral pathogen (Garren et al. 2014), suspended in 0.2-μm-filtered artificial seawater (Instant Ocean; Spectrum Brands, Inc.). Bacterial fluorescence was used to identify cells throughout the well depth by epifluorescence microscopy. One ISCA well was filled with a broad-spectrum chemoattractant (Marine Broth, Becton Dickinson, USA) and another, serving as negative control, with filtered artificial seawater (see Methods; Supplementary Fig. 2). We used 10% Marine Broth inside the ISCA in order to generate signals at ecologically relevant concentrations (Supplementary Note 2). We imaged a predetermined location within each well, scanned over the entire well depth every minute for 60 minutes, and used image analysis to obtain cell counts as a function of time (see Methods).

The ISCA captured the characteristically strong chemotactic response of *V. coralliilyticus*(Garren et al. 2014). An intense accumulation of cells occurred within wells containing Marine Broth (56.1 ± 10.4 % of the microcosm cell density; $n = 3$), whereas the accumulation was negligible in the control wells (4.1 ± 2.4 % of the microcosm cell density; $n = 3$). The ratio of the cell concentrations in treatment and control wells – the chemotactic index (I_c; ratio of cells in treatment to cells in control) – was 14, denoting a strong response to the chemoattractant (Fig. 1b and Supplementary Figs. 3,4). These results confirm that the ISCA

generated robust chemical signals and effectively attracted and retained chemotactic bacteria in the wells (Fig. 1c). The high value of I_c also indicates that random motility – which results in bacteria entering wells even in the absence of chemical gradients – is negligible compared to chemotaxis. Furthermore, experiments with a non-motile bacterium, *Marinobacter adhaerens* (HP15 ΔfliC), did not result in significant cell accumulation relative to the surrounding medium (0.09 ± 0.03 % of the microcosm cell density; $n = 3$; Fig. 1a and Supplementary Fig. 5), implying that environmental factors such as fluid flow do not contribute significantly to the accumulation of cells in the wells under laboratory conditions.

Imaging-based laboratory experiments revealed three phases in the chemotactic accumulation: (*i*) an initial lag phase lasting ~5 min where cells swam into the inlet port but had not yet entered the main cavity of the well; (*ii*) a sharp increase in bacterial abundance in the well as bacteria began to enter, lasting until ~25 min; and (*iii*) a slowdown in the accumulation (at 30–40 min) as the outward diffusive flux of cells began to balance the inward chemotactic flux (Fig. 1b). In the second phase, the spreading of cells from the top of the well downwards (Fig. 1d and Supplementary Figs. 3,6) provides direct visual evidence of the chemotactic dynamics and helps rule out confounding factors such as residual fluid flow in the wells.

To further validate the ISCA, we compared the observed accumulation dynamics with those predicted by a mathematical model of chemotaxis (Methods; Supplementary File 2, Supplementary Videos 1,2 and Supplementary Figs. 6–9). Chemotactic transport models are only well-developed for a few specific model organisms such as *Escherichia coli* (Lewus and Ford 2001), so the model was parameterized for *E. coli* responding to the non-metabolizable chemoattractant α-methylaspartate, a pairing studied extensively in chemotaxis literature (Mesibov and Adler 1972). To allow direct comparison, a laboratory ISCA experiment was

carried out with a fluorescent strain of *E. coli* (AW405) and α-methylaspartate as the chemoattractant (see Methods; Supplementary Fig. 6). In this experiment, image stacks over the entire well's depth were acquired over time at two different locations, one close to the inlet port (1.5 mm from the edge of the inlet) and the second further away (2.5 mm), so that the progression of chemotactic bacteria within the well could be followed. The comparison of experimental results with model predictions demonstrated highly consistent timescales and magnitudes of accumulation, with cells first appearing in the field of view at ~10 min (1.5 mm location) and ~20 min (2.5 mm location) (Supplementary Fig. 9). Furthermore, the chemotactic drift velocity inferred from the time-lag between the appearance of bacteria at the two imaging locations (~1.1–1.85 μm/s; $n = 3$) is consistent with values reported in the literature for *E. coli*(Ahmed and Stocker 2008), further supporting the absence of residual flows within the device. This set of experiments in conjunction with the numerical model confirms that chemotaxis is the primary mode of accumulation in the ISCA.

With experimental results providing confidence in the ISCA's operation, the device was next tested *in situ*. We deployed four replicate ISCAs (each consisting of a 5 × 5 array of wells) for 1 h (a duration well below typical doubling times of marine microbes (Ammerman et al. 1984); Supplementary Note 3) in surface waters (1 m depth) at a coastal marine site in Sydney, Australia (Clovelly Beach; 33.91°S, 151.26°E). To retain consistency with the laboratory-based experiments, we compared the chemotactic response of microbes to wells filled with Marine Broth and to control wells filled with filtered seawater (0.02 μm; see Methods) derived from the deployment site. To prevent density differences between well contents and bulk seawater, which could lead to density-driven flows, this filtered seawater was also used to dilute the Marine Broth.

Although fluid flow into the wells was ruled out in the laboratory experiments, *in situ* conditions are far more dynamic and may potentially disrupt the chemical microplumes emanating from the wells. To prevent this, each ISCA was mounted within a transparent 1.9-liter volume, laser-cut acrylic enclosure (Supplementary Fig. 10). The enclosure was soaked for 48 hr in ddH_2O to remove labile DOM from the acrylic surface. The stable environment provided by the enclosure also ensured that bacteria were not swept past the wells at a speed that overpowered their swimming ability. This replicates the physical environment that cells encounter at the microscale, where bacteria and nutrient hotspots are essentially transported together and movement of one relative to the other is primarily achieved through motility (Taylor and Stocker 2012). After securing the ISCA, the acrylic enclosure was slowly filled with seawater while being submerged and once at its final depth was completely sealed using a plug and left *in situ* for 1 hour (Supplementary Fig. 11). Strong chemotaxis was observed, with the mean number of bacteria in Marine Broth wells 3.6 ± 0.2 times greater than in negative control wells (t-test, $n = 4$, $p < 0.005$; Fig. 2). These results constitute *in situ* confirmation that pelagic marine bacteria exhibit strong chemotaxis, which not only supports results of previous laboratory-based studies (Blackburn, Fenchel, and Mitchell 1998; Smriga et al. 2016; Stocker et al. 2008), but also long-standing hypotheses about the occurrence of this behavior in the pelagic environment (Azam 1998; Azam and Long 2001; Azam and Malfatti 2007).

Chemotactic populations were identified by their 16S rRNA sequences in shotgun metagenomic data obtained using a low DNA-input library preparation procedure (Rinke et al. 2016). Whereas the taxonomic profile of bulk seawater at the sampling site was characteristic of a typical coastal marine community, including a high proportion of non-motile Pelagibacteraceae (Fig. 2), the ISCA wells containing Marine Broth were highly enriched with motile copiotrophs, including

Vibrionales, and Alteromonadales (Supplementary Fig. 12). These groups are well known for their chemotactic capabilities(Smriga et al. 2016) and metabolic versatility (Pedler, Aluwihare, and Azam 2014), which enable them to respond to and use a large number of organic compounds, such as those present in Marine Broth. These results therefore provide *in situ* confirmation that copiotrophic microbes of this type can rapidly respond to microscale nutrient patches (Stocker et al. 2008). In addition, less-studied motile taxa, such as Flammeovirgaceae, were also enriched in the wells containing Marine Broth (Supplementary Fig. 12). The latter finding reveals the power of the ISCA to identify cryptic chemotactic taxa and highlights its potential use in prospecting for taxa capable of responding to specific chemicals, such as pollutants.

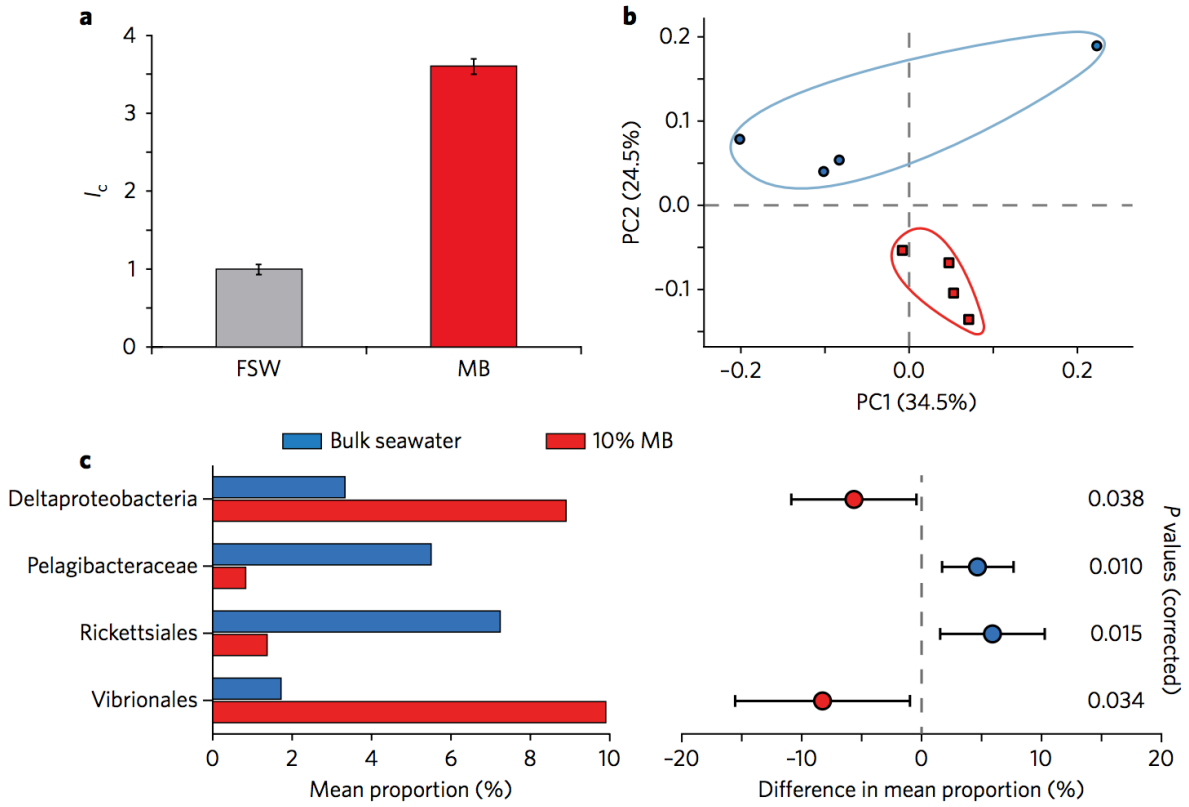

Fig. 2 | Field tests of the ISCA. a, Chemotactic index I_c, denoting the concentration of cells within ISCA wells, normalized by the mean concentration of cells (n =4) within wells containing filtered seawater (FSW), after 60 min field deployment. Cells were enumerated by flow cytometry (MB: $9.4 \pm 0.4 \times 10^3$; FSW: $2.6 \pm 0.3 \times 10^3$ cells ml^{-1}). Note that wells containing 10% MB had significantly more bacteria than the FSW control (t-test, n =4, P <0.05). Error bars represent standard errors. **b**, Principal component analysis comparing family-level taxonomic profiles of bulk seawater from the sampling site with the contents sampled from the ISCA wells containing MB. c, Taxa differing significantly between bulk seawater and ISCA wells containing MB (n =4). P values were corrected for multiple hypothesis testing using the Bonferroni correction (95% confidence intervals).

Conclusion

We believe that the ISCA represents a significant advance in microbial oceanography, enabling the interrogation of the chemically-mediated interactions that support the base of the food web and drive biogeochemical cycles at scales relevant to microorganisms in their natural environment. Here we capitalized on rapid advances made in the fields of microfluidics and low-

input DNA sequencing(Rinke et al. 2016) to couple micro-engineering with genomic analyses. The ISCA is not only deployable in aquatic environments, but also in any system containing a liquid phase (eg. soil and sediment matrices or wastewater systems). Future use of the device will enable high-throughput testing of environmentally-derived chemicals, and when coupled with genomic and metabolomic analyses, will generate rich datasets allowing the behavior and chemical ecology of microbes to be dissected within their natural habitats.

Methods

ISCA design and assembly

A 3D printed mold was designed using SolidWorks 2015 (Dassault Systemes SOLIDWORKS Corp., Concord, USA) and made out of the polymer VeroGrey on an Objet30 3D printer (Stratasys Ltd., Eden Prairie, USA; Supplementary File 1). In the implementation used for the field deployments, each ISCA consisted of an array of 5 × 5 wells. Each well was 6.8 mm in diameter and 3 mm in depth, which corresponds to approximately 110 µL of fluid (Supplementary Fig. 1), a volume selected based on the estimated lower limit of input required for DNA extraction and sequencing. The wells are spaced 17 mm apart between rows (center to center) and 9 mm within a row (Supplementary Fig. 1). The port of each well was offset from the center of the well to allow release of air bubbles during filling of the well (Supplementary Fig. 1). Considering a representative diffusion coefficient (D) of 1×10^{-9} m s^{-1}, the estimated distance L a solute travels in a time t = 1 h is $L = \sqrt{4Dt}$ = 3.8 mm. The spacing used therefore ensures no well-to-well interaction of the diffusion plumes within typical deployment times of 1 h. The port diameter was 800 µm with a depth of 1.6 mm (Supplementary Fig. 1). A high aspect ratio for the inlet port was selected to diminish the effects of cavity flow on device performance (see Supplementary Note 1).

Each mold was filled with 26 g of polydimethylsiloxane (PDMS; 10:1 PDMS base to curing agent, wt/wt; Sylgard 184, Dow Corning Corp., Midland, USA). Curing was carried out overnight at 40°C (the deflection point of VeroGrey is 48°C). The cured PDMS slab (95 mm × 65 mm × 4.6 mm) was cut using a razor blade and carefully peeled from the mold. The PDMS blocks were inspected and any port obstructions cleared using a biopsy punch of the appropriate diameter (ProSciTech, Townsville, Australia). Finally, the devices were UV-sterilised and plasma-bonded to sterile glass microscope slides (100 mm × 76 mm × 1 mm, VWR, Pennsylvania, USA) by exposing both to oxygen plasma for 5 min using a Plasma Cleaner/Sterilizer (Harrick Scientific, New York, USA). Following bonding, the ISCA was heated at 90°C for 10 min to accelerate the formation of covalent bonds and then stored at room temperature until use.

Laboratory experiments

Bacterial cultures

The marine bacterium *Vibrio coralliilyticus* (YB2) was used as a model organism for laboratory experiments due to its high levels of motility and strong chemotactic response (Garren et al. 2014). A glycerol stock of *V. coralliilyticus* was streaked onto Difco 2216 Marine Broth (BD Biosciences, San Jose, USA) agar plates containing 50 μg/ml kanamycin (Axonlab AG, Baden, Switzerland). Individual colonies were then removed and grown in 1% (v/v) 2216 Marine Broth in 0.22 μm filtered artificial seawater (Instant Ocean; Spectrum Brands, Inc., Madison, USA) for 22 h(Garren et al. 2014). The cultures were then diluted 1/20 (v/v) in 0.22-μm filtered Instant Ocean to obtain the bacterial suspension used in the experiments. All cells were grown at 30°C and 180 rpm.

To ensure that bacteria found in the ISCA well had entered them via chemotaxis and not by flushing due to fluid flow or Brownian motion, we carried out an experiment with non-motile bacteria. We used *Marinobacter adhaerens* (HP15 ΔfliC), which is a non-motile mutant lacking fliC, a gene necessary for flagellar synthesis (Sonnenschein et al. 2011). A glycerol stock of *M. adhaerens* HP15 ΔfliC was streaked onto Difco 2216 Marine Broth agar plates containing 50 μg/ml ampicillin (Axonlab AG, Baden, Switzerland). Individual colonies were then suspended in 10% 2216 Marine Broth for 1 d. The cells were then washed three times in Instant Ocean before being diluted 1/10 (v/v) in Instant Ocean to obtain the bacterial suspension used in the experiments. All cells were grown at 30°C and 180 rpm.

To directly compare experimental results to results from the mathematical model of chemotaxis, which was implemented based on parameters for *Escherichia coli* chemotaxis (due to the lack of information on parameters for marine bacterial chemotaxis), we also performed laboratory experiments with *E. coli* (AW405). In order to directly visualize the bacteria in the ISCA wells, *E. coli* were transformed to carry a plasmid constitutively expressing a red fluorescent protein (pFM210) (Kelly et al. 2009; Temme et al. 2012). Cells in log phase (OD = 0.3) were washed and resuspended in 50 mM calcium chloride, heat-shocked in a solution containing plasmid DNA, and spread on tryptone broth plates containing 50 μg/ml kanamycin. Resistant colonies were regrown in tryptone broth containing 50 μg/ml kanamycin and screened for fluorescence. Glycerol stocks (15% v/v) of colonies displaying strong fluorescent signal were made and stored at -80°C. The transformed *E. coli* were streaked onto tryptone broth agar plates containing 50 μg/ml kanamycin. Individual colonies were then removed and grown overnight in tryptone broth containing 50 μg/ml kanamycin. These cells were then diluted 1:100 in tryptone broth and incubated until they reached mid-exponential phase (OD = 0.3). Cells were then diluted 1/20

(v/v) in motility medium (10 mM potassium phosphate, 0.1 mM EDTA, 1 μM methionine, 10 mM lactic acid, pH = 7) to obtain the suspension used in the experiments. All cells were grown at 30°C and 180 rpm.

Assembly of the integrated ISCA for laboratory experiments and chemotaxis experiments with isolates

To visualize chemotactic accumulations in the ISCA wells without interference by external fluid flows, a modified version of the ISCA was integrated into a microcosm designed for use on an inverted microscope. To achieve this, an ISCA was prepared in the same manner as described above, but only four of the wells were excised from the PDMS block to reduce the footprint of the device (Supplementary Fig. 1). The four wells were plasma-bonded to the center of a microscope slide (75 mm × 50 mm × 1 mm) and a four-walled PDMS enclosure was plasma bonded around the wells (Supplementary Fig. 1). The design of the mold used to generate the enclosure is provided in Supplementary File 1. This ISCA-containing microcosm was placed onto the stage of an inverted microscope (Eclipse Ti-E, Nikon, Tokyo, Japan). A well of the integrated ISCA was filled with the prepared bacterial suspension and three stacks of images (80 μm step size, 2960 μm total) were acquired within a well containing the bulk suspension to calculate the bacterial concentration throughout the microcosm. This bacterial concentration (C_0) was subsequently employed to normalize the concentration measured in individual treatments, so that chemotactic accumulations were quantified relative to the absolute concentration of bacteria present in each experiment. The device was then removed from the microscope stage and one well of the device was filled with a chemoattractant (10% Marine Broth for experiments with *V. coralliilyticus*; 100 μM α-methylaspartate for experiments with *E. coli*; Supplementary Figs. 3,6), while a second well was filled with Filtered Artificial seawater (FASW) for experiments

with M. adhaerens and V. coralliilyticus or with Motility Media for experiments with *E. coli*, both serving as negative controls (Supplementary Figs. 4,7). After placing the microcosm back on the microscope stage, an initial image stack was acquired (80 μm step size, 2960 μm total; time $t = 0$). The microcosm was then filled with the bacterial suspension and one image stack was acquired every minute for 60 min (Supplementary Fig. 2). Image stacks acquired within the wells consisted of 1 image every 80 μm of depth, throughout the depth (2960 μm) of the well. Image acquisition was carried out with a 20× objective in all cases using Nikon Elements software (Nikon, Tokyo, Japan) and a Zyla 4.2 PLUS sCMOS camera (Andor, Belfast, Ireland).

Image analysis

To quantify cells in our laboratory experiments it was necessary to accurately identify cells in each image, while excluding out-of-focus cells and debris. To accomplish this, image processing and analysis was carried out in MATLAB 2015a (The MathWorks, Natick, USA) using the Image Processing Toolbox. The image stacks obtained in Nikon Elements were first filtered with a bandpass Gaussian filter to reduce high-frequency noise and remove larger objects due to uneven illumination or out-of-focus halos. These processed images were then segmented to identify candidate bacteria. These candidates were subsequently gated based on average pixel intensity and object area to enumerate the cells in each image. The resulting cell counts were manually verified for a subset of images in each image stack. Videos displaying the success of image analysis in identifying cells can be found in the supplementary material (Supplementary Videos 5-7). The analysis was successful in identifying the majority of cells while excluding out-of-focus cells.

To determine absolute cell concentrations it was necessary to quantify the depth of field for each of the three strains of bacteria used, so that cell concentration could be computed from the

number of cells and the imaging volume. The detection of cells described above depends on the choice of gating parameters and the fluorescent intensity of the cells themselves. The depth of field was determined empirically by the analysis of vertical image stacks of fluorescently labeled cells on a horizontal surface. The image processing described above was carried out and the depth of field was defined as twice the height at which the number of detected in-focus cells was <10% of the value at the surface. This depth of field was then used consistently throughout the analysis to determine cell concentrations. The cell concentration in each well, C, was normalized by the cell concentration in the initial bacterial suspension, C_0, measured in a well filled with that suspension.

Mathematical model of chemotaxis into ISCA wells

We compared our laboratory observations with the predictions from a mathematical model, implemented in COMSOL Multiphysics 5.1 (COMSOL Inc., USA) using the 'Transport of Diluted Species' and 'Coefficient Form PDE' modules. The model domain consisted of a single three-dimensional ISCA well and the fluid (1 ml) outside the inlet port (Supplementary Fig. 8). The model, based on coupled partial differential equations, solves for the spatiotemporal distribution of the chemoattractant (Supplementary Video 1), which is then used as input into a transport equation for populations of chemotactic or non-chemotactic bacteria, modeled as a concentration of cells (Ahmed, Shimizu, and Stocker 2010) (Supplementary Video 2 and Supplementary Fig. 9). The mesh consisted of two domains (port and well; Supplementary Fig. 8) and boundary layers were enabled, with edges trimmed. The chemical field and bacterial field were initialized as opposing smoothed step functions, with the transition zone determined by the penetration depth of a cavity flow (Supplementary Note 1). Because chemotactic transport models are only well-developed for specific model organisms, and in particular *Escherichia coli*

(Lewus and Ford 2001), the model was parameterized for *E. coli* responding to the non-metabolizable chemoattractant α-methylaspartate, based on a model described previously (Ahmed and Stocker 2008). The model was initialized with the bulk fluid containing 1×10^5 cells ml^{-1} and the well contained 100 μM α-methylaspartate. The model then ran in two stages: an initial, 1-s long stage with 0.1-s time-steps and a subsequent, 1-h long stage with 10-s time-steps. This two-stage method saves on computation time while allowing sufficient temporal resolution early in time, when very steep gradients occur. The output of the model consisted in the concentration of chemoattractant and bacteria over the full computational domain and over time, which was then used to compare with experimental observations. The COMSOL model file (Supplementary File 2) can be found in the supplementary materials.

Field deployments

Field deployments occurred in April 2016 at Clovelly Beach (33.91° S, 151.26° E), situated on the eastern coast of Australia. To ensure the initial absence of microbial cells in the seawater used as both a negative control and as a base for chemoattractant suspensions, seawater from the site was subjected to a triple-filtration process: 50 ml was collected and first filtered through a 0.2-μm Sterivex filter (Millipore, USA), followed by a 0.2-μm Millex FG (Millipore, USA) and finally through a 0.02-μm Anotop filter (Whatman, England). Five 80-μl samples of this ultra-filtered seawater were fixed into 2% glutaraldehyde for subsequent flow cytometry analysis, which confirmed the effectiveness of this filtration protocol in removing all bacterial cells.

For initial testing of the ISCA in the field we used a broad-spectrum chemoattractant, Marine Broth 2216 (Beckton Dickson, NJ, USA), a common growth medium for marine microbes, which contains peptone (5 g/l) and yeast extract (1 g/l). A 10% final concentration of Marine Broth was resuspended in freshly ultra-filtered seawater from the deployment site immediately

before loading in the ISCA wells. The ISCA wells were filled with the port facing up: sterile 1-ml syringes and 27G needles (Terumo, Japan) were used to load samples into the wells. The diameter of the needle being smaller than the port allows air to escape as the well is filled. This procedure was found to be optimal in ensuring complete filling and no residual air bubbles in the wells.

Across each ISCA, treatments (filtered seawater or Marine Broth) were randomly allocated to an ISCA row (consisting of five wells). All wells in a row acted as technical replicates and four different ISCAs were deployed in parallel to act as biological replicates. Each ISCA was secured inside a deployment enclosure (Supplementary Fig. 10), which was sealed by pressure-sensitive tape (Scotch, 3M, USA) and an enclosure plug to seal the bottom drain (Supplementary Fig. 11). Each enclosure was then attached to a modified vice enabling the deployed ISCA to be firmly secured to a rigid structure (e.g., pontoon, ladder, pole) to minimize enclosure movement and standardize the deployment depth at 1 m. As the enclosures were submerged, they slowly filled with seawater through the enclosure inlets. Once completely filled with seawater, the enclosure inlets were plugged (to seal the enclosure) and the ISCAs were left *in situ* for 1 h.

Upon retrieval of the enclosures, the side outlets were unsealed progressively to slowly drain the seawater. Once the enclosure were completely empty, the contents of ISCA wells were then collected using 1-ml syringes and 27G needles (Terumo, Japan), with the ports facing down. For each ISCA, the liquid in the wells acting as technical replicates was pooled (five wells per treatment) in order to increase the amount of DNA collected per sample. The total volume of each pooled sample was 550 µL, out of which 80 µL was fixed with filtered glutaraldehyde (2% final concentration) for flow cytometry analysis (conducted on fresh samples the same day) and 470 µL was snap-frozen immediately in liquid nitrogen for subsequent DNA extraction and

sequencing. In addition to the ISCA samples, bulk seawater samples (n = 4) were also collected for both flow cytometry and DNA sequencing. Water temperature and salinity were recorded with a multiprobe meter (WTW Multiparameter Meter, WTW, Germany).

Although the deployment enclosure was required to generate a microenvironment that is analogous to that experienced by planktonic bacteria interacting with chemical hotspots in the water column, the manner in which the ISCA is housed is entirely dependent on the scientific question investigated. One may wish to study the interaction of bacteria with cues released from surfaces, such as in the benthic environment. In this case, the surface is stationary but the bacteria are advected by the flow, a scenario that is best replicated by deploying the ISCA without an enclosure.

Flow cytometry analysis

Samples for flow cytometry were transferred into sterile Titertube micro test tubes (Bio-Rad, CA, USA), stained with SYBR-Green I (Thermo-Fisher, MA, USA), incubated for 15 min in the dark, and analyzed on a BD Accuri C6 flow cytometer (Becton Dickinson, NJ, USA) with filtered MilliQ water as the sheath fluid. For each sample, forward scatter (FSC), side scatter (SSC), green (SYBR-green), and red (chlorophyll) fluorescence were recorded. The samples were analyzed at a flow rate of 35 µl min^{-1}. Microbial populations were characterized according to SSC and SYBR Green fluorescence (Marie et al. 1997) and cell abundances were calculated by running a standardized volume of sample (50 µl). To quantify the strength of chemotaxis, the Chemotactic Index (I_C) was calculated by dividing the number of cells present in the chemoattractant treatment by the number of cells present in the filtered seawater (FSW) negative control.

Molecular analysis

DNA extraction, library preparation, sequencing and bioinformatics

DNA extraction from seawater samples was performed using the UltraClean® Tissue & Cells DNA Isolation Kit, following the manufacturer's instructions with minor modifications described previously (Rinke et al. 2016). Libraries for shotgun metagenomic sequencing were prepared using the Nextera XT DNA Sample Preparation Kit (Illumina Inc., San Diego, CA, USA) following a previously described modified protocol designed for generating low DNA input libraries (Rinke et al. 2016). All libraries were sequenced with an Illumina NextSeq 500 platform 2× with 150 bp High Output v.1 run chemistry. Libraries were pooled on an indexed shared sequencing run, resulting in 1/37 of a run or ~3.2 Gbp per sample. The raw fastq read files were deposited on the Microscale Ocean webpage (http://microscaleocean.org/data/category/12-in-situ-chemotaxis-assay).

To characterize the composition of bacterial communities, 16S rRNA gene-based taxonomic profiles of the samples were generated with GraftM (http://geronimp.github.io/graftM) using the 16S rRNA package (4.39.2013_08_greengenes_97_otus.better_tree.gpkg). The pipeline was designed to identify reads encoding 16S rRNA genes based on HMMs and to assign taxonomic classifications by comparison against a reference taxonomy. A detailed feature description, user manual, and example runs are available on the GitHub wiki (https://github.com/geronimp/graftM/wiki). For the heatmap, the GraftM output was manually curated, whereby mitochondrial and chloroplast sequences were removed. Relative abundances were calculated and trimmed (>5% max) in the software environment R (www.r-project.org), and the data was displayed as a heat-map (pheatmap). Differences in 16S rRNA gene abundance

between samples (n = 4) were compared via ANOVA, using the Statistical Analysis of Metagenomic Profiles (STAMP) software(Parks et al. 2014).

In addition, a reference genome based taxonomic classification approach was employed using the bacterial genome collection in GTDB (gtdb.ecogenomic.org). Reads were aligned back with Bowtie2(Langmead and Salzberg 2012), BAM files were created and reads counted with SAMtools (Kelly et al. 2009). Taxonomy parsing and cross-reference of sequences was performed using MGKit (bitbucket.org/setsuna80/mgkit) and analysis performed in Python (www.python.org) and Pandas (pandas.pydata.org/) environments. Counts were grouped to the class level and relative abundances calculated. Taxonomic assignments that accounted for less than 5% of the total reads were filtered and a clustered heatmap produced with Seaborn (http://seaborn.pydata.org/index.html).

Contributions

Bennett Lambert (B.L.), Jean-Baptiste Raina (JB. R.), Justin Seymour (J.S.), and Roman Stocker (R.S.) designed research. B.L. and JB. R. carried out laboratory experiments. B.L. and Vicente Fernandez (V.F.) performed image analysis. B.L. developed the numerical model and analyzed model output. B.L., JB. R., & Nachshon Siboni (N.S.) carried out field deployments. JB. R. and Chris Rinke (C.R.) carried out molecular work. C.R., Francesco Rubino (F.R.), Gene Tyson (G.T.), and Phil Hugenholtz (P.H.) analyzed sequencing data. B.L., JB.R., J.S. & R.S. wrote the paper. All above reviewed the paper before submission.

Supplementary notes

Supplementary Note 1 | Cavity flow in a T-junction

Upon submersion, the ISCA experiences a transient fluid flow across the surface of the device. In order to understand how fluid motion may affect the performance of the device a simple model was implemented in COMSOL Multiphysics (5.1) using the Laminar Flow module. The model was of fluid flow over a solid surface with a T-junction placed 15 mm away from the edge, representing an ISCA port closest to the edge of the PDMS layer. The model captured the steady flow for three representative mean flow velocities (0.1 cm s^{-1}, 0.01 cm s^{-1}, and 0.001 cm s^{-1}). Streamlines were then plotted and the penetration depth of the recirculating cavity flow was determined. This penetration depth was then used as the distance over which the initial chemical and bacterial fields were smoothed. In all cases the cavity flow penetrated approximately 700 μm into the port (which corresponds approximately to the port diameter).

Supplementary Note 2 | Concentrations of compounds emitted from the ISCA

Marine Broth is a mixture of many compounds and the peptone present within the media is composed quite evenly of nearly 20 amino acids (BD Biosciences, 2015), which serve as major chemoattractants. Thus, when considering the concentration of chemoattractants, one must consider that the attractant field is divided among a great number of compounds.

For example, we consider serine, one of the 20 amino acids present in Marine Broth. In our experiment, we used 10% Marine Broth which contains 0.5 g/L of peptone. According to the manufacturer, peptone contains nearly even concentrations of the different amino acids, none of which are present in greater proportion than 17% of total amino acids (BD Biosciences, 2015). Serine (MW = 105.09 g/mol) has been used extensively in chemotaxis research(Mesibov and Adler 1972). If we consider a conservative scenario, where serine is present as 17% of the total

amino acid concentration, converting the mass concentration into molarity we obtain the following serine concentration:

$$0.5\ \text{g/L} \times \frac{1\ \text{mol}}{105.09\text{g}} \times 17\% = 808\ \mu\text{M} \quad (1)$$

Using this concentration in order to rescale the numerical model in the manuscript (e.g., Video S1, Fig. N1a) we obtain the concentration profile of serine over the depth of the well, in the port, and directly outside (Fig. N1b): directly at the port mouth the concentration of serine is ~120 μM and a distance of 1 mm from the port it is ~20 μM. For other dominant amino acids present in Marine Broth (Alanine, Arginine, Lysine) at lower concentrations (1.2%, 2.8%, 2.2% of free amino acid content in BD Bacto Peptone, respectively), the concentrations are even lower.

Thus the chemical signal described here is within the same order of magnitude as what may occur for DMSP (50 μM) and DMSO (780 μM) during phytoplankton cell lysis(Bucciarelli et al. 2013; Stocker and Seymour 2012) or ammonium as a result of zooplankton excretion(Jackson 1980).

Supplementary Note 3 | Bacterial growth in ISCA wells

To assess the potential for growth within ISCA wells, the growth kinetics of *Vibrio coralliilyticus* (Figure N2) exposed to the same nutrient concentration present in the ISCA wells during our tests were determined. The cells were initially grown under the same conditions used for laboratory experiments. The data indicate a lag time of longer than 90 minutes before measureable growth was observed. This confirms that the substantial increase in cell numbers

observed during our 60 minute deployment time were purely a consequence of chemotaxis, with an absence of any confounding effects of growth

Supplementary note figures

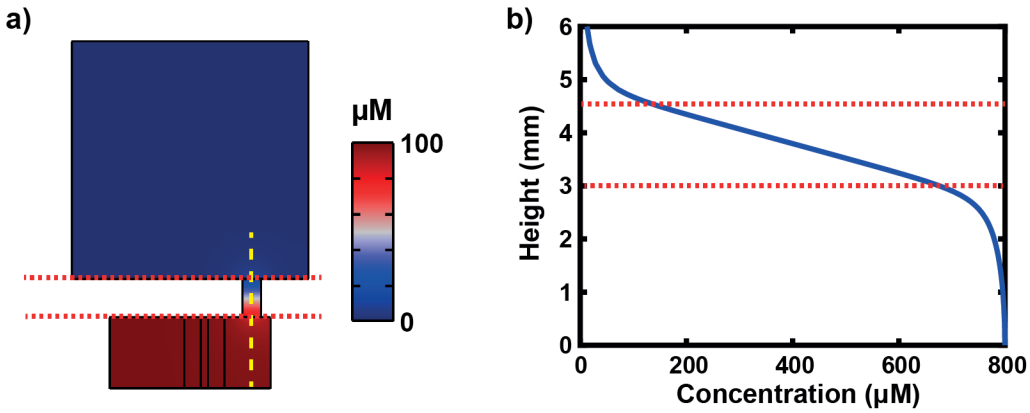

Figure N1 | a) Predicted concentration field of alpha-methylaspartate after 1 h. Cross-section of the COMSOL model domain for an individual ISCA well. Red dashed lines correspond to port entrance and exit and the yellow dashed line indicates the location of the cutline used to generate the data in panel (b). **b)** Rescaled concentration corresponding to serine.

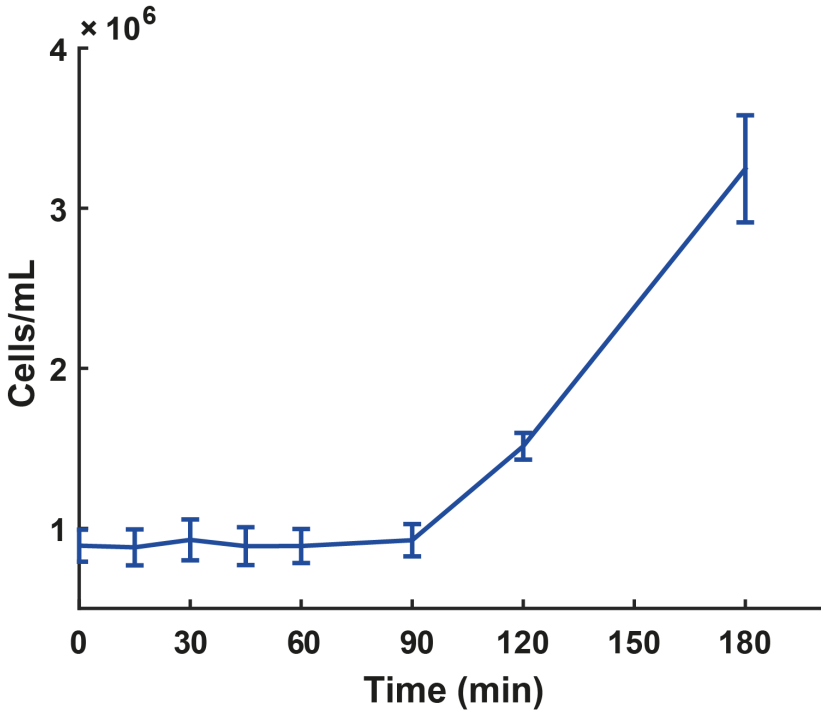

Figure N2 | Growth of *Vibrio coralliilyticus* upon exposure to 10% Marine Broth. A lag time of 90 minutes occurred before significant growth was observed. Error bars represent standard deviations (*n=4*).

Supplementary figures

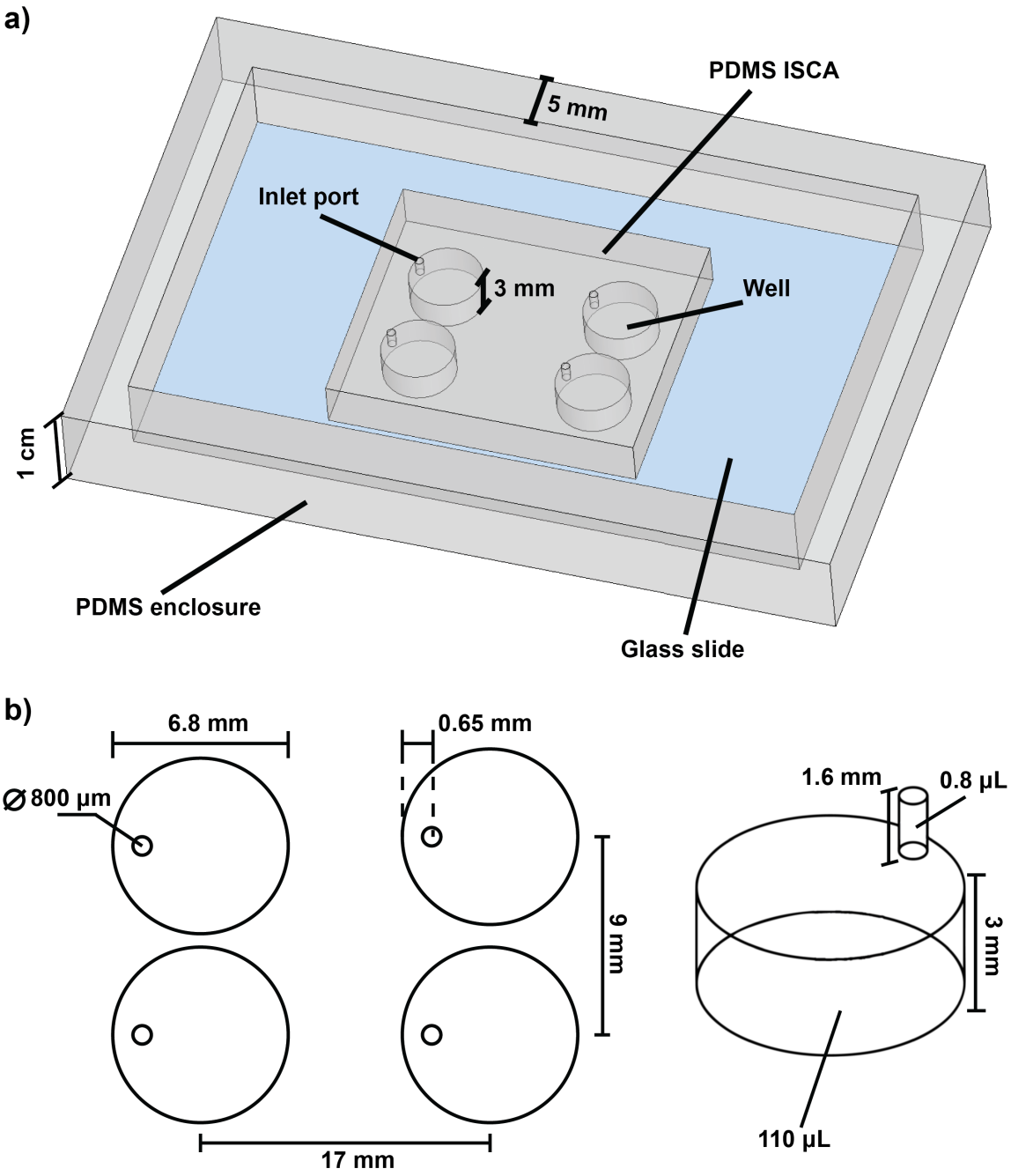

Supplementary Figure 1 | Schematic of the ISCA in the version used for laboratory experiments. (**a**) The laboratory microcosm consists of four wells centered on a microscope slide and surrounded by a PDMS enclosure. (**b**) Plan view schematic of ISCA wells in the laboratory version, and a perspective view of a single well, showing dimensions of the different elements and distances between wells. All dimensions were the same in the field-going ISCA. Computer-aided-design files for the microcosm mold may be found in **Supplementary File 1**.

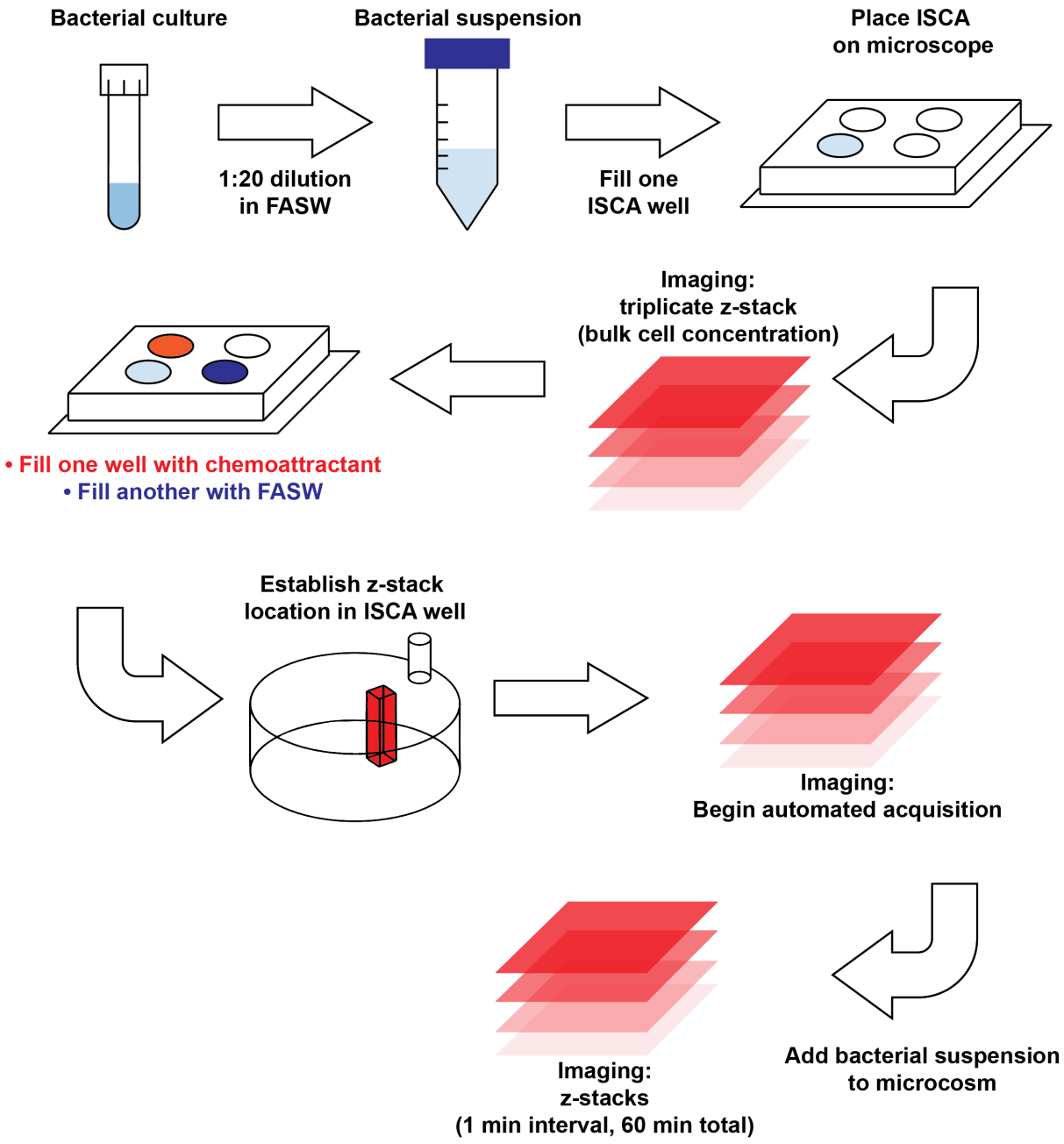

Supplementary Figure 2 | Flow diagram showing the experimental procedure used for laboratory ISCA experiments (see Methods). FASW = filtered artificial seawater. A z-stack denotes a series of images acquired over the depth of the well.

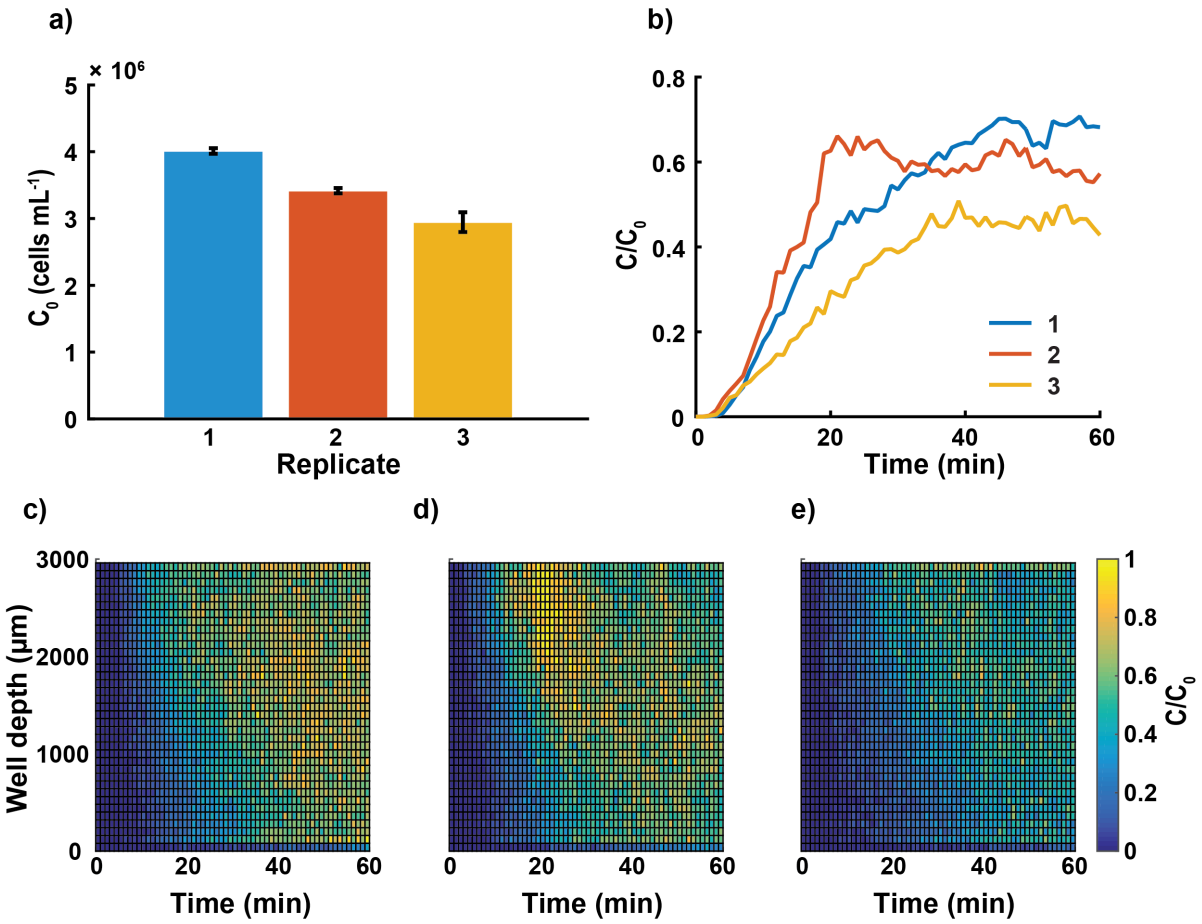

Supplementary Figure 3 | Response of *V. coralliilyticus* to 10% Marine Broth in laboratory experiments with the ISCA, quantified by imaging. (**a**) Cell concentration in the microcosm (C_0) (mean and standard deviation) (see Methods). Between separate trials the initial concentration in the microcosm was similar. (**b**) Time history of the mean concentration of cells over the imaging volume for ISCA wells containing 10% Marine Broth, normalized by the mean concentration of cells in the microcosm, C_0. Numbers and colors in panels (a) and (b) refer to replicate experiments. (**c-e**) The concentration of cells in the imaging volume, C, over the height of the well, Z, and over time, for wells containing 10% Marine Broth. The resolution is 80 µm in the depth and 1 min in time and the three panels denote replicate ISCA experiments, performed independently using different cultures (see **Supplementary Video 3**).

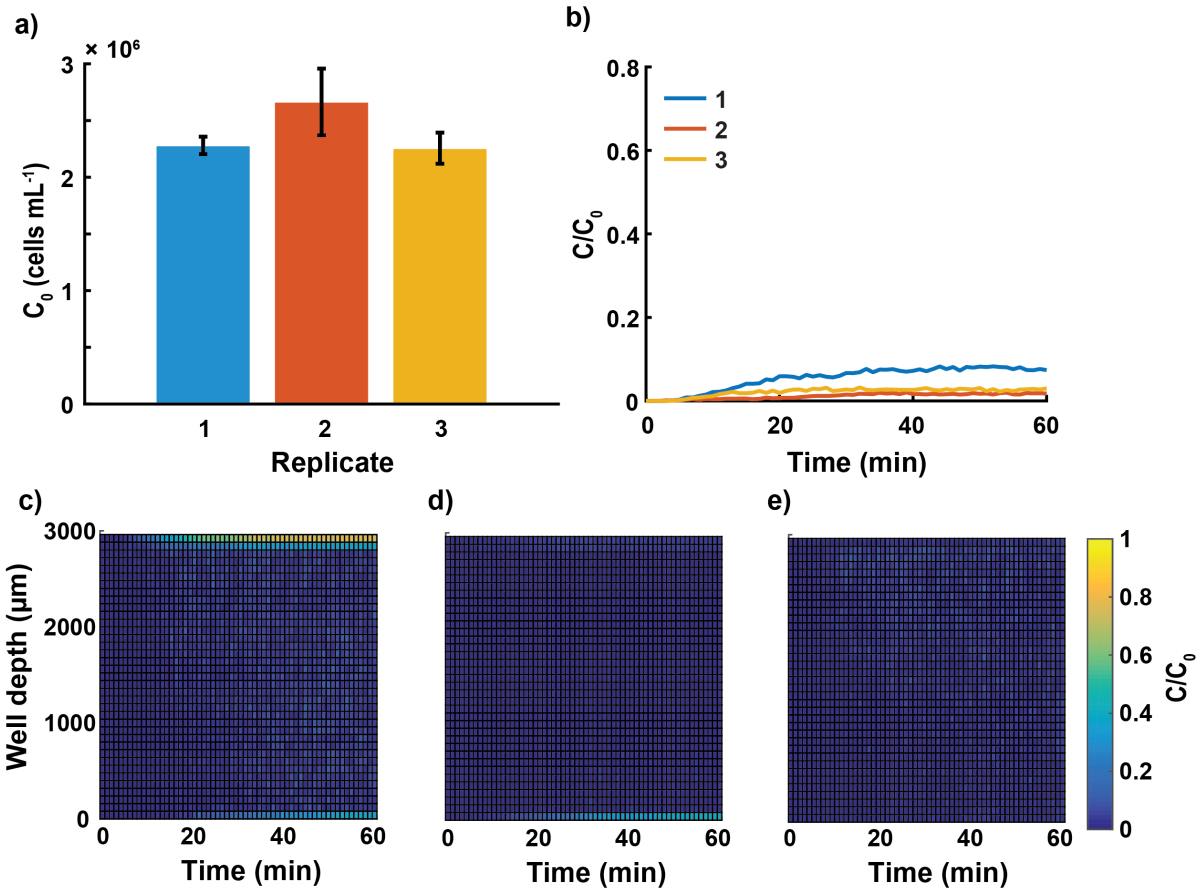

Supplementary Figure 4 | Response of *V. coralliilyticus* to filtered artificial seawater in laboratory experiments with the ISCA, quantified by imaging. (**a**) Cell concentration in the microcosm (C_0) (mean and standard deviation) (see Methods). Between separate trials the initial concentration in the microcosm was similar. (**b**) Time history of the mean concentration of cells over the imaging volume for ISCA wells containing filtered artificial seawater, normalized by the mean concentration of cells in the microcosm, C_0. Numbers and colors in panels (a) and (b) refer to replicate experiments. The resolution is 80 µm in the depth and 1 min in time. (**c-e**) The concentration of cells in the imaging volume, C, over the height of the well, Z, and over time, for wells containing filtered artificial seawater. The three panels denote replicate ISCA experiments, performed independently using different cultures (see **Supplementary Video 4**).

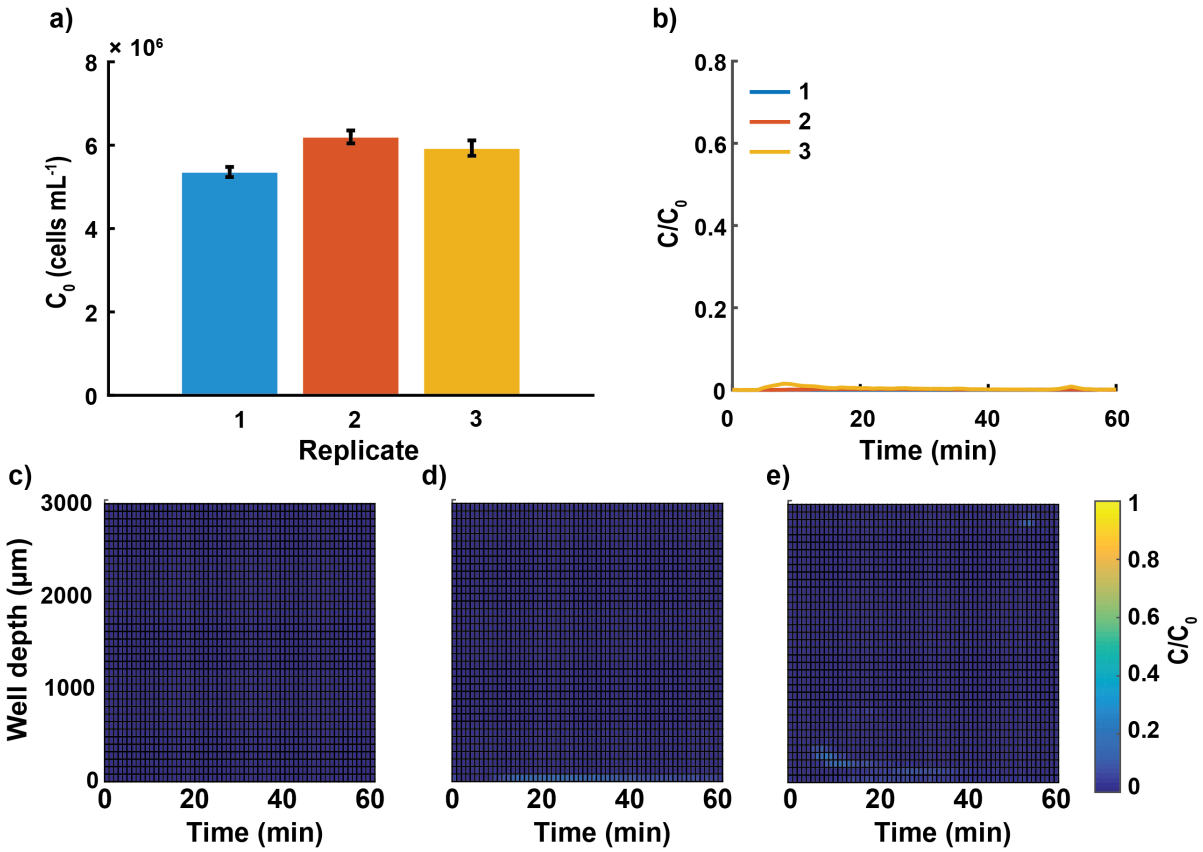

Supplementary Figure 5 | Response of *M. adhaerens* (ΔfliC) to filtered artificial seawater in laboratory experiments with the ISCA, quantified by imaging. (**a**) Cell concentration in the microcosm (C_0) (mean and standard deviation) (see Methods). Between separate trials the initial concentration in the microcosm was similar. (**b**) Time history of the mean concentration of cells over the imaging volume for ISCA wells containing filtered artificial seawater, normalized by the mean concentration of cells in the microcosm, C_0. Numbers and colors in panels (a) and (b) refer to replicate experiments. The resolution is 80 µm in the depth and 1 min in time. (**c-e**) The concentration of cells in the imaging volume, C, over the height of the well, Z, and over time, for wells containing filtered artificial seawater. The three panels denote replicate ISCA experiments, performed independently using different cultures.

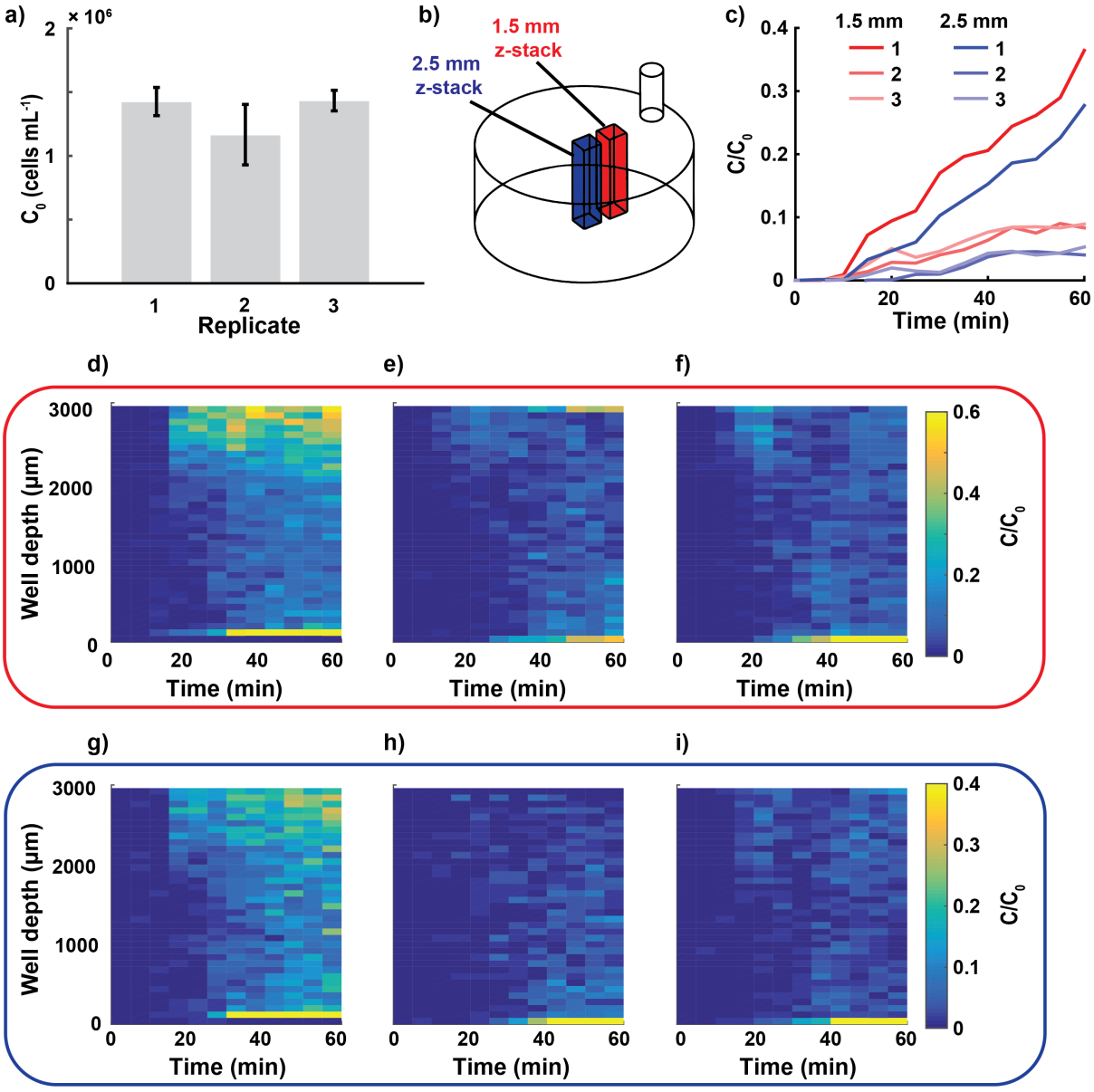

Supplementary Figure 6 | Response of *E. coli* to 100 µM α-methylaspartate in laboratory experiments with the ISCA, quantified by imaging. (**a**) Cell concentration in the microcosm (mean and standard deviation) (see Methods). Between separate trials the initial concentration in the microcosm was similar. (**b**) Schematic showing the two imaging volumes inside a well, color-coded red (1.5 mm from inlet port) and blue (2.5 mm from the inlet port) for ease of reference in subsequent panels. For each imaging volume, a time series of z-stacks of images over the depth of the well was acquired. (**c**) The mean concentration of cells over the imaging volume for ISCA wells containing 100 µM α-methylaspartate, normalized by the mean concentration of cells in the microcosm, C_0. Red and blue curves correspond to the two imaging locations in panel b, respectively, and shading intensity denotes different replicates. (**d-f**) The concentration of cells in the imaging volume, C, over the height of the well, Z, and over time, for wells containing 100 µM α-methylaspartate, acquired 1.5 mm from the inlet port (red imaging volume in panel b). (**g-i**) Same as panels (d-f), but acquired 2.5 mm from the inlet port (blue imaging volume in panel b). The resolution is 80 µm in the depth and 5 min in time.

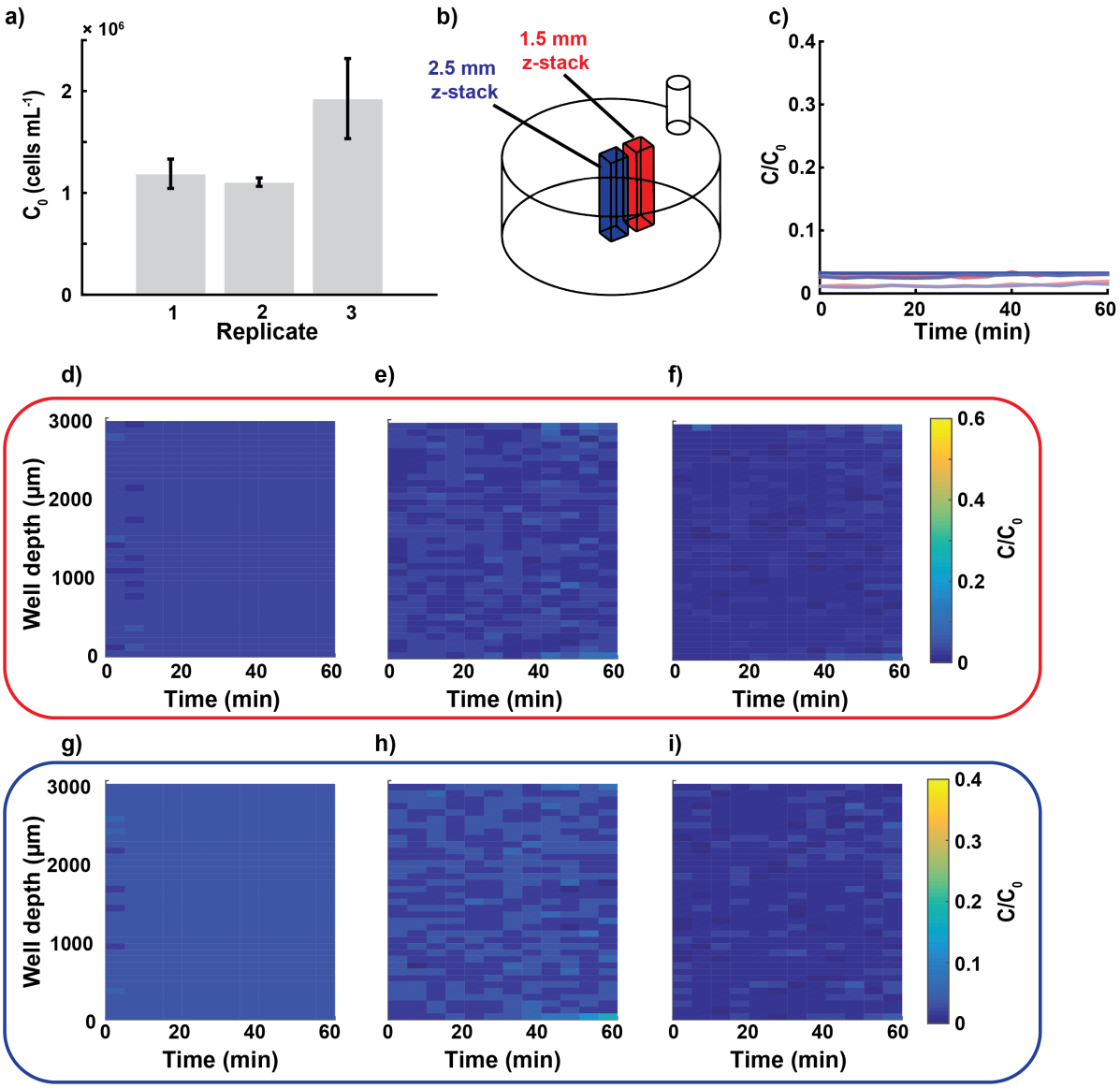

Supplementary Figure 7 | Response of *E. coli* to Motility Medium in laboratory experiments with the ISCA, quantified by imaging. (**a**) Cell concentration in the microcosm (mean and standard deviation) (see Methods). Between separate trials the initial concentration in the microcosm was similar. (**b**) Schematic showing the two imaging volumes inside a well, color-coded red (1.5 mm from inlet port) and blue (2.5 mm from the inlet port) for ease of reference in subsequent panels. For each imaging volume, a time series of z-stacks of images over the depth of the well was acquired. (**c**) The mean concentration of cells over the imaging volume for ISCA wells containing Motility Medium, normalized by the mean concentration of cells in the microcosm, C_0. Red and blue curves correspond to the two imaging locations in panel b, respectively, and shading intensity denotes different replicates. (**d-f**) The concentration of cells in the imaging volume, C, over the height of the well, Z, and over time, for wells containing Motility Medium acquired 1.5 mm from the inlet port (red imaging volume in panel b). (**g-i**) Same as panels (d-f), but acquired 2.5 mm from the inlet port (blue imaging volume in panel b). The resolution is 80 µm in the depth and 5 min in time.

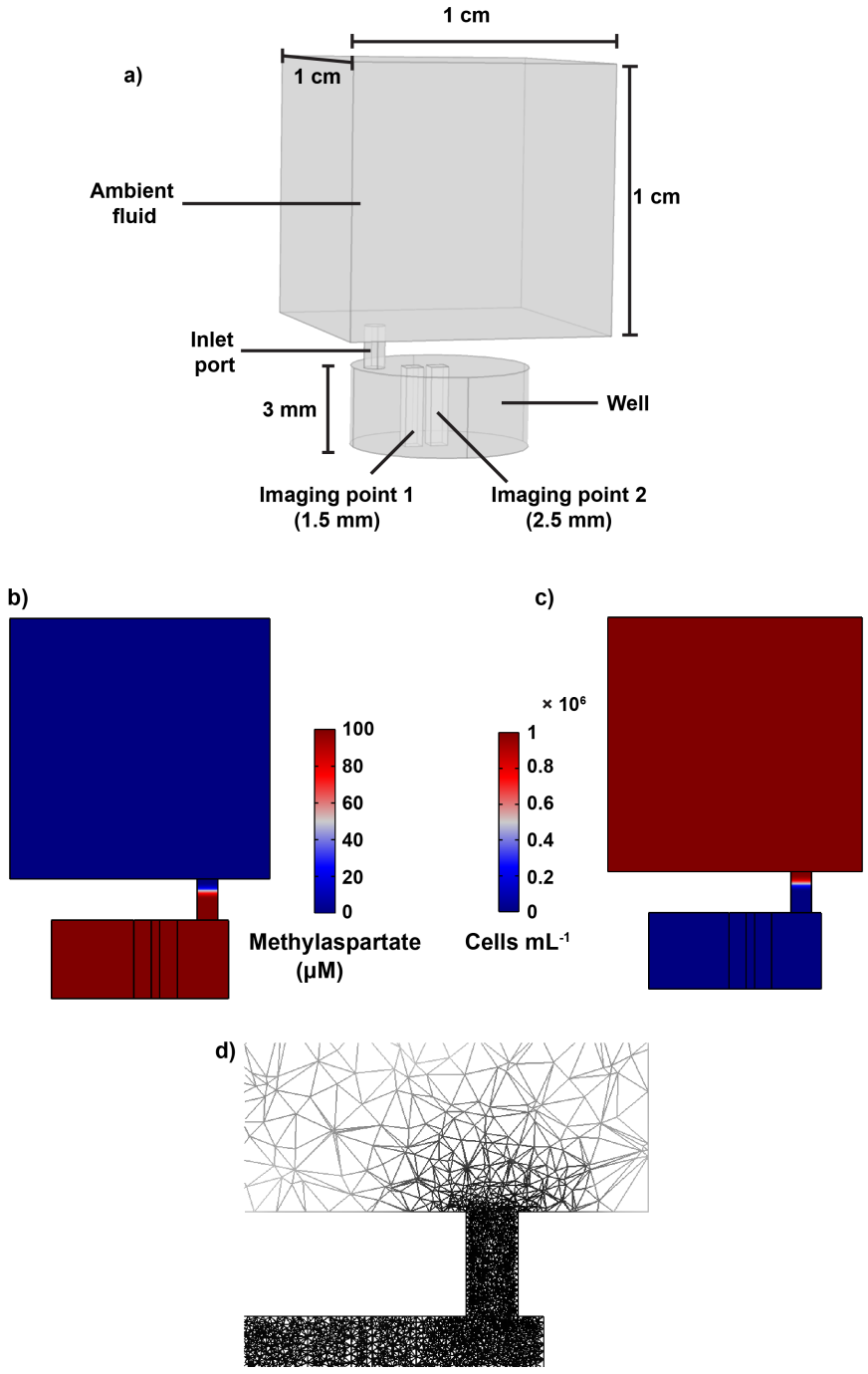

Supplementary Figure 8 | Geometry and initial conditions of the mathematical model of chemotaxis into ISCA wells. (a) The model consists of a single well with two observation regions inside the well (corresponding to the two imaging locations in Fig. S6b). The well is connected to a cube of fluid ('external fluid'; 1 ml volume) by an inlet port. (**b**) The concentration field is initialized as a smoothed step function, ramping down from 100 μM α-methylaspartate (in the well) to 0 μM over a distance of 700 μm from the top of the well into the inlet port. (**c**) The bacterial field is initialized as a smoothed step function, ramping down from 10^6 cells/ml (in the external fluid) to 0 cells/ml over a distance of 700 μm from the top of the inlet port downwards (see Methods). (**d**) Mesh applied to model domain in the COMSOL program used to solve the mathematical model, shown is the region surrounding the inlet port of the ISCA well (see Methods).

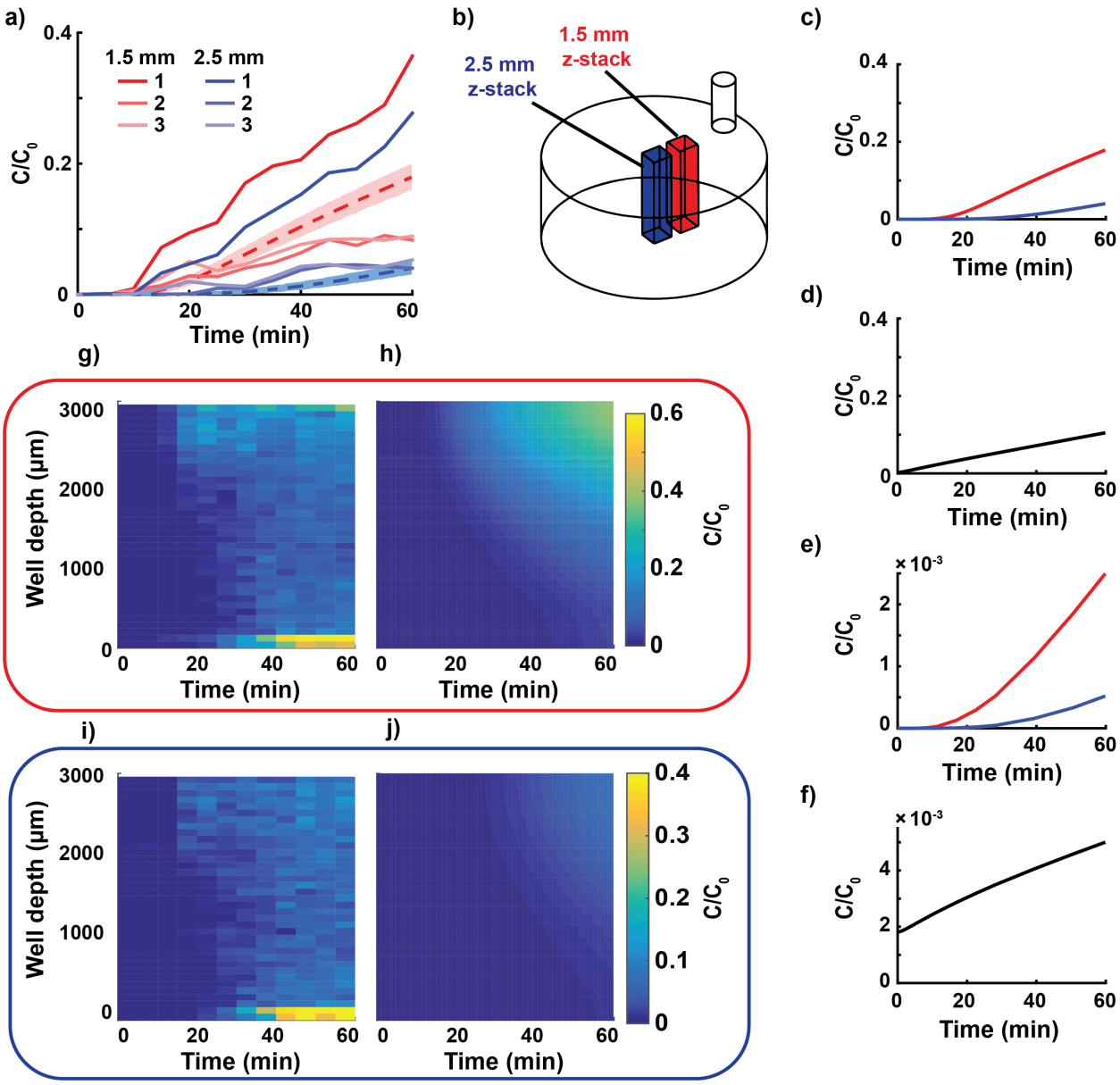
a)
1.5 mm
2.5 mm
1
2
3
C/C0
Time (min)
b)
1.5 mm
z-stack
2.5 mm
z-stack
c)
d)
e)
f)
g)
h)
i)
j)
Well depth (µm)
Time (min)
C/C0
×10-3

Supplementary Figure 9 | Accumulation of cells into ISCA wells predicted by the mathematical model, and comparison with experimental observations. (**a**) Mean concentration of cells in the imaging volume normalized by the mean concentration of cells in the microcosm, for the experiments (solid lines) and the model (dashed lines). For the model results, the shaded region represents the 95% confidence interval (see Methods). In all panels, red and blue correspond to the imaging volume located 1.5 mm and 2.5 mm from the inlet port, respectively. (**b**) Schematic of a well showing the two imaging volumes. (**c**) Time series of the concentration of bacteria in the two imaging volumes (color-coded as in panel b) predicted by the mathematical model. (**d**) Time series of the concentration of bacteria over the entire well predicted by the mathematical model. (**e**) Time series of the concentration of bacteria in the two imaging volumes (color-coded as in panel b) predicted by the mathematical model, in the absence of chemotaxis (i.e., random swimming). (**f**) Time series of the concentration of bacteria over the entire well predicted by the mathematical model, in the absence of chemotaxis (i.e., random swimming). (**g-h**) Concentration of *E. coli*, *C*, in the imaging volume, over the height of the well, Z, and over time, for wells containing 100 μM α-methylaspartate, acquired 1.5 mm from the inlet port (red imaging volume in panel b), from the experiments (g) and the model (h). (**i-j**) Same as panels (g-h), but acquired 2.5 mm from the inlet port (blue imaging volume in panel b). For experimental data the resolution is 80 μm in the depth and 5 min in time.

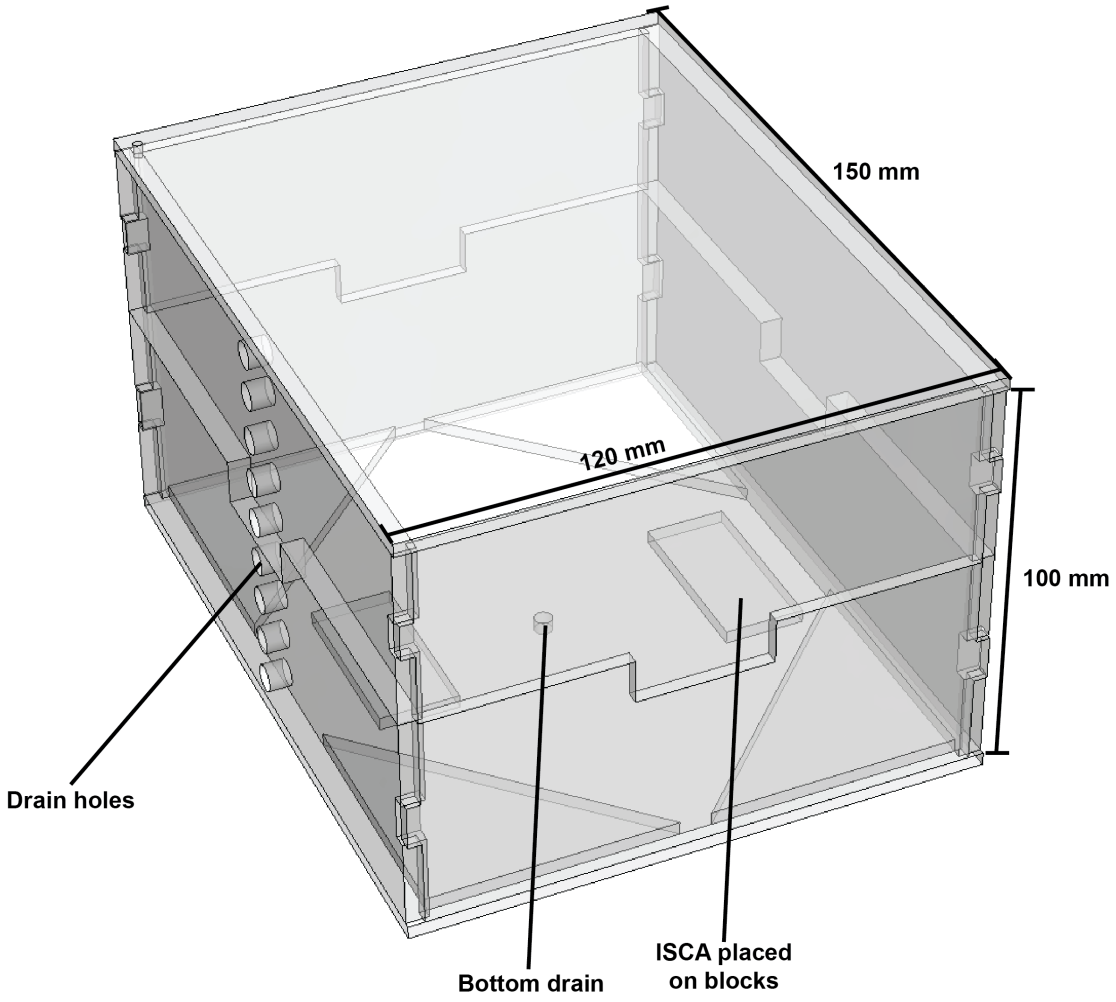

Supplementary Figure 10 | Field deployment enclosure for the ISCA. The ISCA is placed on blocks of height 6 mm on the bottom of the enclosure at the beginning of the experiment and secured using two fine strips of pressure sensitive tape (Scotch, 3M, USA). The enclosure is slowly immersed at the field site. The elevated placement of the ISCA allows the initial transient flow to subside by the time the ISCA comes in contact with the seawater, minimizing the effect of turbulent fluid motion. After the enclosure is completely filled with seawater, the bottom drain hole is sealed and the set-up left *in situ* for the duration of the experiment (typically, 1 h). The field deployment enclosure was built out of laser-cut acrylic (see Methods). Computer-aided-design files can be found in **Supplementary File 1**.

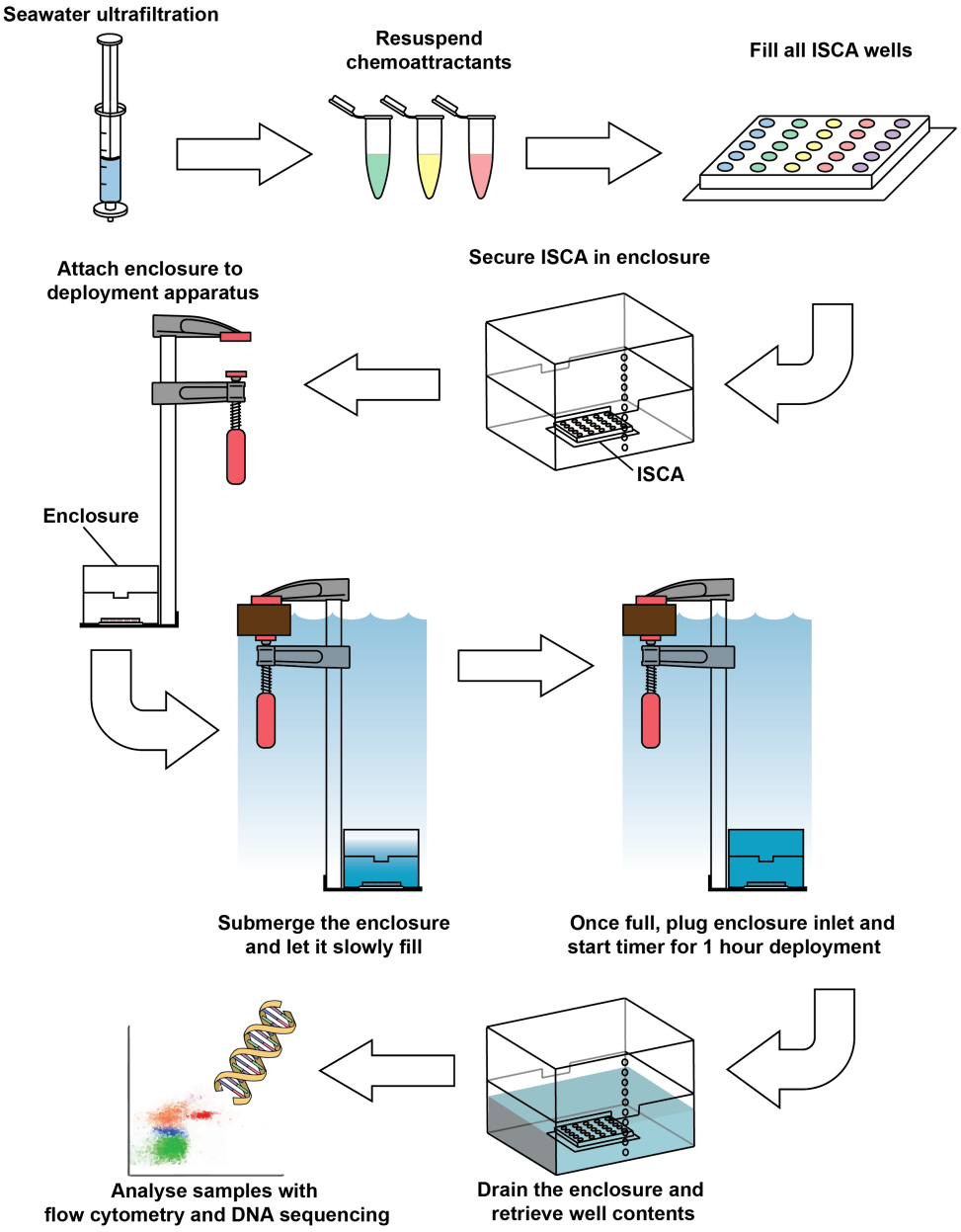

Supplementary Figure 11| Flow diagram showing the experimental procedure used for field deployment of the ISCA (see Methods).

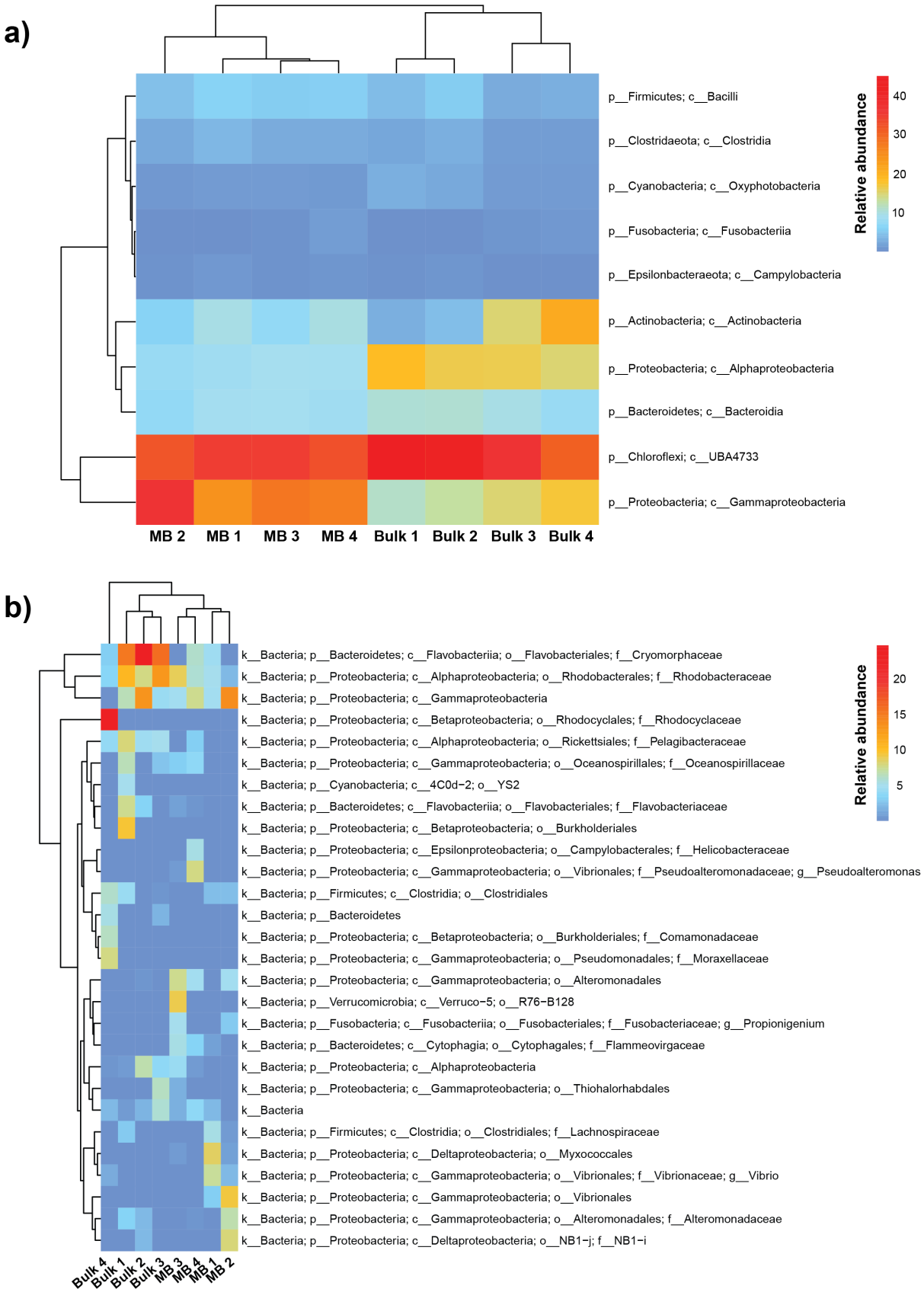
a)
p__Firmicutes; c__Bacilli
p__Clostridaeota; c__Clostridia
p__Cyanobacteria; c__Oxyphotobacteria
p__Fusobacteria; c__Fusobacteriia
p__Epsilonbacteraeota; c__Campylobacteria
p__Actinobacteria; c__Actinobacteria
p__Proteobacteria; c__Alphaproteobacteria
p__Bacteroidetes; c__Bacteroidia
p__Chloroflexi; c__UBA4733
p__Proteobacteria; c__Gammaproteobacteria
MB 2
MB 1
MB 3
MB 4
Bulk 1
Bulk 2
Bulk 3
Bulk 4
Relative abundance
40
30
20
10
b)
k__Bacteria; p__Bacteroidetes; c__Flavobacteriia; o__Flavobacteriales; f__Cryomorphaceae
k__Bacteria; p__Proteobacteria; c__Alphaproteobacteria; o__Rhodobacterales; f__Rhodobacteraceae
k__Bacteria; p__Proteobacteria; c__Gammaproteobacteria
k__Bacteria; p__Proteobacteria; c__Betaproteobacteria; o__Rhodocyclales; f__Rhodocyclaceae
k__Bacteria; p__Proteobacteria; c__Alphaproteobacteria; o__Rickettsiales; f__Pelagibacteraceae
k__Bacteria; p__Proteobacteria; c__Gammaproteobacteria; o__Oceanospirillales; f__Oceanospirillaceae
k__Bacteria; p__Cyanobacteria; c__4C0d−2; o__YS2
k__Bacteria; p__Bacteroidetes; c__Flavobacteriia; o__Flavobacteriales; f__Flavobacteriaceae
k__Bacteria; p__Proteobacteria; c__Betaproteobacteria; o__Burkholderiales
k__Bacteria; p__Proteobacteria; c__Epsilonproteobacteria; o__Campylobacterales; f__Helicobacteraceae
k__Bacteria; p__Proteobacteria; c__Gammaproteobacteria; o__Vibrionales; f__Pseudoalteromonadaceae; g__Pseudoalteromonas
k__Bacteria; p__Firmicutes; c__Clostridia; o__Clostridiales
k__Bacteria; p__Bacteroidetes
k__Bacteria; p__Proteobacteria; c__Betaproteobacteria; o__Burkholderiales; f__Comamonadaceae
k__Bacteria; p__Proteobacteria; c__Gammaproteobacteria; o__Pseudomonadales; f__Moraxellaceae
k__Bacteria; p__Proteobacteria; c__Gammaproteobacteria; o__Alteromonadales
k__Bacteria; p__Verrucomicrobia; c__Verruco−5; o__R76−B128
k__Bacteria; p__Fusobacteria; c__Fusobacteriia; o__Fusobacteriales; f__Fusobacteriaceae; g__Propionigenium
k__Bacteria; p__Bacteroidetes; c__Cytophagia; o__Cytophagales; f__Flammeovirgaceae
k__Bacteria; p__Proteobacteria; c__Alphaproteobacteria
k__Bacteria; p__Proteobacteria; c__Gammaproteobacteria; o__Thiohalorhabdales
k__Bacteria
k__Bacteria; p__Firmicutes; c__Clostridia; o__Clostridiales; f__Lachnospiraceae
k__Bacteria; p__Proteobacteria; c__Deltaproteobacteria; o__Myxococcales
k__Bacteria; p__Proteobacteria; c__Gammaproteobacteria; o__Vibrionales; f__Vibrionaceae; g__Vibrio
k__Bacteria; p__Proteobacteria; c__Gammaproteobacteria; o__Vibrionales
k__Bacteria; p__Proteobacteria; c__Gammaproteobacteria; o__Alteromonadales; f__Alteromonadaceae
k__Bacteria; p__Proteobacteria; c__Deltaproteobacteria; o__NB1−j; f__NB1−i
Bulk 4
Bulk 1
Bulk 2
Bulk 3
MB 3
MB 4
MB 1
MB 2
Relative abundance
20
15
10
5

Supplementary Figure 12 | Microbial community profiles obtained from ISCA field deployments. The different columns show 4 samples from the ambient seawater ('Bulk') and four samples from wells containing 10% Marine Broth ('MB'). The heatmaps show: (**a**) grouping at the class level using a reference genome based taxonomic classification approach (see Methods); (**b**) the relative abundance of operational taxonomic units (0–20%). Taxonomy was assigned based on 16S rRNA gene sequence detection of shotgun sequencing reads (see Methods) and the taxonomic assignment is provided down to the genus level if available, otherwise to the best available taxonomic rank.

Supplementary files

Files may be found on the associated USB storage device.

Supplementary File 1 | Computer aided design (CAD) file for the ISCA mold; CAD file for the laboratory ISCA microcosm; CAD file for the ISCA field deployment enclosure.

Supplementary File 2 | Mathematical model of chemotaxis into an ISCA well implemented in COMSOL.

Supplementary videos

Supplementary Video 1 | Evolution of the chemoattractant concentration field as it diffuses from the ISCA well, as predicted by the mathematical model.

Supplementary Video 2 | Accumulation of bacteria into an ISCA well predicted by the mathematical model.

Supplementary Video 3 | Fluorescently labeled *Vibrio coralliilyticus* cells at mid-depth in an ISCA well containing 10% Marine Broth.

Supplementary Video 4 | Fluorescently labeled *Vibrio coralliilyticus* cells at mid-depth in an ISCA well containing filtered artificial seawater.

Supplementary Video 5 | Example of cell enumeration through image analysis in laboratory ISCA experiments, for *Vibrio coralliilyticus.*

Supplementary Video 6 | Example of cell enumeration through image analysis in laboratory ISCA experiments, for *Escherichia coli.*

Supplementary Video 7 | Example of cell enumeration through image analysis in laboratory ISCA experiments, for *Marinobacter adhaerens.*

Chapter 4: An *in situ* millifluidic platform to study rapid microbial responses to resource encounter

Work presented in this chapter is in preparation for submission as "Bennett S. Lambert, Jean-Baptiste Raina, Donovan H. Parks, Nachshon Siboni, Lauren F. Messer, Vicente I. Fernandez, Sammy Frenk, Cameron J. Arnet, Christian Rinke, Francesco Rubino, Philip Hugenholtz, Gene W. Tyson, Justin R. Seymour, & Roman Stocker. An *in situ* millifluidic platform to study rapid microbial responses to resource encounter".

Introduction

Marine microorganisms inhabit a patchy environment, where encounters with nutrient sources of diverse composition can be intermittent and short-lived (Blackburn, Fenchel, and Mitchell 1998; Stocker and Seymour 2012). These microscale patches are for example derived from phytoplankton cells (Seymour et al. 2017; Smriga et al. 2016), zooplankton fecal pellets (Jefferson 2002), and other organic particles (Kiørboe et al. 2002), each representing nutrient rich hotspots that can persist from minutes to days (Blackburn, Fenchel, and Mitchell 1998; Newell, Lucas, and Linley 1981). Differences in the rate of encounter with and duration of exposure to resource hotspots strongly influences trophic strategies observed within the marine environment. Two extreme ends of the trophic-strategy spectrum are apparent: copiotrophs, which often exhibit behaviors to increase encounter and residence time in favorable microenvironments and possess the ability to rapidly uptake nutrients when they are encountered (Dang and Lovell 2016; Lauro et al. 2009); and oligotrophs, which rely on streamlined genomes (Giovannoni et al. 2005) and efficient resource usage (Roller and Schmidt 2015) to thrive on very low resource concentrations. Important factors in the relative fitness of these strategies are

the resource patch density and quality of the environment the organisms inhabit, the frequency with which they encounter these patches, and their ability to exploit short-lived and diverse substrates.

Many copiotrophs exhibit physiological and behavioral adaptations to life in heterogeneous landscapes. Marine copiotrophs possess large genomes containing a vast array of genes targeted at resource uptake and metabolism (Lauro et al. 2009). Together with this broad metabolic potential, they often leverage motility and chemotaxis – the ability to alter swimming behavior in response to a chemical gradient – to increase encounter and residence time within high nutrient microenvironments in the ocean. Chemotaxis and motility are known to play a central role in phytoplankton-bacteria interactions (Seymour et al. 2017), the colonization of particles (Kiørboe et al. 2002; Kiørboe and Jackson 2001), and microbial foraging (Yawata et al. 2014). In a cell's travels through the marine environment, each successive resource patch may have an entirely different chemical nature or duration. Ongoing efforts to characterize how microbial behavior impacts ecology at the microscale have highlighted the complexity of interactions between microbes within these chemical-rich microenvironments (Amin et al. 2015; Durham et al. 2015). However, a fundamental question surrounding life in such a patchy environment remains – how do marine microbes tune their physiology to cope with short-lived encounters with diverse resources?

Here we introduce the Millifluidic *In Situ* Enrichment (MISE), an instrument purpose-built to interrogate a microbial community's response to encounters with ephemeral microscale hotspots. The millifluidic design of the MISE circumvents many limitations of conventional transcriptomics sampling schemes, allowing rapid addition of both a chemical stimulus and RNA preservative. The MISE enables insight into rapid transcriptional responses of whole

communities to chemical stimuli *in situ*, opening a window into mechanisms leveraged by marine microorganisms to maximize access to critical resources. Combining this new *in situ* platform with digital droplet PCR reveals that microorganisms respond within minutes upon amendment with an organic substrate. The MISE represents a significant advance in *in situ* instrumentation developed to understand life at the microscale, and results presented here demonstrate its potential to interrogate the impact that microscale patchiness may have on larger-scale biogeochemical fluxes.

In order to test the MISE, we carried out field deployments using the algal osmolyte dimethylsulfoniopropionate (DMSP; 100 μM final concentration) as a chemical stimulus. DMSP plays a central role in the global sulfur cycle as a precursor to the climatically active gas dimethylsulfide (DMS) (Lovelock, Maggs, and Rasmussen 1972; Moran et al. 2011), as a key nutrient to marine microbes (Kiene, Linn, and Bruton 2000) and as a foraging cue for zooplankton and marine bacteria (Seymour, Simó, et al. 2010). Microbial processing of DMSP serves as a particularly interesting test case, as there are two competing pathways by which microorganisms degrade the compound – demethylation and cleavage (Moran et al. 2011). The process of demethylation involves breakdown of DMSP to methylmercaptopropionate and 5-methyl-tetrahydrofolate through the *dmdA* protein and results in cells retaining both carbon and sulfur from the DMSP molecule to sustain their growth. Cleavage is carried out by a variety of enzymes, collectively termed *ddd*- (DMSP-dependent DMS production), and breaks DMSP into DMS and either acrylate or 3-hydroxypropionate and leads to incorporation of carbon from the initial DMSP molecule. A layer of complexity is added to this story in that some marine bacteria house genes encoding both pathways within their genome (Moran et al. 2011). The environmental factors causing bacteria to favor one pathway over another are still poorly

understood, but the current hypothesis put forth by Kiene and co-authors suggests that cells with rapid growth rates and accordingly high sulfur demand will favor the demethylation pathway in an attempt to fulfill their sulfur needs (Kiene, Linn, and Bruton 2000). In the alternative scenario, water column concentrations of sulfur are high and slow growing cells can easily obtain sulfur via other means and will favor the cleavage pathway to use DMSP as a carbon source (Kiene, Linn, and Bruton 2000). However, the plot continues to thicken, with new proteins involved in DMSP degradation and synthesis also being identified in marine bacteria (Sun et al. 2016; Todd et al. 2011; Curson et al. 2017). One of our major goals for the MISE was to incorporate unique design features to test competing ideas about resource preference and use within patches in the aquatic environment and enable researchers to examine how that preference shifts with environmental conditions and throughout the lifetime of microscale nutrient hotspots.

Results

In order to interrogate patch-scale processes in a controlled manner, we designed and constructed the Millifluidic *In Situ* Enrichment (MISE; Fig. 1a). The MISE consists of a series of 18 microcosms (wells) organized in three rows (Fig. 1a), which fill with seawater from the site upon deployment. These wells are then automatically sealed, encapsulating natural microbial communities. Following an automated routine (Fig. 1b, see Methods), the MISE injects simultaneously a chemical stimulus into nine treatment wells (arranged on 3 rows, $n = 3$ replicate treatments per row) and ultrafiltered seawater from the site into nine control wells (3 rows, $n = 3$ replicate treatments per row). Following an incubation period, wells within a row are injected with RNA preservative at predetermined times (resulting in sample preservation at three different time points; see Methods, Fig. 1b-c). This yields a time series comparing microbial community transcription in response to a chemical stimulus to that of a control.

The MISE has several key features that enable investigation of rapid timescale phenomena. First, the amendment and preservation of samples occurs *in situ*. This reduces the potential for confounding stressors (*e.g.*, changes in light or temperature) that may induce rapid shifts in expression (Morimoto 1993; Pfannschmidt, Nilsson, and Allen 1999) and make data interpretation challenging. Second, the chemical additives are mixed at a consistent and rapid timescale (approximately 6 s; Fig. 2), exposing organisms within the microcosms to the same condition nearly simultaneously. The conventional approach employed in marine metatranscriptomics involves filtering samples prior to preservation, which often takes as long as 20-30 minutes (Poretsky Rachel et al. 2009; Vila-Costa et al. 2010), defeating any attempt to obtain finely-resolved time series or access small volumes. In the MISE, the RNA preservative is mixed rapidly throughout the microcosm volume as a result of the small dimensions of this volume, ensuring a well-resolved snapshot of community transcription at that time. This significantly accelerated timescale is achieved through a delicate balance between turbulent mixing and diffusion-driven mixing, which is a direct result of the physics of mixing at small scales (Purcell 1977). This is of fundamental importance when interrogating processes that occur on the order of minutes.

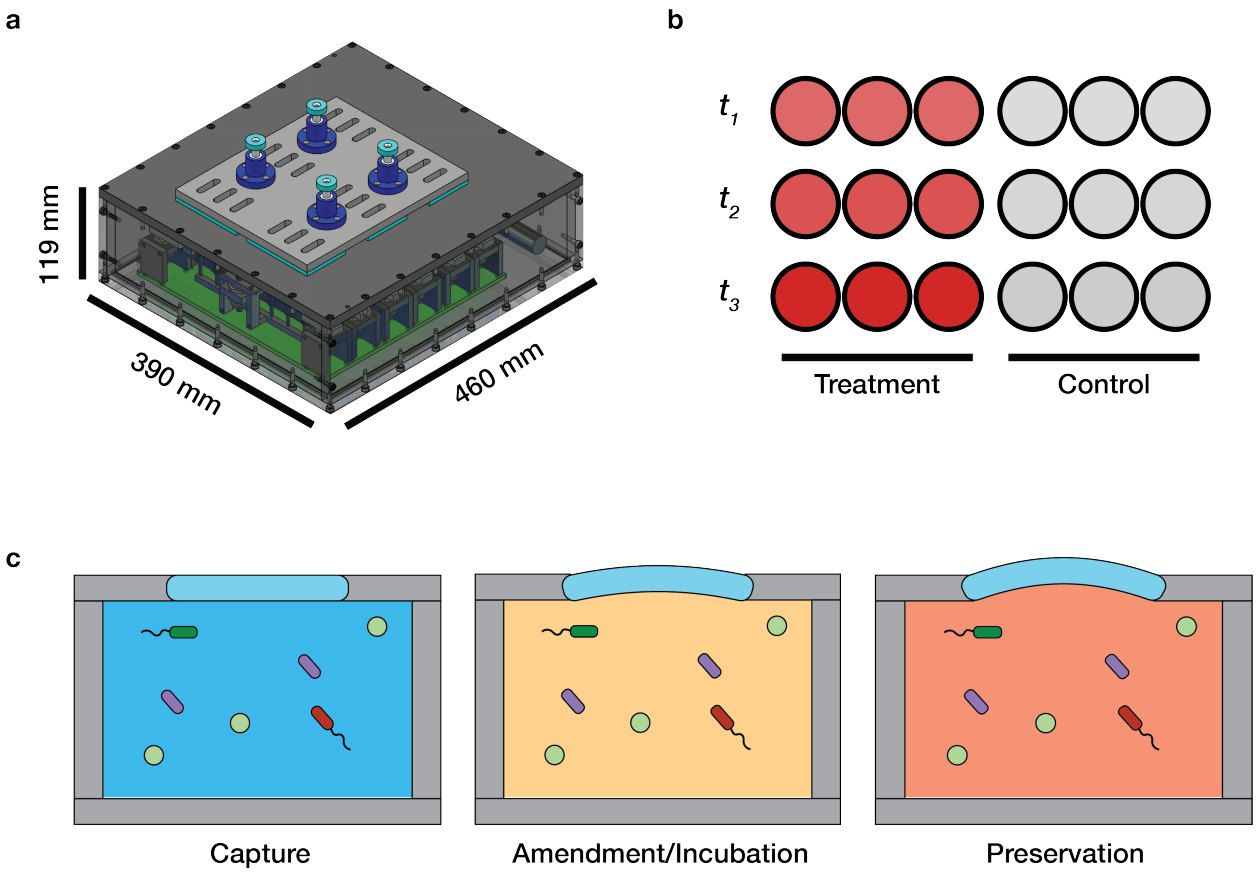

Fig. 1 | (a) The Millifluidic *In Situ* Enrichment (MISE). Syringes are driven by pneumatic actuators to generate rapid amendment and preservation of samples under *in situ* light and temperature conditions. **(b)** Schematic layout of the MISE microcosms. Each row corresponds to a time point (t_1-t_3) within the time series of RNA preservation. Measurements are obtained in triplicate for treatment and control. **(c)** The automated routine of the MISE. The microbial community is captured *in situ* in enclosed microcosms and then subjected to a chemical amendment or filtered seawater control. Wells are incubated for a predetermined period until RNA is preserved via injection of a mixture of Trizol and ProtectRNA.

An essential element in the MISE's performance is the formation of a tight seal around each well, allowing each one to act as an isolated microcosm. To ensure that there was no cross-contamination or leakage from wells, experiments were carried out with a fluorescent dye in a seawater mesocosm (see Methods). During these tests there was no observable leakage from MISE wells and no evidence of cross-contamination on timescales of $>$ 1 hr. These simple tests

provided assurance that the final concentrations of chemical treatments and RNA preservative that were injected into each well were accurate and reproducible between MISE deployments.

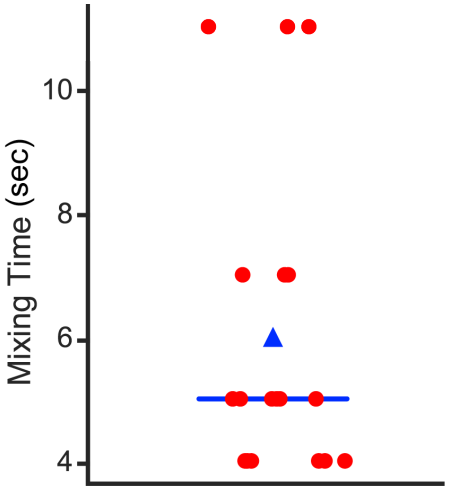

Fig. 2 | Mixing time of RNA preservative with the contents of the MISE wells. Mixing time was determined from video recordings of field deployments (n = 18 wells; see Methods) as the time for RNA preservative to transit the MISE well. Mean mixing time was 6 ± 2.52 s (blue triangle) with a median of 5 s (blue line). Mixing (quenching of RNA activity) is rapid in comparison with the timescale of experiments (typically on the order of minutes). Data points are staggered in the horizontal axis for clarity.

To characterize rapid transcriptional responses carried out by the microbial community upon exposure to DMSP, we coupled digital droplet polymerase chain reaction (ddPCR; see Methods) focused on select genes related to DMSP metabolism with MISE deployments. The MISE deployments yielded preserved community RNA at 10, 20, and 30 minutes following DMSP amendment. After samples were retrieved, RNA was extracted, cDNA was synthesized, and ddPCR was carried out targeting *dddP* (a cleavage protein) and *dmdA* (a demethylation protein; see Methods). Preliminary analysis revealed that marine microorganisms up-regulated the *dddP*

gene following DMSP amendment, while *dmdA* transcription was unaltered relative to the control (Fig 3a).

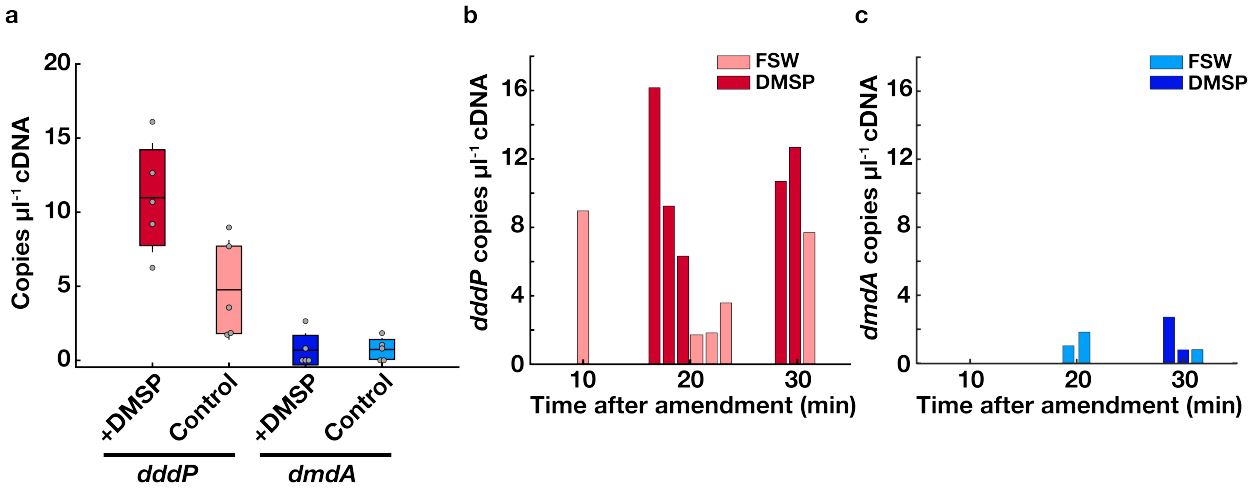

Fig. 3 | Expression of DMSP degradation genes determined by digital PCR. Following RNA extraction and cDNA synthesis (see Methods), ddPCR was carried out targeting the *dddP* and *dmdA* genes. The resulting copy number was normalized by the volume of input cDNA. Upon amendment with DMSP in the MISE device, the microbial community present at the deployment site increased expression of *dddP* relative to the control. *dmdA* expression was unaltered relative to the control at the timescales selected for this study. **(a)** Binned expression by treatment from the MISE time series (10, 20 and 30 minutes post amendment). Grey dots represent individual replicates within the MISE. In each boxplot, the center line represents the mean of replicates, the box extremities represent standard error of the mean, and whiskers represent one standard deviation. **(b)** Expression of *dddP* at each time point within the time series, where data is available. **(c)** Expression of *dmdA* at each time point within the time series, where data is available. In both **b, c** time points with expression levels of 0 copies μl^{-1} cDNA were not plotted. There are an equal number of measurements for both *dddP* and *dmdA*.

The binned results (Fig. 3a) indicate up-regulation of *dddP* relative to the filtered seawater control during the experiment. In contrast, there is no observable shift in *dmdA* expression level. The higher expression level of *dddP* in the control compared to *dmdA* is consistent with the higher copy number present in DNA extracted from the field site (781 copies μl^{-1} *dddP* vs 114 copies μl^{-1} *dmdA*; see Methods). At the time of this writing, the ddPCR analysis is still ongoing and data points are currently missing for the chemical treatment at 10 minutes post-amendment

(Fig. 3b-c). However, from the data available for *dddP* expression (Fig. 3b) no significant difference is apparent between *dddP* expression at 20 and 30 minutes post-amendment. This suggests that up-regulation of *dddP* might occur at timescales shorter than 20 minutes.

Discussion

The MISE was purpose-built to examine transcriptional responses of aquatic microbial communities to resource encounter at relevant patch timescales and several design elements of the MISE are essential towards that end. The injection system operated well during deployments in both a seawater mesocosm and the field site. The rapid mixing timescale of approximately 6 seconds easily enables time series with intervals of as little as 5 minutes. Together with the firm seal provided by the well layers of the instrument, the MISE enables researchers to extend the boundaries of our knowledge concerning the strategies that microbes employ to navigate life in a fluctuating environment. For copiotrophic cells maneuvering through the chemically heterogeneous landscape present at the ocean's microscale, the lifetime of a single patch may be a timescale of fundamental importance and with the MISE we are closing in on the ability to interrogate these processes directly.

To demonstrate the MISE's capabilities, we deployed it in coastal waters with DMSP as a chemical treatment. The up-regulation of the DMSP lyase *dddP* during this deployment points to two intriguing possible explanations: either the hypothesis put forth by Kiene and co-authors holds true and these cells have a greater demand for carbon relative to sulfur and thus favor use of the lyase, or the lyase is upregulated rapidly because it is a small protein (189 amino acids vs. 369 for *dmdA*) that the cell can generate on timescales relevant to a single patch encounter. These explanations are not mutually exclusive, and in this case we cannot rule out one or the other. However, it is likely that the community has an overabundance of sulfur available due to

the coastal nature of the site, providing the conditions necessary for the hypothesis of Kiene and co-authors (Kiene, Linn, and Bruton 2000) to hold true.

The time series in the transcription response provided by MISE deployments will enable researchers to investigate questions beyond simple up- or down-regulation, including transcriptional cascades. The ddPCR analysis for the deployment with DMSP is still in progress, however from the available data it appears that microbes may up-regulate *dddP* on a timescale less than 20 min. Up-regulation of key genes, such as the DMSP lyase on these timescales indicates that a portion of the microbial community may be adapted to rapid shifts in metabolism upon encounter with resources. Although 20 minutes may be too long to exploit a patch resulting from a lysis event (Jackson 2012), it is conceivable that cells maintain close physical proximity to phytoplankton over significantly longer periods. Further analysis is needed to examine the identity and metabolic repertoire of responsive microbes, but my initial hypothesis is that responsive cells will be motile copiotrophs with large genomes. As these cells explore the water column, their capability to exploit a vast array of substrates (Lauro et al. 2009), combined with a strategy of rapidly shifting their transcriptome would likely enable them to encounter and exploit diverse resource patches.

Studies comparing the regulatory cascades of marine microbes from diverse environments to that of model microorganisms present an exciting opportunity to look for commonalities between regulatory systems leveraged in the microbial world. Further analysis is required with the samples presented within this thesis to thoroughly examine the time series data. While there are many scientific avenues to explore, the simple experiment presented here provides a proof of concept that the MISE can interrogate the shifts in gene expression occurring upon exposure to nutrient upshifts.

MISE operation and recommendations

The MISE performed well during deployments at the coastal site. However, through multiple deployments we observed several potential improvements that would enhance the precision, ease-of-use, and safety of the instrument. (*i*) In terms of precision, the aluminum mechanisms present in the device were robust and more than able to withstand deployment, but we found that the nuts fixing the linear actuators were sensitive to vibration and prone to loosening. This presents not only a technical issue, but also a matter of safety, as these nuts directly affect the alignment of the syringes within the housing and could lead to accidental discharge of Trizol into the instrument housing. This issue can be easily overcome through the use of thread-locker. (*ii*) Another issue related to the linear actuators was their limited lifetime. Through a series of deployments, we discovered that the performance of individual linear actuators degraded rapidly in a random manner. During development, we constructed custom circuitry from FR-1 and milled circuits using a desktop CNC mill. This allowed us to freely and rapidly modify circuit layouts, but the finished circuits were not as robust as etched printed circuit boards. It is therefore our recommendation that future construction makes use of etched printed circuit boards instead. (*iii*) Lastly, there exists a need for additional safety precautions to be engineered into the instrument. An array of pressurized syringes, some containing toxic compounds, calls for dedicated safety measures, both through rigorous adherence to a thorough protocol and through redesign of instrument elements to allow for unobstructed handling of syringes. To facilitate syringe handling and the operation of the syringe banks, the MISE lid containing the septa should be transparent. The opaque nature of the prototype presented here did not easily allow identification of potential misalignment of syringe needles with their through-holes. Another element that could improve needle alignment would be alteration of the syringe through-hole in the MISE lid. In the current design, the through-hole is simply cylindrical and if the needle is

misaligned, it will bend over upon placement of the lid, which can lead to discharge of toxic and highly corrosive compounds into the MISE housing. Future design should implement conical through-holes that will guide the needles and limit risks of bending and accidental discharge. The instrument as presented here should be considered a prototype and future work should be carried out with an eye for improving user safety during deployment.

Conclusions and outlook

To understand microbial life at the microscale requires new tools and techniques in the microbial ecologist's toolkit. Here we introduced the Millifluidic *In Situ* Enrichment, a purpose-built instrument to study links between life in a fluctuating environment and the physiology of marine microbes. Using DMSP as a test case, we demonstrated the MISE's capability to manipulate microbial communities in the natural environment and to preserve RNA reliably during deployment in the field. Leveraging digital droplet PCR, we observed that a coastal marine community up-regulated the DMSP-lyase *dddP* on the order of tens of minutes in response to encounter with DMSP. As improved molecular techniques reduce the material required for analysis, an exciting future avenue is coupling low-input metatranscriptomics with MISE deployments for a more holistic understanding of microbial strategies to cope with resource fluctuation.

Methods

Construction of the Millifluidic In Situ Enrichment

The exterior housing and chambers of the MISE were constructed out of CNC-milled polyvinyl chloride (PVC). Briefly, a waterproof housing was constructed by assembling milled PVC, extrusion welding the housing seams, and sealing interior edges with silicone. The PVC faceplate compressed an O-ring (Kubo Tech AG) when fastened into place, providing a

waterproof seal. Four inlet ports were milled into the housing for cable routing and actuator placement: a push-button to begin the experiment, a push-button acting as a safety stop, and two cable ports to route the servo (D-845WP; HiTec RCD, USA) logic and power cables. Each port was waterproofed with silicone sealant after component placement or cable routing. Punched silicone rubber inserts (Food grade silicone, 3/16" thickness, 20 mm diameter; McMaster Carr, USA) were placed in the PVC faceplate, providing a sacrificial self-healing septum for the syringes to pierce during experiments. The high-torque servos were mounted on the faceplate and a Teflon attachment used to reduce friction between the top well layer and the servo arm during the initial phase of experiments. The bottom well layers (Fig. 4) were fastened in place on top of the faceplate, further compressing the silicone inserts. Prior to experiments, two thin silicone layers (0.032" thickness; Stockwell Elastomerics Inc., USA) were attached to the top well layer (Fig. 5) and the assembled layer was placed on guide rails with the spring assembly primed to create compressive force.

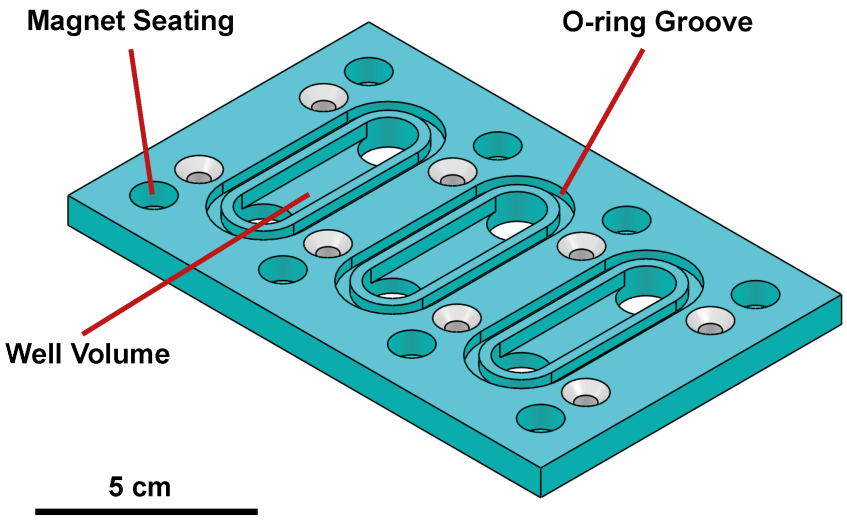

Fig. 4 | The lower well layer of the MISE. The layer contains openings where 2 kg pull neodymium magnets are press fit. Countersunk openings allow the lower layer to be fastened to the MISE housing. O-rings seated in a CNC milled groove provide a leak-proof seal surrounding each microcosm. Each unit contains three wells, and six units are used in one MISE device.

The interior mechanical structures were fabricated from aluminum (Fig. 6-8). Linear actuators (SMC Corporation, Switzerland) and 500 µL luer lock syringes (ILS syringes, Germany) were housed within the aluminum structure, together forming the basis of the injection system. The linear actuators were connected to a solenoid valve manifold (SMC Corporation, Switzerland) via one-touch fittings (Festo, Switzerland) and semi-rigid tubing (Festo, Switzerland). Pressurized CO_2 was supplied to the manifold through a stabilizer (0–200 psi; Palmer Pursuit Shop, USA) connected to an 1800 psi CO_2 bottle (20 oz. CO_2 tank; Palmer Pursuit Shop, USA).

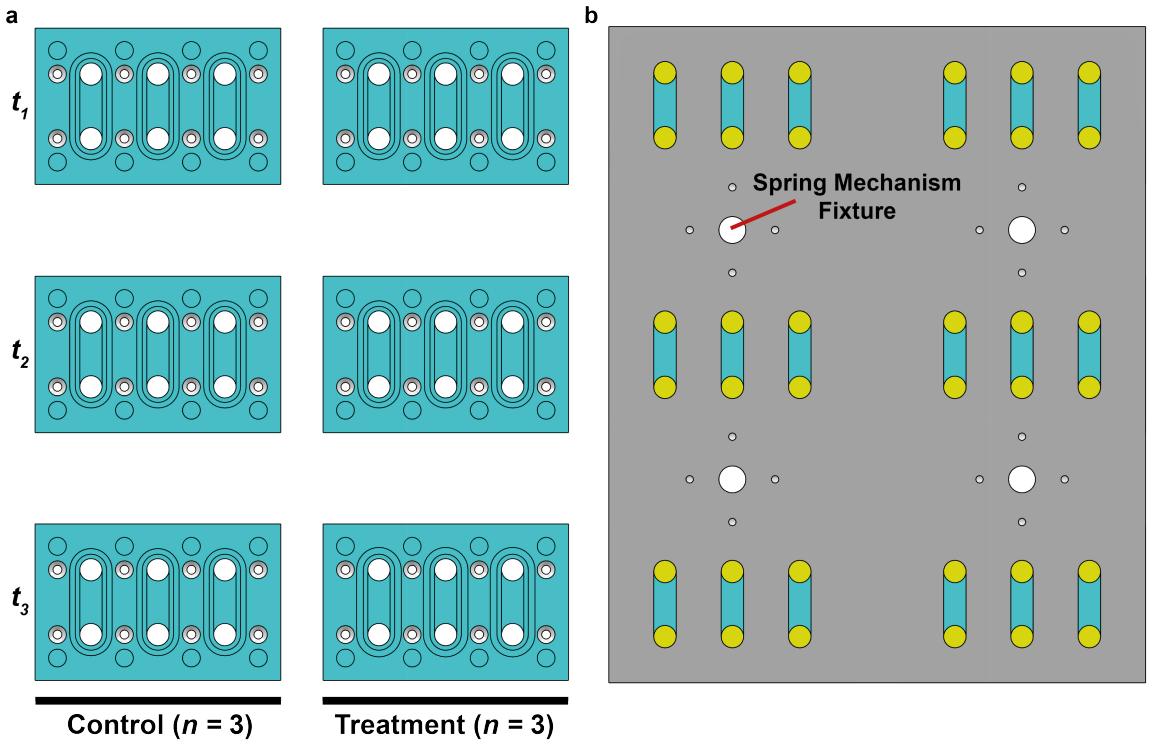

Fig. 5 | The well layer layout of the MISE. (**a**) Lower well layer sections are separated according to treatment vs. control and time point within the time series (t_1-t_3). (**b**) The upper well layer consists of a single milled piece of PVC with several added elements. Flexible silicone sheeting is placed between the upper and lower layers and acts as a displaceable membrane during injection. The four spring mechanisms generate compression upon activation and are fixed on the upper well layer.

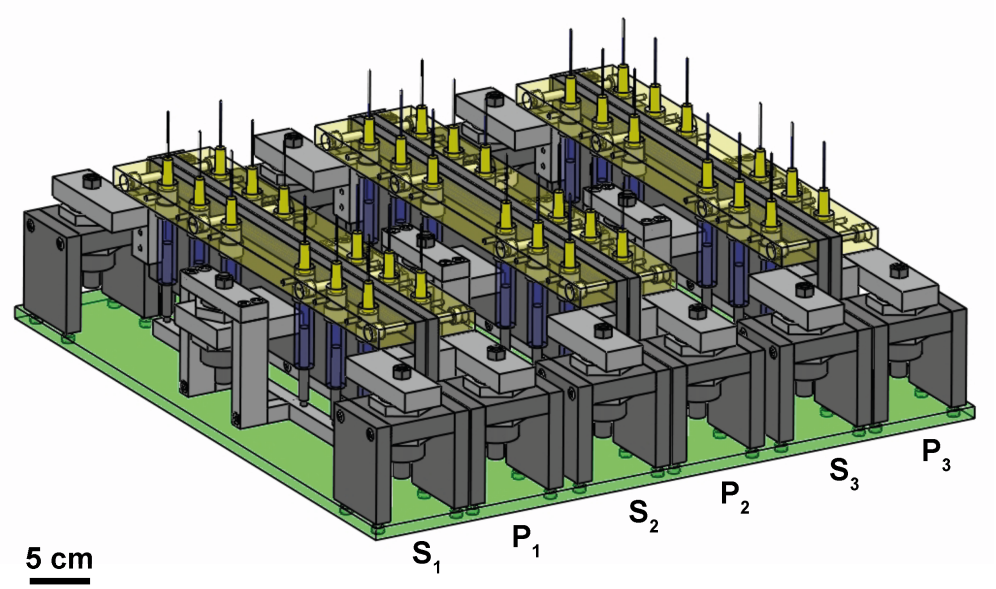

Fig. 6 | The chemical delivery system of the MISE. The system consists of six independent syringe banks (see Fig. 7). Stimulus banks (S_1-S_3) deliver either chemical treatment or filtered seawater control and preservative banks (P_1-P_3) deliver the Trizol and ProtectRNA mixture.

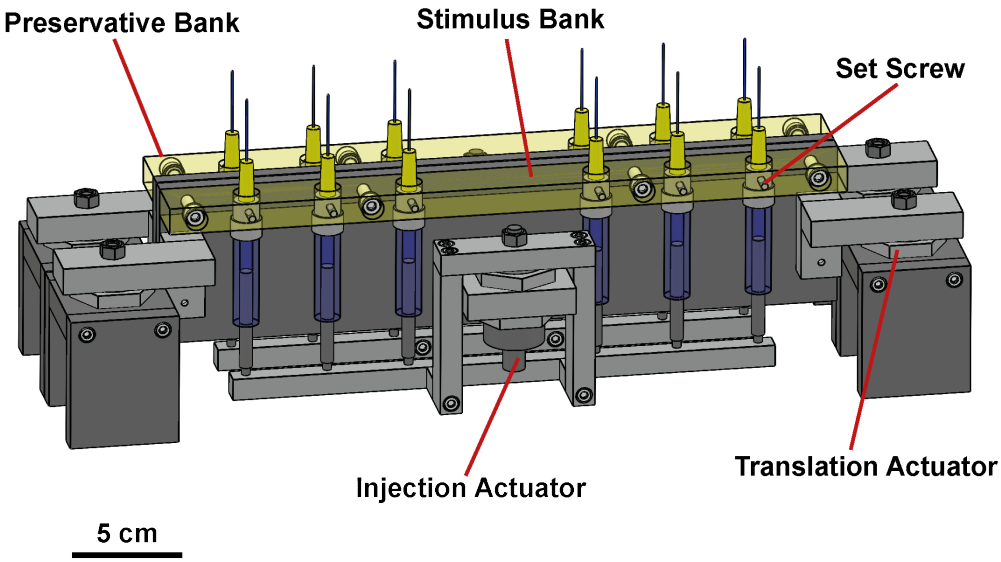

Fig. 7 | One pair of syringe banks of the MISE. Syringes are held into place by set screws. Prior to loading, syringes are filled with the chemical amendment, a filtered seawater control, or RNA preservative. The translation actuator shifts the entire bank upwards, causing the needles to pierce the septa covering the wells in the lower layer. Following a brief pause, the injection actuator drives the syringe plungers, injecting the contents of the syringes into the MISE microcosms. Stimulus and preservative banks move independently, with their injection marking the beginning and end of a set of experimental replicates, respectively.

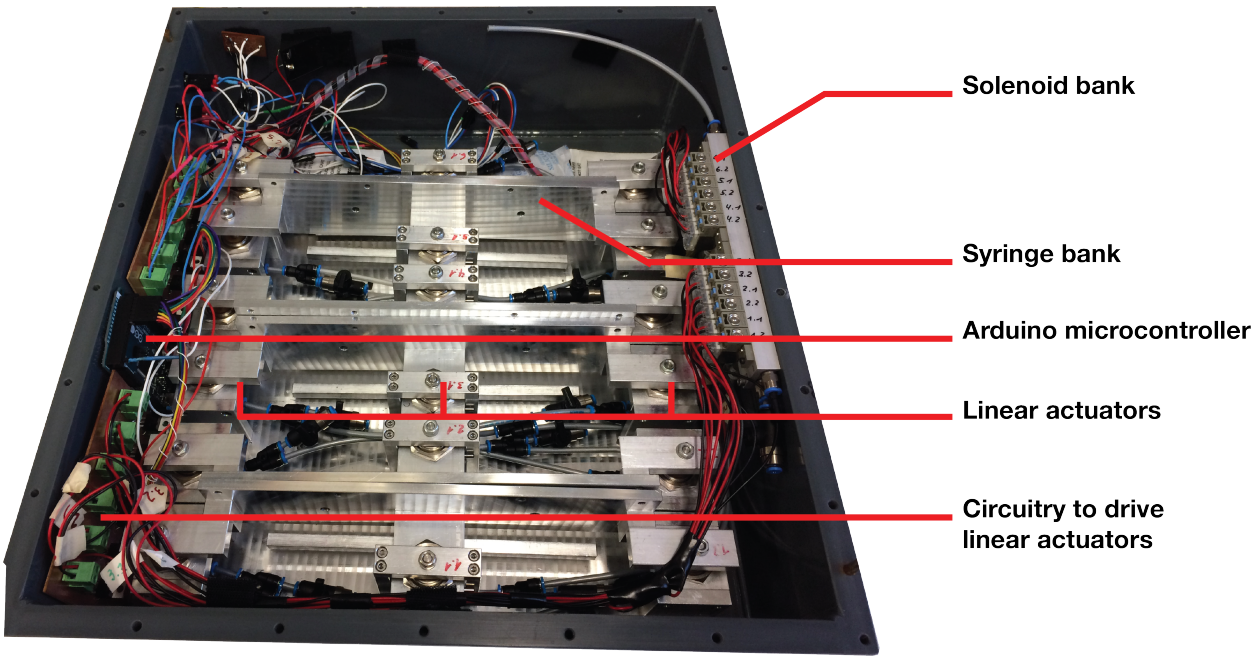

Fig. 8 | The internal mechanical, pneumatic, and electrical systems of the MISE. Each syringe bank within the MISE housing is connected to three linear actuators. The outer two actuators serve to translate the syringe bank upwards and cause the needles to pierce the well layer septa. The center actuator drives the syringe plungers, injecting the contents of each syringe into the well above. The linear actuators are connected to a solenoid bank that controls when CO_2 is delivered to pressurize the actuators. For each independent bank, the outer two actuators act together and are connected to a single solenoid valve and the center actuator is connected to a separate valve. The solenoid valves are controlled via an Arduino microcontroller and custom circuitry (see Fig. 9).

Custom circuitry for the MISE was designed using the open-source environment KiCad EDA (available under GNU GPLv3+; Supplementary File 1). Circuit boards were then milled out of double-sided FR-1 (OTHERMACHINE Co., USA) using a desktop CNC mill and the companion software, (OtherMill; OtherPlan; OtherMachine Co., USA). Electrical components were then soldered to circuit boards and the assembly mounted inside the PVC housing. Circuit schematics were laid out using standard autorouting options in KiCad (Fig. 9). The logic and control of the electronic system was managed using an Arduino Mega 2560 (Arduino, Italy), programmed using the Arduino IDE's built-in libraries (see Supplementary Note 1).

A complete list of mechanical and electronic components can be found in Tables 1 and 2 respectively. An engineering drawing of the MISE is available in Supplementary File 2.

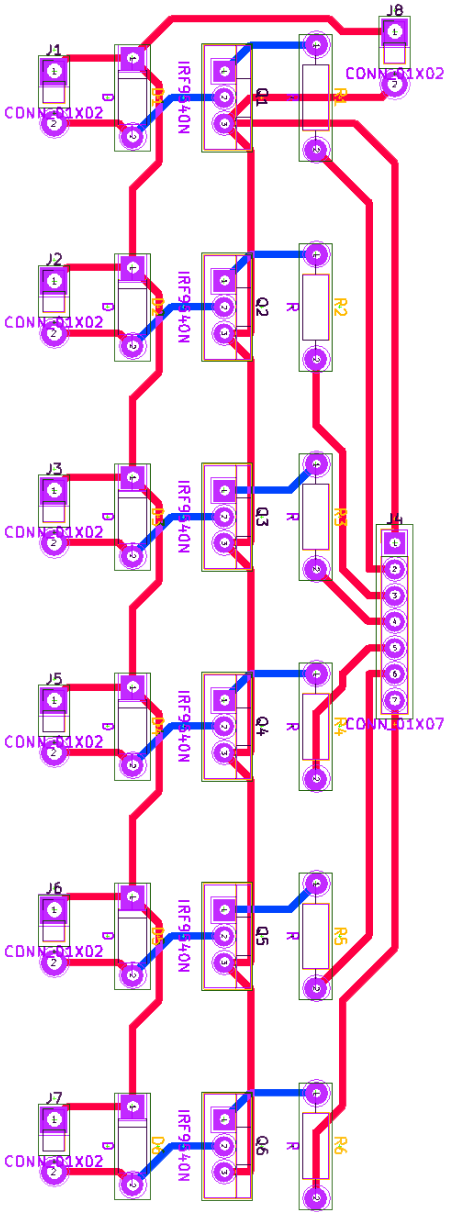

Fig. 9 | Circuit schematic for the MISE. A 5-V pulse is delivered from the Arduino to a transistor acting as a switch allowing current from a battery to drive each solenoid. Design files for circuitry used in the MISE can be found in Supplementary File 1.

Field deployment of the MISE

The test site selected for the MISE was Clovelly Beach in Sydney, Australia (33.91° S, 151.26° E). The MISE was deployed at 1 meter using a custom mounting apparatus (Fig. 10), the pneumatic system pressurized to 7 bar, and the experimental protocol initiated by depressing the device start button. The MISE then carried out an automated routine, whereby samples were enriched, incubated, and preserved. Preservation occurred at 10, 20, and 30 minutes following chemical amendment. Amendment and RNA preservative (1:50 mixture of ProtectRNA (Millipore Sigma, Germany) and TRIZOL (ThermoFisher, USA)) were injected to a final ratio of 1:10 (vol/vol) representing a final DMSP concentration of 100 μM. As both the RNA preservative and concentrated DMSP (Millipore Sigma, Germany) are much denser than water, the instrument was deployed first at an angle to enhance stimuli mixing and then rotated to a state that enhances mixing of the Trizol and ProtectRNA mixture (Fig. 10). Upon retrieval of the instrument, the upper silicone membrane was pierced with a syringe and preserved samples were withdrawn and snap-frozen in liquid N_2.

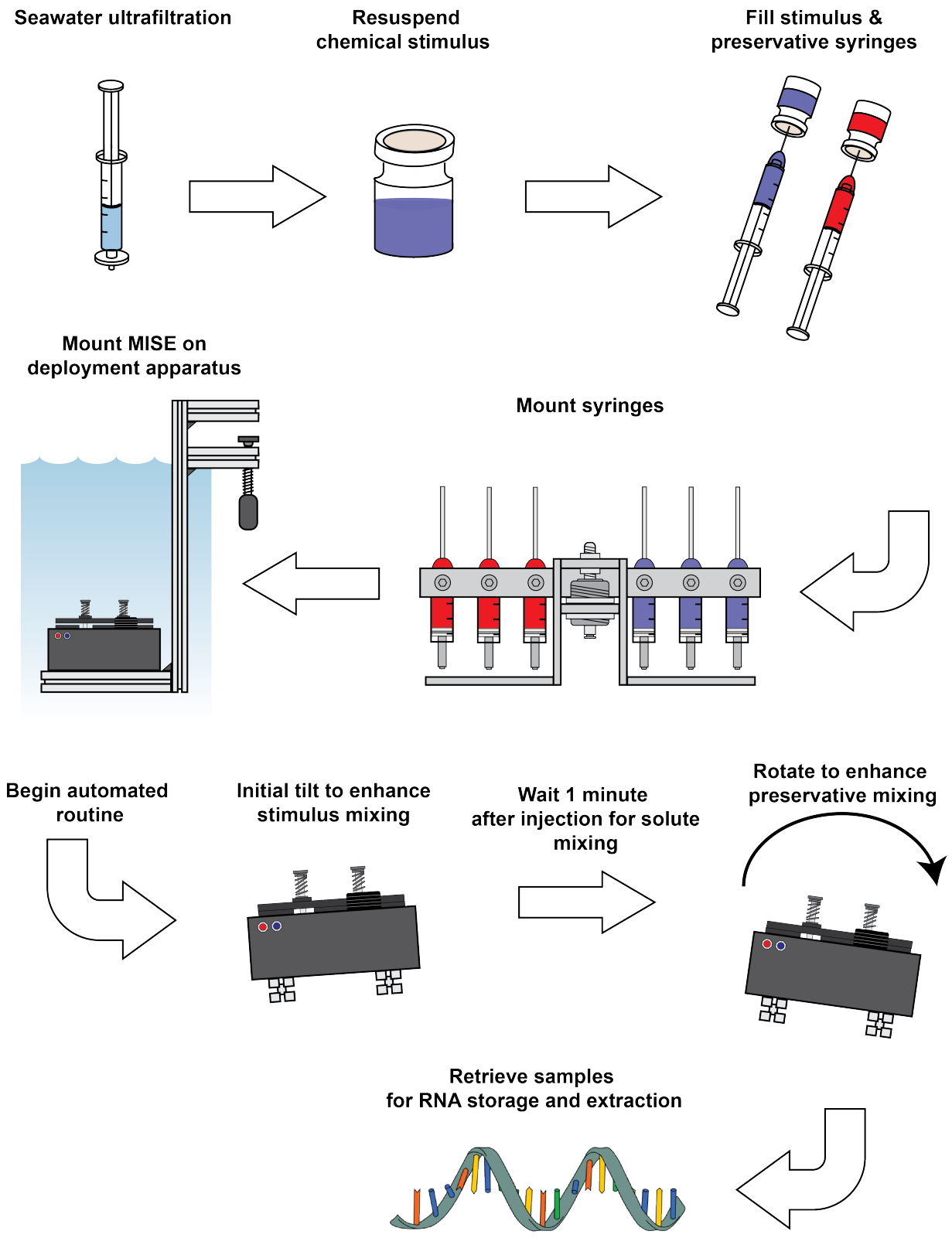

Fig. 10 | Deployment of the Millifluidic *In Situ* Enrichment. (see Methods)

RNA extraction

Samples were extracted using a modified phenol:chloroform:isoamyl alcohol (PCI) extraction(Kim et al. 2012; Griffiths et al. 2000; Feinstein, Sul, and Blackwood 2009; Angel, Claus, and Conrad 2011; Henckel, Friedrich, and Conrad 1999). Briefly, snap-frozen samples were thawed, and then PCI, phosphate buffer, TNC buffer(Henckel, Friedrich, and Conrad 1999), and 2-mercaptoethanol added to the pelleted sample. Samples were then subjected to 3 cycles of freezing in liquid N_2 followed by thawing in 50 $^{\circ}$C water bath. Bead beating (4500 rpm; 4 × 10 sec intervals; 0.1 mm and 0.5 mm glass beads) was then used to ensure complete cell lysis. An equal volume of chloroform was added and the suspension was spun down to remove impurities. Ampure RNA magnetic beads (Beckman Coulter, USA) were added to the samples in a 1.8:1.5 (bead solution/sample) ratio to bind nucleic acids and two washes with 70% ethanol were carried out. RNAse-out (ThermoFisher, Germany) was then added to eluted nucleic acids and the mixture subjected to two rounds (30 min at 37 $^{\circ}$C) of DNAse treatments using Turbo DNAse (ThermoFisher, Germany). RNA was once again retrieved using Ampure beads followed by two washes with 70% ethanol. Following the second DNA depletion step, EDTA was added to a final concentration of 15 mM and the solution heated at 75 $^{\circ}$C for 10 minutes to inactivate the DNAse. Finally, the solution was cleaned again using Ampure beads, two washes with 70% ethanol, and eluted in RNAse free water.

DNA extraction

10 l of seawater from the deployment was filtered through a 0.22 μm Sterivex filter (Millipore, USA) and snap frozen in liquid N_2. Following thawing of the Sterivex filters, a phenol-chloroform extraction was carried out. Briefly, one port of the Sterivex filter was sealed with parafilm and 1.8 ml of 0.22 μm filter sterilized lysis buffer (50 mM Tris-HCl, pH 8.0; 40 mM

EDTA, pH 8.0; 256 g/l Sucrose) was added to the Sterivex cartridge. 18 µl Lysozyme (100 mg/ml; Thermo Fisher, USA) was then added to the Sterivex cartridge. The second port was then securely sealed with parafilm and the cartridge was incubated for 1 hr at 37 °C. Following incubation, the top port was opened and 200 µl of Proteinase K (2 mg/ml; Thermo Fisher, USA) was added to the cartridge, the port was again securely sealed with parafilm, and the cartridge incubated for 1 hr at 55 °C on a rolling table. Lysate was then recovered and Phenol:Choloroform:IAA (25:24:1; Sigma-Aldrich, USA) was added in equal volume and mixed by inversion. Samples were then centrifuged (16, 000 g for 10 min) and the aqueous phase recovered. Choloroform/IAA (24:1) was then added in a volume equal to the sample, mixed by inversion, and the samples centrifuged (16, 000 g for 10 min). The aqueous phase was recovered and 100 µl of Sodium Acetate (3M) was added. DNA was then precipitated: 600-1000 µl of Isopropanol, was added gently mixed through inversion, incubated at room temperature for 15 min, centrifuged (20,000 g for 20-30 min at 4 ºC), and the supernatant disposed. 500 µl of 70% EtOH was then added to remove impurities from the precipitated DNA, the samples centrifuged (20,000 g for 15 min), and the supernatant discarded. Samples were then air-dried to ensure removal of EtOH, resuspended in MilliQ water, and stored at 4 ºC.

Digital PCR

Digital PCR was first introduced as a concept in 1992(Baker 2012; Sykes et al. 1992). Since then it has become an increasingly employed technique to quantify the copy number of rare genes and an effective technique for samples with a high degree of contamination(Taylor et al. 2015). Digital PCR does not require the same controls as traditional quantitative PCR and often has much better inter-experiment reproducibility, a major limitation of qPCR(Baker 2012; Taylor et al. 2015). Combined with its high dynamic range, these factors make digital droplet PCR

(ddPCR) an appealing technology to assay gene expression in samples with small quantities of genetic material(Baker 2012; Hindson et al. 2011; Taylor et al. 2015).

RNA libraries were generated using a SMARTer Stranded RNA-Seq Kit (Takara, USA) following manufacturer's instructions, and used as template in ddPCR reactions. The PCR assays were carried out using the QX100 Droplet Generator Bio-Rad system (Bio-Rad, USA) on two published primer sets: *dmdA* A/1-spFP (5'-ATGGTGATTTGCTTCAGTTTCT-3'), A/1-spRP (5'-CCCTGCTTTGACCAACC-3') that targets *dmdA* predominantly in roseobacters(Varaljay et al. 2015); and *dddP*_874F (5'-AAYGAAATWGTTGCCTTTGA-3'), 971R (5'-GCATDGCRTAAATCATATC-3') which targets *dddP* in roseobacters(Levine et al. 2012). Assays were carried out with EvaGreen Supermix (Bio-Rad, USA), run with positive and negative controls on a C1000 PCR, read on a QX200 Droplet Reader and analyzed with QuantaSoft Software (Bio-Rad, USA). Reaction volume was 23 µl, with 2 µl of RNA templates and a primer concentration of 0.1 µM. Assays were run according to the instruction manual (https://www.bio-rad.com/webroot/web/pdf/lsr/literature/10028376.pdf), with the *dmdA*-assay run as a two-step reaction (annealing/extension both occurring at 53 °C) and the *dddP*-assay run as a three-step reaction (temperature difference between annealing was 41 °C followed by 72 °C, each for 30 sec).

Mixing time observations

To determine mixing time within the MISE wells, video footage (GoPro Hero 3) of RNA preservative injection obtained during field deployments was analyzed. As the MISE wells are much larger in the horizontal plane than the vertical dimension, the mixing was assumed to be largely two dimensional and the mixing time was defined as the timescale over which the RNA preservative mixed fully in the horizontal plane.

Well cross-contamination tests

To ensure that each MISE well served as an independent microcosm, it was essential that there was no exchange between well volumes or leakage on timescales similar to the duration of MISE experiments. To test for leakage and cross-contamination mock deployments were carried out in a seawater mesocosm. During these deployments, alternating syringes were filled with filtered seawater from the mesocosm and fluorescein diacetate suspended in seawater from the mesocosm. A modified version of the automated injection routine was then carried out, whereby only a single row of wells was injected with amendments (fluorescein solution or seawater). The MISE wells were illuminated with violet light and the instrument left submerged for a 1-hour deployment time. Within this time no leakage or cross-contamination of fluorescein into the surrounding seawater and adjacent wells was observed.

Contributions

Bennett Lambert (B.L.), Jean-Baptiste Raina (JB.R.), Justin Seymour (J.S.), and Roman Stocker (R.S.) designed research. B.L., Vicente Fernandez (V.F.), and Toni Blunschi (T.B.) designed the MISE pneumatic and mechanical systems. B.L. and T.B. assembled the MISE. B.L. and Cameron Arnet (C.A.) designed and constructed electronics and wrote the microcontroller code. B.L., JB.R., and Nachshon Siboni (N.S.) carried out field deployments. JB. R., Lauren Messer (L.M.), Sammy Frenk (S.F.) and Chris Rinke (C.R.) carried out molecular work. N.S. performed digital droplet PCR assays. B.L. and JB. R. wrote the first draft of the manuscript from which this chapter was derived.

Item	Catalog Number	Manufacturer	Notes
500 µL Syringe	2666915	ILS Syringes	Corrosion resistant seals
Fine-Ject Syringe Tips	4710006025	Henke Sass Wolf	
Pneumatic Check Valve	AKH-05-A-Nil-M5-S	SMC Corp.	
Solenoid Valve Manifold	VV100-S41-16-M5	SMC Corp.	
10 mm Stroke Linear Act.	CJPB15-10H4	SMC Corp.	
15 mm Stroke Linear Act.	CJPB15-15H4	SMC Corp.	
Solenoid Valve	V1-1-4-Nil-R-H-S-Nil-M5	SMC Corp.	3.3V with leads attached
One-Touch-Fittings Ball Valve	QH-QS-4	Festo	
One-Touch-Fittings Y-Junction	QSMY-4-100	Festo	
One-Touch-Fittings L-Type	QSMLV-M5-4-I		
Pneumatic Tubing	PAN 4x0.75	Festo	
20 oz. CO_2 Bottle	TANK2	Palmer Pursuit Shop	
Pressure Stabilizer	PPSP010LP200	Palmer Pursuit Shop	
Food Grade Silicone Rubber (3/16”)	86045K98	McMaster Carr	For septa
Silicone Sheet (0.032”)	HT6240	Stockwell Elastomerics	For upper well layer
Hex M4x10	83.1215.04010	Hasler + Co AG	
Hex M3x12	83.1215.03012	Hasler + Co AG	
Hex M3x8	83.1215.03008	Hasler + Co AG	
Hex M5x22	83.1215.05022	Hasler + Co AG	
O-Ring (70 Shore, 32 × 2.5)	0101-001394	Kubo Tech AG	

Table 1. Mechanical materials list for assembly of the Millifluidic *In Situ* Enrichment.

Item	Catalog Number	Manufacturer
1 × 7 Pin Connector	1906	Pololu Corp.
1 × 2 Pin Connector	1901	Pololu Corp.
Pre-crimped Wires	1800	Pololu Corp.
Male Headers	1065	Pololu Corp.
TIP120G Transistor	774-3653	RS Electronics
1N4001 Diode	110-52-622	Distrelec
Male 2 Pin Connector	300-43-025	Distrelec
Female 2 Pin Connector	300-43-003	Distrelec
1.1 kΩ Resistor	148-512	RS Electronics
Arduino Mega 2560 Rev3		Arduino
Waterproof Servo	D-845WP	HiTec RCD

Table 2. Electrical components for assembly of MISE circuitry.

Supplementary information

Supplementary Note 1 | Arduino program used in this study.

```
#include <Servo.h>
//pins for solenoid circuits and input button
Servo myservo1;
Servo myservo2;
const int start_button_pin = 22;
const int chem_push_pin1 = 44; // 6.2 orange
const int chem_push_pin2 = 50; // 4.2 purple
const int chem_push_pin3 = 49; // 2.2 green
const int chem_plunge_pin1 = 42; // 6.1 red
const int chem_plunge_pin2 = 52; // 4.1 blue
const int chem_plunge_pin3 = 47; // 2.1 yellow
const int kill_push_pin1 = 46; // 5.2 green
const int kill_push_pin2 = 51; // 3.2 orange
const int kill_push_pin3 = 43; // 1.2 purple
const int kill_plunge_pin1 = 48; // 5.1 yellow
const int kill_plunge_pin2 = 53; // 3.1 red
const int kill_plunge_pin3 = 45; // 1.1 blue
int val = 0;
int flag = 0;
int token = 0;
//half hour time point, 30 minutes = 1.8 million ms
const unsigned long CHEMTIME = 30000; // 30 seconds
const unsigned long KILLTIME1 = 600000; // 10 minutes
const unsigned long KILLTIME2 = 1200000; // 20 minutes
const unsigned long KILLTIME3 = 1800000; // 30 minutes
```

```
//30, 60, 100 minute deployment
//const unsigned long CHEMTIME = 30000; // 30 seconds
//const unsigned long KILLTIME1 = 1800000; // 30 minutes
//const unsigned long KILLTIME2 = 3600000; // 60 minutes
//const unsigned long KILLTIME3 = 6000000; // 100 minutes
void setup() {
//Start serial so you can debug using the serial monitor if necessary
 Serial.begin(9600);
  pinMode(start_button_pin, INPUT);
  digitalWrite(chem_push_pin1, LOW);
  digitalWrite(chem_push_pin2, LOW);
  digitalWrite(chem_push_pin3, LOW);
  digitalWrite(chem_plunge_pin1, LOW);
  digitalWrite(chem_plunge_pin2, LOW);
  digitalWrite(chem_plunge_pin3, LOW);
  digitalWrite(kill_push_pin1, LOW);
  digitalWrite(kill_push_pin2, LOW);
  digitalWrite(kill_push_pin3, LOW);
  digitalWrite(kill_plunge_pin1, LOW);
  digitalWrite(kill_plunge_pin2, LOW);
  digitalWrite(kill_plunge_pin3, LOW);
  myservo1.attach(10, 900, 2100); // 2
  myservo2.attach(11, 900, 2100); // 1
  myservo1.write(180);
  myservo2.write(90);
}
```

```
//Uncomment below and comment the main loop to run the debug program
//It's good to run this and listen for audible clicks from the solenoids WITHOUT PRESSURE
//void loop(){
//  digitalWrite(chem_push_pin1, HIGH);
//  delay(1000);
//  digitalWrite(chem_push_pin1, LOW);
//  delay(1000);
//  digitalWrite(chem_plunge_pin1, HIGH);
//  delay(1000);
//  digitalWrite(chem_plunge_pin1, LOW);
//  delay(1000);
//  digitalWrite(chem_push_pin2, HIGH);
//  delay(1000);
//  digitalWrite(chem_push_pin2, LOW);
//  delay(1000);
//  digitalWrite(chem_plunge_pin2, HIGH);
//  delay(1000);
//  digitalWrite(chem_plunge_pin2, LOW);
//  delay(1000);
//  digitalWrite(chem_push_pin3, HIGH);
//  delay(1000);
//  digitalWrite(chem_push_pin3, LOW);
//  delay(1000);
//  digitalWrite(chem_plunge_pin3, HIGH);
//  delay(1000);
//  digitalWrite(chem_plunge_pin3, LOW);
//  delay(1000);
//  digitalWrite(kill_push_pin1, HIGH);
```

```
//  delay(1000);
//  digitalWrite(kill_push_pin1, LOW);
//  delay(1000);
//  digitalWrite(kill_plunge_pin1, HIGH);
//  delay(1000);
//  digitalWrite(kill_plunge_pin1, LOW);
//  delay(1000);
//  digitalWrite(kill_push_pin2, HIGH);
//  delay(1000);
//  digitalWrite(kill_push_pin2, LOW);
//  delay(1000);
//  digitalWrite(kill_plunge_pin2, HIGH);
//  delay(1000);
//  digitalWrite(kill_plunge_pin2, LOW);
//  delay(1000);
//  digitalWrite(kill_push_pin3, HIGH);
//  delay(1000);
//  digitalWrite(kill_push_pin3, LOW);
//  delay(1000);
//  digitalWrite(kill_plunge_pin3, HIGH);
//  delay(1000);
//  digitalWrite(kill_plunge_pin3, LOW);
//  delay(1000);
//while (0<1){}
//}
void loop() {
//  Serial.println("main loop");
Serial.println(val);
```

```
val = digitalRead(start_button_pin);
if (val == HIGH){
  flag = 1;
  myservo1.write(90);
  myservo2.write(180);
  delay(1000);
  while (flag == 1){
    digitalWrite(chem_push_pin1, LOW);
    digitalWrite(chem_push_pin2, LOW);
    digitalWrite(chem_push_pin3, LOW);
    digitalWrite(chem_plunge_pin1, LOW);
    digitalWrite(chem_plunge_pin2, LOW);
    digitalWrite(chem_plunge_pin3, LOW);
    digitalWrite(kill_push_pin1, LOW);
    digitalWrite(kill_push_pin2, LOW);
    digitalWrite(kill_push_pin3, LOW);
    digitalWrite(kill_plunge_pin1, LOW);
    digitalWrite(kill_plunge_pin2, LOW);
    digitalWrite(kill_plunge_pin3, LOW);
    //Main function that carries out all the syringe insertion
    //and plunging
    MISE_it();
    int k = 1;
    while (k==1) {}
    //This infinite loop keeps the program from trying to run again.
  }
}
```

```
}
void MISE_it(){
//Serial.println("something");
  token = 2;
  unsigned long start_time = millis();
  unsigned long current_time;
  while(token == 2){
    current_time = millis();
    if(current_time - start_time == CHEMTIME){
      push_chem();
      delay(1);
      plunge_chem();
      delay(1);
    }
    if(current_time - start_time == KILLTIME1){
      kill1();
      delay(1);
    }
    if(current_time - start_time == KILLTIME2){
      kill2();
      delay(1);
    }
    if(current_time - start_time == KILLTIME3){
      kill3();
      delay(1);
      token = 3; //exit the MISE_it function
    }
  }
```

```
}
void push_chem(){
  Serial.print("here");
  digitalWrite(chem_push_pin1, HIGH);
  delay(2000);
  digitalWrite(chem_push_pin1, LOW);
  delay(2000);
  digitalWrite(chem_push_pin2, HIGH);
  delay(2000);
  digitalWrite(chem_push_pin2, LOW);
  delay(2000);
  digitalWrite(chem_push_pin3, HIGH);
  delay(2000);
  digitalWrite(chem_push_pin3, LOW);
  delay(2000);
}
void plunge_chem(){
  digitalWrite(chem_plunge_pin1, HIGH);
  delay(2000);
  digitalWrite(chem_plunge_pin1, LOW);
  delay(2000);
  digitalWrite(chem_plunge_pin2, HIGH);
  delay(2000);
  digitalWrite(chem_plunge_pin2, LOW);
  delay(2000);
  digitalWrite(chem_plunge_pin3, HIGH);
  delay(2000);
  digitalWrite(chem_plunge_pin3, LOW);
```

```
  delay(2000);
}
void kill1(){
  digitalWrite(kill_push_pin1, HIGH);
  delay(2000);
  digitalWrite(kill_push_pin1, LOW);
  delay(2000);
  digitalWrite(kill_plunge_pin1, HIGH);
  delay(2000);
  digitalWrite(kill_plunge_pin1, LOW);
  delay(2000);
}
void kill2(){
  digitalWrite(kill_push_pin2, HIGH);
  delay(2000);
  digitalWrite(kill_push_pin2, LOW);
  delay(2000);
  digitalWrite(kill_plunge_pin2, HIGH);
  delay(2000);
  digitalWrite(kill_plunge_pin2, LOW);
  delay(2000);
}
void kill3(){
  digitalWrite(kill_push_pin3, HIGH);
  delay(2000);
  digitalWrite(kill_push_pin3, LOW);
  delay(2000);
  digitalWrite(kill_plunge_pin3, HIGH);
```

```
  delay(2000);
  digitalWrite(kill_plunge_pin3, LOW);
  delay(2000);
}
```

Supplementary files

Files may be found on the associated USB storage device.

Supplementary File 1 | Circuit schematic for MISE electronics.

Supplementary File 2 | Engineering drawing for the MISE mechanical elements.

Chapter 5: Motility drives bacterial encounter with particles responsible for carbon export throughout the ocean

Work presented here has been submitted for journal publication, and is currently under review, as "Bennett S. Lambert, Vicente I. Fernandez, & Roman Stocker. Motility drives bacterial encounter with particles responsible for carbon export throughout the ocean".

Main Text

Marine bacteria play central roles in the oceans' biogeochemical cycles. Quantifying the impact of their collective metabolisms, as well as the prevalence of different adaptations and the relative importance of different taxa remain topics of active research, and the answers will lie at the heart of our ability to model the role of the oceans in elemental cycling. Recently, Zehr and colleagues (Zehr, Weitz, and Joint 2017) highlighted the importance and numerical dominance in the open ocean of small, non-motile bacteria, which acquire nutrients by diffusion from the surrounding oligotrophic (*i.e.*, nutrient-deplete) waters. The arguments they presented give a general reader the impression that microbial motility is insignificant in the open ocean. Here we provide a counterpoint to that implication, by considering the role of motility in one of the most prominent biogeochemical processes in the ocean, the biological pump. Specifically, bacterial colonization of the particles that drive carbon export is strongly favored by motility even in the nutrient-depleted open ocean, because motility more than compensates for the usually low numerical abundance of motile bacteria by vastly increasing their encounter rates with particles.

Numerical abundance is only a partial metric of ecological importance, and the complexity and beauty of marine systems show their true color when ecosystem processes are interpreted

through the lens of the turnover rates and functional roles of participating microorganisms, particularly those driving prominent components of biogeochemical cycles. As an example from a different domain, apex predators play a major role in structuring trophic interactions in many ecosystems even though they occur in low numbers. Analogously, even numerically underrepresented groups of marine bacteria can dominate important components of biogeochemical cycles. Using literature data and a simple mathematical model, we show that motile bacteria encounter particles at disproportionate rates, which greatly enhances their ability to dominate particle-associated communities. Actual dominance on particles will be further influenced by additional factors such as metabolic capacity and microbial interactions (which will often further favor motile bacteria because of their copiotrophic adaptations (Dang and Lovell 2016; Herndl and Reinthaler 2013)), but the 1000-fold enhancement in colonization rate we highlight through our model provides motile bacteria a major starting advantage. Our calculation thus supports prior reports – though these are limited in number for the oligotrophic ocean – that motile bacteria often dominate particle communities (Fontanez et al. 2015). As a result, motile bacteria are expected to be primary agents in setting the magnitude of the biological pump, even in the open ocean.

Whether motile or non-motile, it has long been recognized that bacteria live in a world dominated by diffusion (Purcell 1977; Karp-Boss, Boss, and Jumars 1996). Zehr and colleagues compare the relative contribution of motility and molecular diffusion in the uptake of ammonium. However, it has long been known that swimming does not itself increase the instantaneous uptake rate for small microorganisms (Karp-Boss, Boss, and Jumars 1996), but rather serves them to find new nutrient sources (Purcell 1977). This year marks the 40th anniversary of Edward Purcell's seminal realization that a bacterium "*... does not move like a*

cow that is grazing a pasture – it moves to find greener pastures" (Purcell 1977). For a heterotrophic marine bacterium, there are no greener pastures than particles rich in organic matter.

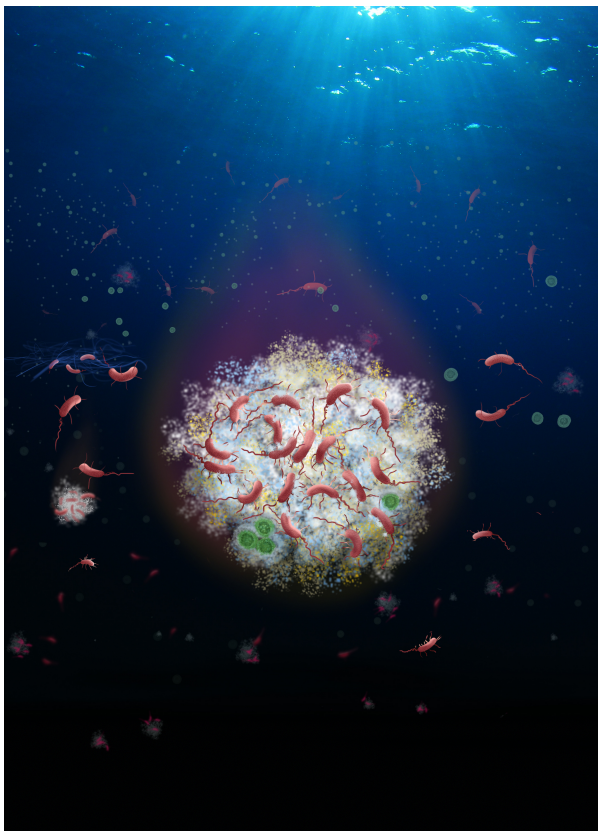

Figure 1 | Copiotrophic bacteria, which are often motile, frequently dominate over small, non-motile bacteria in communities inhabiting and degrading marine particles and thus play a dominant role in reducing the magnitude of the ocean's biological pump, the downward transport of vast quantities of carbon driven by sinking particles.

The role of sinking particles in driving the biological pump has traditionally been recognized for the productive coastal oceans (Muller-Karger et al. 2005), yet recently a comparable contribution was found to come from the open ocean (Jahnke 1996; Muller-Karger et al. 2005). New

approaches have revealed that particle concentrations in the open ocean can be much higher than measured by sediment traps (Pilskaln et al. 2005), including conspicuous amounts of non-sinking organic particles (Baltar et al. 2010), and that the aggregation of the characteristically small cells of the open ocean produces particles with sinking speeds similar to those in coastal waters (Richardson and Jackson 2007). This challenges the notion that the oligotrophic waters of the open ocean are devoid of microscale heterogeneity and suggests that even in this environment, particles are an important niche for motile bacteria, which thus make a major contribution to carbon export dynamics throughout the ocean (Fig. 1). The following discussion illustrates multiple lines of evidence for this view.

Particle-associated microbial communities are often found to be taxonomically distinct from their free-living counterparts (Ganesh et al. 2014; Fontanez et al. 2015). Physiologically, particle-attached bacteria are typically much larger (Dang and Lovell 2016) and exhibit greater uptake and exoenzyme production rates (Dang and Lovell 2016). Genes characteristic of a copiotrophic lifestyle are strongly enriched in the particle-associated fraction compared to the free-living population, not just in coastal waters (Ganesh et al. 2014), but also in the open ocean (Fontanez et al. 2015), and recent data from *Tara* Oceans point to the importance of copiotrophic taxa and motility for carbon export in the open ocean (Guidi et al. 2016).

While small, non-motile bacteria dominate by numerical abundance in the free-living fraction of open-ocean surface waters, evidence is accumulating that the oceans' interior is rich in bacteria adapted to a particle-associated lifestyle (Lauro and Bartlett 2008; Herndl and Reinthaler 2013). Copiotrophic bacteria with large genomes are preeminent members of the deep-sea community (Lauro and Bartlett 2008; Herndl and Reinthaler 2013) and sequenced genomes contain a large number of genes responsible for flagellar synthesis, signal transduction, and response to

gradients (Lauro and Bartlett 2008). Together with the prevalence of dissolved, particle-degrading enzymes indicative of surface-attached communities (Herndl and Reinthaler 2013), this evidence points to an active community of particle-attached copiotrophic bacteria in the open ocean's interior, where bacteria colonize particles through motility and remineralize them.

As a direct consequence of motility, motile bacteria in the oligotrophic ocean encounter particles at disproportionate rates compared to non-motile bacteria (Fig. 2), often more than outweighing the numerical dominance of non-motile bacteria in the bulk. Swimming greatly increases the volume of water that bacteria explore in a given time and thus the rate at which they encounter particles. At the small scale of bacteria, the 'ability to explore and encounter' also corresponds to a diffusivity, which for motile bacteria is 100–8 000 times greater than for non-motile bacteria, which explore the environment through Brownian motion (Supplementary Note). Strikingly, even when motile bacteria make up only 0.1% of bacteria in the bulk (e.g., *(Vergin et al. 2013)*, they will account for 70% of bacterial encounters with particles, and even more if chemotaxis is considered (Fig. 2). The composition of bacterial communities on particles is certainly influenced by factors other than just encounter rates. One key factor is the metabolic repertoire of bacteria encountering and residing on particles, which often further favors motile copiotrophic bacteria because of their capacity for rapid growth and broad range of substrate utilization (Dang and Lovell 2016; Herndl and Reinthaler 2013; Lauro and Bartlett 2008). A second factor is the pre-existence of bacteria on particles, yet this simply pushes back the question to encounters between bacteria and the constituent parts of particles and would be similarly impacted by motility. Ultimately, however, the striking enhancement in encounter rates makes motility a major determinant of which groups of bacteria are most abundant on particles, and thus likely to contribute to particle degradation and the magnitude of the biological pump.

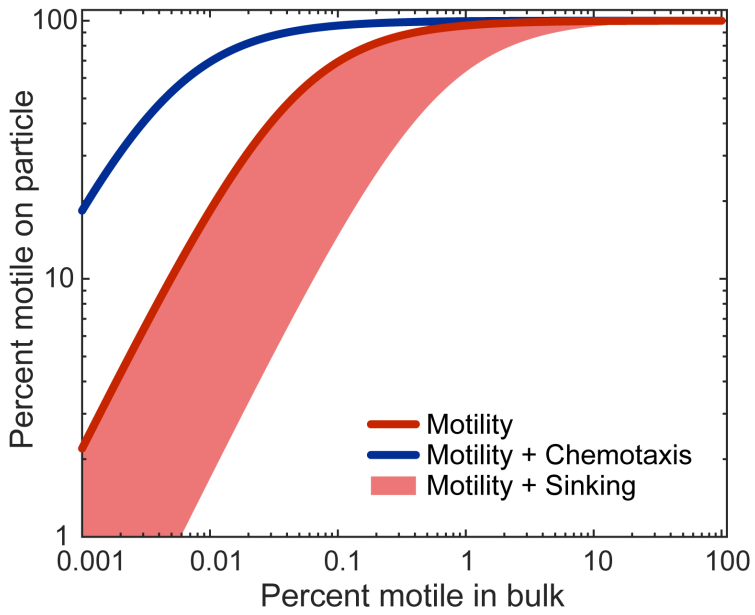

Figure 2 | In the colonization of particles, motile bacteria dominate despite their low numerical abundance in the bulk. Shown is the percentage of motile bacteria (relative to total bacteria) that encounter a particle (red solid curve), as a function of the percentage of motile bacteria in the bulk, predicted by a simple mathematical model (Supplementary Note). Also shown is the additional effect of chemotaxis (blue) and the effect of particle sinking (shaded red), represented as an envelope to account for different sinking speeds. Motility and chemotaxis vastly enhance the encounter rate of bacteria with particles, leading to a vastly disproportionate contribution of motile bacteria to particle colonization. Note that results are independent of particle size.

Are distances between particles too large for motile bacteria to rely on them as nutrient sources? A simple calculation shows that this is often not the case in the open ocean (see Supplementary Note). Based on particle abundances and size spectra from the North Pacific and focusing on particles in the diameter range of 20 µm to 5 mm, the time for a fast motile bacterium in the open ocean to find a particle is 3.3 – 27.3 h on average, but 10% of the bacteria find one in 20 – 170 min and 1% find one in 1 – 16 min. For slower bacteria the time increases approximately ten-fold, yet many bacteria still find a particle within a day. Whether bacteria can search for particles over these timescales will depend to some extent on the cost of motility. For comparison, in

laboratory settings bacteria have been observed to swim for 20–72 h in depleted environments (Malmcrona-Friberg, Goodman, and Kjelleberg 1990; Seymour, Ahmed, et al. 2010). Furthermore, motility does not need to be a viable strategy for every individual as long as a significant fraction of a clonal population survives. This ability to search for particles is of course not uniform across the open ocean. For example, at the highly oligotrophic center of the South Pacific gyre, where particle abundances can be 100-fold lower, even the top 10% of bacteria have to search for 3.6 days to find a particle, making motility less viable. This variability, and the paucity of data for particles in the open ocean, makes a general conclusion of where and when motility is a viable nutrient acquisition strategy in the open ocean currently impossible. What appears clear from combining the above calculations, however, is that particle hopping is a viable strategy where a sufficient concentration of particles exists, and thus in regions of the open ocean that most contribute to carbon export, and that motile bacteria are expected to play a major role in those regions because of their high encounter rates with particles.

Even in the open ocean, different nutritional niches coexist, allowing for both oligotrophic and copiotrophic strategies. Small, non-motile bacteria such as *Pelagibacter ubique* and *Prochlorococcus marinus* dominate in the surface of the open ocean, where sunlight dominates as an energy source and photosynthate provides a relatively steady if low nutrient supply to heterotrophs. Below the sunlit ocean, the situation changes rapidly and particulate organic matter becomes a central component of the deep-sea microbial loop(Herndl and Reinthaler 2013). In light of current oceanographic evidence and biophysical modeling results, motile bacteria dominate particle dynamics even when numerically rare overall – because they encounter them at disproportionate rates through swimming – and thus govern critical biogeochemical fluxes, including carbon export to the depths of the oceans. Advancing our understanding of the role and

relevance of different groups of bacteria in the ocean necessitates us to look with fresh eyes and a focus on microbial activity and functional impact. Constructing this new view will require appropriate measurement tools, significant field data and sound biophysical modeling, making this one of the most exciting frontiers in microbial ecology.

Supplementary Note

Diffusivity comparison. A non-motile bacterium with radius r = 0.5 μm has a diffusivity due to Brownian motion of $D = kT/(6\pi\eta r) \approx 10^{-12}$ m^2/s, where k is Boltzmann's constant, T is temperature and η is the dynamic viscosity. The diffusivity of motile bacteria, originating from their random-walk behavior, is $D \approx v^2\tau/3$, where v is the swimming speed and τ is the run time (Berg 1993). Strains isolated from particles were found to have $D = (0.1 - 8)\times10^{-9}$ m^2/s, *i.e.*, 100- to 8000-fold higher than small non-motile bacteria (Kiørboe 2008).

Encounter rate of motile and non-motile bacteria with particles. The rate of encounter of bacteria (concentration B) with a particle of radius a is $R = 4\pi aDB$. Neglecting differences in growth, the fraction of bacteria on a particle that are motile is the rate of encounter of motile bacteria divided by the combined rate of encounter of motile and non-motile bacteria, i.e.:

$$F_{mot,particle} = \frac{R_{mot}}{R_{mot} + R_{non}} = \frac{(D_{mot}/D_{non})\, F_{mot,bulk}}{(D_{mot}/D_{non})\, F_{mot,bulk} + (1 - F_{mot,bulk})}.$$

where $F_{mot,bulk}$ is the fraction of motile bacteria in the bulk. For chemotaxis, the radius of the particle was increased 10-fold for motile bacteria, based on recent observations(Smriga et al. 2016). For sinking particles, the encounter rate becomes additionally proportional to $D^{-1/3}$ (Kiørboe 2008), yielding:

$$F_{mot,sinking\ particle} = \frac{1}{(D_{non}/D_{mot})^{2/3}\ (1 - F_{mot,bulk})/F_{mot,bulk} + 1}.$$

Frequency of particle encounters. To calculate the search time of motile bacteria for particles in the open ocean we used observations of particle spectra and abundances from the North Pacific (Pilskaln et al. 2005; Kostadinov, Siegel, and Maritorena 2009) and the South Pacific gyre (Stemmann et al. 2008). We assumed that bacteria encounter particles only by random motility (with $D = 8\times10^{-10}$ or 8×10^{-9} m^2/s^1). To find the time required for a bacterium to encounter any particle in the range considered (10 μm – 2.5 mm) we follow previous studies[2] combining the particle size spectrum with the size-specific encounter rate model that includes the effect of particle sinking. Integrating over the particle size range, one calculates the average search time T_S $(1/E_{tot})$ that a bacterium has with particles in that size range. Modeling particle encounters as a Poisson process, the cumulative distribution function of the time to the first encounter is $P(t < T_{bulk}) = 1 - e^{-T_{bulk}/T_S}$, used to find the maximum search time for the shortest 10% and 1% of searches given in the main text.

Contributions

Bennett Lambert (B.L.), Vicente Fernandez (V.F.), and Roman Stocker (R.S.) designed research. B.L. and V.F. gathered data and developed the particle encounter model. All authors wrote the paper.

Chapter 6: Future Directions

Engineering and ocean science have always been intimately intertwined as a result of the challenges of research at sea. Whether observing the deepest reaches of the seafloor (Kato et al. 1998; Taira et al. 2004), sampling hydrothermal vents where local fluid temperatures can reach hundreds of degrees Celsius(Fornari et al. 1998), carrying out global observations of ocean color via remote sensing (Dickey, Lewis, and Chang 2006), or extended *in situ* time series of physical, chemical, and molecular data (Karl and Lukas 1996), engineering has been and continues to be an integral component of our efforts to characterize the biology, physics, and chemistry of the oceans.

Instrumentation to study natural communities of marine microbes at scales relevant to the individual remains an underdeveloped field in ocean engineering. To contribute to address this gap, in this thesis I have presented three devices that have the potential for wide adoption (in particular the ISCA) and can enhance our capacity to sample the ocean at the microscale. Techniques to study the ecology of natural communities of marine microbes at appropriate spatiotemporal scales offer an exciting opportunity to begin to assemble a mechanistic understanding of the microbial processes that underlie larger-scale ecosystem dynamics.

However far we have come, there still exists a world of opportunity and intrigue to explore through the development and application of new field-based techniques to observe microscale processes. Results presented in Chapter 3 and preliminary results from follow-up experiments suggest we have a poor understanding of the phylogenetic diversity of marine microbes that make use of motility and chemotaxis as resource acquisition strategies. Furthermore, we are still

far from a comprehensive understanding of how these behaviors impact the ecology of participating microorganisms in the water column. Through the techniques presented here, coupled with advances in molecular techniques and analytical chemistry, we begin to have the power to move forward and describe life at the microscale in greater detail than ever before.

Beyond application of the techniques presented within this thesis, there remains a fundamental engineering challenge that mirrors the task faced by oceanographers throughout history. The instruments presented within this thesis can sample or are currently deployable at depths of less than approximately 3 m. Micro- and millifluidic devices often rely on materials that cannot withstand the immense pressure of the ocean's interior and are sensitive to mechanical disruption. Considerable effort will be required to establish techniques that are extremely simple and robust to the stress of deep-sea deployment. When considering key microscale processes that make significant contributions to the chemical heterogeneity of the water column, the nature of each process depends strongly on the depth at which it occurs. For example, consider marine snow particles sinking through the water column. Motility and chemotaxis play an important role in establishing the microbial communities present on the individual components prior to formation of the marine snow particle (see Chapter 5). Following this initial colonization, these behaviors continue to play a critical role in structuring the composition of the microbial community encountering, residing on, and degrading the particle through its lifetime. This is a particularly interesting example, as the chemical composition of the aggregate changes with depth (Lee, Wakeham, and Arnosti 2004) (and therefore the chemical cues emanating from it) and the background microbial community also shifts in function and composition with depth (DeLong et al. 2006; Mende et al. 2017). Particle foraging in the deep sea is hypothesized to be a critical component of microbial life in the dark ocean (Herndl and Reinthaler 2013; Lauro and

Bartlett 2008), however we know precious little about the ecology, biology, and behavior of the microbes that occupy one of the largest biomes on earth. Enabling the study of these communities represents one of the most exciting frontiers in ocean engineering and marine microbial ecology and success on this front will surely lead to a wealth of new information about the strategies these organisms use to occupy extreme environments.

The rapid development of novel microfabrication techniques is consistently introducing new technologies that are well suited to marine microbial ecology. The advent of biocompatible 3D printer resins (Urrios et al. 2016) and a push to higher resolution (Anscombe 2010) are making digital manufacturing an appealing alternative to traditional photolithography. Similarly, laser-cutting of polymethyl methacrylate (PMMA)(Klank, Kutter, and Geschke 2002) or mixed PDMS/PMMA devices (Sunkara et al. 2011) has recently emerged as another viable rapid prototyping option. The rate-limiting process at this point is adapting these devices to marine deployment, which proves to be a particularly challenging task. Many microfluidic techniques rely on bulky external hardware. Reducing complexity and waterproofing these devices often requires a great deal of ingenuity. As with many technologies and burgeoning fields, it will take some time to develop tricks of the trade and design rules that can be applied to the development of marine microdevices. With refinement and automation, these techniques can be extended to carry out time series analyses and biogeographic surveys of critical microscale processes and, together with environmental metadata, will allow us to assemble an understanding of the impact of microscale phenomena on ecosystem-level processes. With the ISCA, the use of widely available rapid-prototyping techniques broadened the potential user base immediately. Furthermore, the use of 3D printing as opposed to traditional lithography-based work flows reduced the degree of labor and cost per device. We are currently in the process of improving

this even further through the development of an injection-moulded ISCA, where each device will cost on the order of ten dollars and can be produced in high-throughput. The continued refinement of the ISCA places it in a prime position to be adopted as a standard technique in the microbial ecologist's toolkit and an increase in the breadth of environmental conditions under which the ISCA is deployed will provide insight into the factors that drive motility in the environment.

The capability to probe specific compartments of the microbial communities under natural conditions is critical to understand how microbial communities self-assemble and interact. Interactions at these fine scales drive central processes in the marine environment, from host-symbiont systems (Mandel et al. 2012), to coral disease (Garren et al. 2014), to interactions between phytoplankton and bacteria ranging from mutualistic to antagonistic (Seymour et al. 2017), to the biological pump (Kiørboe et al. 2002). A mechanistic understanding of life at the microscale is essential if we are to predict how earth's changing climate and the predicted shift in phytoplankton community composition (Flombaum et al. 2013; Morán et al. 2010) will affect the ecology of heterotrophic microbes and the balance of the biogeochemical cycles they drive. Here we have taken some first steps in establishing *in situ* micro- and millifluidic tools for microbial oceanography with the aim of driving the effort to understand the ocean at the microscale forward.

References

Ackermann, M. 2015. 'A functional perspective on phenotypic heterogeneity in microorganisms', *Nat Rev Microbiol*, 13: 497-508.

Adler, J., and M. Dahl. 1967. 'A Method for Measuring the Motility of Bacteria and for Comparing Random and Non-random Motility', *Microbiology*, 46: 161-73.

Ahmed, Tanvir, Thomas S. Shimizu, and Roman Stocker. 2010. 'Microfluidics for bacterial chemotaxis', *Integrative Biology*, 2: 604-29.

Ahmed, Tanvir, and Roman Stocker. 2008. 'Experimental Verification of the Behavioral Foundation of Bacterial Transport Parameters Using Microfluidics', *Biophysical Journal*, 95: 4481-93.

Amin, S. A., L. R. Hmelo, H. M. van Tol, B. P. Durham, L. T. Carlson, K. R. Heal, R. L. Morales, C. T. Berthiaume, M. S. Parker, B. Djunaedi, A. E. Ingalls, M. R. Parsek, M. A. Moran, and E. V. Armbrust. 2015. 'Interaction and signalling between a cosmopolitan phytoplankton and associated bacteria', *Nature*, 522: 98.

Ammerman, J.W., J.A. Fuhrman, A. Hagstrom, and F. Azam. 1984. 'Bacterioplankton growth in seawater: I. Growth kinetics and cellular characteristics in seawater cultures', *Mar. Ecol. Prog. Ser.*, 18: 31-39.

Angel, Roey, Peter Claus, and Ralf Conrad. 2011. 'Methanogenic archaea are globally ubiquitous in aerated soils and become active under wet anoxic conditions', *The Isme Journal*, 6: 847.

Anglès, Sílvia, Antoni Jordi, and Lisa Campbell. 2015. 'Responses of the coastal phytoplankton community to tropical cyclones revealed by high-frequency imaging flow cytometry', *Limnology and Oceanography*, 60: 1562-76.

Anscombe, Nadya. 2010. 'Direct laser writing', *Nature Photonics*, 4: 22.

Armbrust, E. V., J. D. Bowen, R. J. Olson, and S. W. Chisholm. 1989. 'Effect of light on the cell cycle of a marine *Synechococcus* strain', *Appl Environ Microbiol*, 55: 425-32.

Armbrust, E. Virginia, Sallie W. Chisholm, and Robert J. Olson. 1990. 'Role of light and the cell cycle on the induction of spermatogenesis in a centric diatom', *Journal of Phycology*, 26: 470-78.

Azam, F., and R. A. Long. 2001. 'Sea snow microcosms', *Nature*, 414: 495, 97-8.

Azam, Farooq. 1998. 'Microbial Control of Oceanic Carbon Flux: The Plot Thickens', *Science*, 280: 694-96.

Azam, Farooq, and Francesca Malfatti. 2007. 'Microbial structuring of marine ecosystems', *Nat Rev Micro*, 5: 782-91.

Baker, L. J., and P. F. Kemp. 2014. 'Exploring bacteria– diatom associations using single-cell whole genome amplification', *Aquatic Microbial Ecology*, 72: 73-88.

Baker, Monya. 2012. 'Digital PCR hits its stride', *Nature Methods*, 9: 541.

Baltar, Federico, Javier Arístegui, Eva Sintes, Josep M. Gasol, Thomas Reinthaler, and Gerhard J. Herndl. 2010. 'Significance of non-sinking particulate organic carbon and dark CO2 fixation to heterotrophic carbon demand in the mesopelagic northeast Atlantic', *Geophysical Research Letters*, 37.

Becker, Jamie, Paul Berube, Christopher Follett, John Waterbury, Sallie Chisholm, Edward DeLong, and Daniel Repeta. 2014. 'Closely related phytoplankton species produce similar suites of dissolved organic matter', *Frontiers in Microbiology*, 5.
Berg, Howard C. 1993. *Random walks in biology* (Princeton University Press: Princeton, N.J.).
Blackburn, Nicholas, Farooq Azam, and Åke Hagström. 1997. 'Spatially explicit simulations of a microbial food web', *Limnology and Oceanography*, 42: 613-22.
Blackburn, Nicholas, Tom Fenchel, and Jim Mitchell. 1998. 'Microscale Nutrient Patches in Planktonic Habitats Shown by Chemotactic Bacteria', *Science*, 282: 2254.
Bonato, Simon, Urania Christaki, Alain Lefebvre, Fabrice Lizon, Melilotus Thyssen, and Luis Felipe Artigas. 2015. 'High spatial variability of phytoplankton assessed by flow cytometry, in a dynamic productive coastal area, in spring: The eastern English Channel', *Estuarine, Coastal and Shelf Science*, 154: 214-23.
Boutte, Cara C., and Sean Crosson. 2013. 'Bacterial lifestyle shapes stringent response activation', *Trends in Microbiology*, 21: 174-80.
Brosnahan, M. L., S. Farzan, B. A. Keafer, H. M. Sosik, R. J. Olson, and D. M. Anderson. 2014. 'Complexities of bloom dynamics in the toxic dinoflagellate *Alexandrium fundyense* revealed through DNA measurements by imaging flow cytometry coupled with species-specific rRNA probes', *Deep Sea Res Part 2 Top Stud Oceanogr*, 103: 185-98.
Bucciarelli, Eva, Céline Ridame, William G. Sunda, Céline Dimier-Hugueney, Marie Cheize, and Sauveur Belviso. 2013. 'Increased intracellular concentrations of DMSP and DMSO in iron-limited oceanic phytoplankton *Thalassiosira oceanica* and *Trichodesmium erythraeum*', *Limnology and Oceanography*, 58: 1667-79.
Campbell, Lisa, Robert J. Olson, Heidi M. Sosik, Ann Abraham, Darren W. Henrichs, Cammie J. Hyatt, and Edward J. Buskey. 2010. 'First harmful *Dinophysis* (Dinophyceae, Dinophysiales) bloom in the U.S. revealed by automated imaging flow cytometry', *Journal of Phycology*, 46: 66-75.
Chatterji, Dipankar, and Anil Kumar Ojha. 2001. 'Revisiting the stringent response, ppGpp and starvation signaling', *Current Opinion in Microbiology*, 4: 160-65.
Chisholm, Sallie W., Robert J. Olson, and Clarice M. Yentsch. 1988. 'Flow cytometry in oceanography: Status and prospects', *Eos, Transactions American Geophysical Union*, 69: 562-72.
Chisholm, Sallie W., Robert J. Olson, Erik R. Zettler, Ralf Goericke, John B. Waterbury, and Nicholas A. Welschmeyer. 1988. 'A novel free-living prochlorophyte abundant in the oceanic euphotic zone', *Nature*, 334: 340.
Cucci, T. L., S. E. Shumway, W. S. Brown, and C. R. Newell. 1989. 'Using phytoplankton and flow cytometry to analyze grazing by marine organisms', *Cytometry*, 10: 659-69.
Curson, Andrew R. J., Ji Liu, Ana Bermejo Martínez, Robert T. Green, Yohan Chan, Ornella Carrión, Beth T. Williams, Sheng-Hui Zhang, Gui-Peng Yang, Philip C. Bulman Page, Xiao-Hua Zhang, and Jonathan D. Todd. 2017. 'Dimethylsulfoniopropionate biosynthesis in marine bacteria and identification of the key gene in this process', *Nature Microbiology*, 2: 17009.
Dang, H., and C. R. Lovell. 2016. 'Microbial surface colonization and biofilm development in marine environments', *Microbiol Mol Biol Rev*, 80: 91-138.
DeLong, Edward F., Christina M. Preston, Tracy Mincer, Virginia Rich, Steven J. Hallam, Niels-Ulrik Frigaard, Asuncion Martinez, Matthew B. Sullivan, Robert Edwards, Beltran

Rodriguez Brito, Sallie W. Chisholm, and David M. Karl. 2006. 'Community Genomics Among Stratified Microbial Assemblages in the Ocean's Interior', *Science*, 311: 496.
Dickey, T., M. Lewis, and G. Chang. 2006. 'Optical oceanography: Recent advances and future directions using global remote sensing and in situ observations', *Reviews of Geophysics*, 44.
Drescher, Knut, Yi Shen, Bonnie L. Bassler, and Howard A. Stone. 2013. 'Biofilm streamers cause catastrophic disruption of flow with consequences for environmental and medical systems', *Proceedings of the National Academy of Sciences*, 110: 4345.
Durham, Bryndan P., Shalabh Sharma, Haiwei Luo, Christa B. Smith, Shady A. Amin, Sara J. Bender, Stephen P. Dearth, Benjamin A. S. Van Mooy, Shawn R. Campagna, Elizabeth B. Kujawinski, E. Virginia Armbrust, and Mary Ann Moran. 2015. 'Cryptic carbon and sulfur cycling between surface ocean plankton', *Proceedings of the National Academy of Sciences*, 112: 453.
Falkowski, Paul G., Tom Fenchel, and Edward F. Delong. 2008. 'The microbial engines that drive earth's biogeochemical cycles', *Science*, 320: 1034-39.
Fawcett, Sarah E., Michael W. Lomas, John R. Casey, Bess B. Ward, and Daniel M. Sigman. 2011. 'Assimilation of upwelled nitrate by small eukaryotes in the Sargasso Sea', *Nature Geoscience*, 4: 717.
Feinstein, Larry M., Woo Jun Sul, and Christopher B. Blackwood. 2009. 'Assessment of Bias Associated with Incomplete Extraction of Microbial DNA from Soil', *Applied and Environmental Microbiology*, 75: 5428-33.
Fenchel, T. 2002. 'Microbial behavior in a heterogeneous world', *Science*, 296: 1068-71.
Flombaum, Pedro, José L. Gallegos, Rodolfo A. Gordillo, José Rincón, Lina L. Zabala, Nianzhi Jiao, David M. Karl, William K. W. Li, Michael W. Lomas, Daniele Veneziano, Carolina S. Vera, Jasper A. Vrugt, and Adam C. Martiny. 2013. 'Present and future global distributions of the marine Cyanobacteria *Prochlorococcus* and *Synechococcus*', *Proceedings of the National Academy of Sciences*, 110: 9824.
Fontanez, K. M., J. M. Eppley, T. J. Samo, D. M. Karl, and E. F. DeLong. 2015. 'Microbial community structure and function on sinking particles in the North Pacific Subtropical Gyre', *Front Microbiol*, 6: 469.
Ford, Roseanne M., Bret R. Phillips, John A. Quinn, and Douglas A. Lauffenburger. 1991. 'Measurement of bacterial random motility and chemotaxis coefficients: I. Stopped-flow diffusion chamber assay', *Biotechnology and Bioengineering*, 37: 647-60.
Fornari, D. J., T. Shank, K. L. Von Damm, T. K. P. Gregg, M. Lilley, G. Levai, A. Bray, R. M. Haymon, M. R. Perfit, and R. Lutz. 1998. 'Time-series temperature measurements at high-temperature hydrothermal vents, East Pacific Rise 9°49′–51′N: evidence for monitoring a crustal cracking event', *Earth and Planetary Science Letters*, 160: 419-31.
Ganesh, S., D. J. Parris, E. F. DeLong, and F. J. Stewart. 2014. 'Metagenomic analysis of size-fractionated picoplankton in a marine oxygen minimum zone', *ISME J*, 8: 187-211.
Garren, Melissa, Kwangmin Son, Jean-Baptiste Raina, Roberto Rusconi, Filippo Menolascina, Orr H. Shapiro, Jessica Tout, David G. Bourne, Justin R. Seymour, and Roman Stocker. 2014. 'A bacterial pathogen uses dimethylsulfoniopropionate as a cue to target heat-stressed corals', *ISME J*, 8: 999-1007.
Giovannoni, S. J., H. J. Tripp, S. Givan, M. Podar, K. L. Vergin, D. Baptista, L. Bibbs, J. Eads, T. H. Richardson, M. Noordewier, M. S. Rappe, J. M. Short, J. C. Carrington, and E. J.

Mathur. 2005. 'Genome streamlining in a cosmopolitan oceanic bacterium', *Science*, 309: 1242-5.
Griffiths, Robert I., Andrew S. Whiteley, Anthony G. O'Donnell, and Mark J. Bailey. 2000. 'Rapid Method for Coextraction of DNA and RNA from Natural Environments for Analysis of Ribosomal DNA- and rRNA-Based Microbial Community Composition', *Applied and Environmental Microbiology*, 66: 5488-91.
Grossart, Hans-Peter, Lasse Riemann, and Farooq Azam. 2001. 'Bacterial motility in the sea and its ecological implications', *Aquatic Microbial Ecology*, 25: 247-58.
Guidi, L., S. Chaffron, L. Bittner, D. Eveillard, A. Larhlimi, S. Roux, Y. Darzi, S. Audic, L. Berline, J. Brum, L. P. Coelho, J. C. I. Espinoza, S. Malviya, S. Sunagawa, C. Dimier, S. Kandels-Lewis, M. Picheral, J. Poulain, S. Searson, coordinators Tara Oceans, L. Stemmann, F. Not, P. Hingamp, S. Speich, M. Follows, L. Karp-Boss, E. Boss, H. Ogata, S. Pesant, J. Weissenbach, P. Wincker, S. G. Acinas, P. Bork, C. de Vargas, D. Iudicone, M. B. Sullivan, J. Raes, E. Karsenti, C. Bowler, and G. Gorsky. 2016. 'Plankton networks driving carbon export in the oligotrophic ocean', *Nature*, 532: 465-70.
Guillard, Robert R. L. 1975. 'Culture of Phytoplankton for Feeding Marine Invertebrates.' in Walter L. Smith and Matoira H. Chanley (eds.), *Culture of Marine Invertebrate Animals: Proceedings — 1st Conference on Culture of Marine Invertebrate Animals Greenport* (Springer US: Boston, MA).
He, Kuang, and Carl E. Bauer. 2014. 'Chemosensory signaling systems that control bacterial survival', *Trends in Microbiology*, 22: 389-98.
Henckel, Thilo, Michael Friedrich, and Ralf Conrad. 1999. 'Molecular Analyses of the Methane-Oxidizing Microbial Community in Rice Field Soil by Targeting the Genes of the 16S rRNA, Particulate Methane Monooxygenase, and Methanol Dehydrogenase', *Applied and Environmental Microbiology*, 65: 1980-90.
Herndl, G. J., and T. Reinthaler. 2013. 'Microbial control of the dark end of the biological pump', *Nat Geosci*, 6: 718-24.
Hindson, Benjamin J., Kevin D. Ness, Donald A. Masquelier, Phillip Belgrader, Nicholas J. Heredia, Anthony J. Makarewicz, Isaac J. Bright, Michael Y. Lucero, Amy L. Hiddessen, Tina C. Legler, Tyler K. Kitano, Michael R. Hodel, Jonathan F. Petersen, Paul W. Wyatt, Erin R. Steenblock, Pallavi H. Shah, Luc J. Bousse, Camille B. Troup, Jeffrey C. Mellen, Dean K. Wittmann, Nicholas G. Erndt, Thomas H. Cauley, Ryan T. Koehler, Austin P. So, Simant Dube, Klint A. Rose, Luz Montesclaros, Shenglong Wang, David P. Stumbo, Shawn P. Hodges, Steven Romine, Fred P. Milanovich, Helen E. White, John F. Regan, George A. Karlin-Neumann, Christopher M. Hindson, Serge Saxonov, and Bill W. Colston. 2011. 'High-Throughput Droplet Digital PCR System for Absolute Quantitation of DNA Copy Number', *Analytical Chemistry*, 83: 8604-10.
Hol, F. J., and C. Dekker. 2014. 'Zooming in to see the bigger picture: microfluidic and nanofabrication tools to study bacteria', *Science*, 346: 1251821.
Iglesias-Rodríguez, María Débora, Oscar M. Schofield, Jacqueline Batley, Linda K. Medlin, and Paul K. Hayes. 2006. 'Intraspecific genetic diversity in the marine coccolithophore *Emiliania huxleyi* (Prymnesiophyceae): The use of microsatellite analysis in marine phytoplankton population studies', *Journal of Phycology*, 42: 526-36.
Jackson, George A. 1980. 'Phytoplankton growth and Zooplankton grazing in oligotrophic oceans', *Nature*, 284: 439-41.

———. 2012. 'Seascapes: the world of aquatic organisms as determined by their particulate natures', *The Journal of Experimental Biology*, 215: 1017.
Jahnke, Richard A. 1996. 'The global ocean flux of particulate organic carbon: Areal distribution and magnitude', *Global Biogeochemical Cycles*, 10: 71-88.
Jefferson, T. Turner. 2002. 'Zooplankton fecal pellets, marine snow and sinking phytoplankton blooms', *Aquatic Microbial Ecology*, 27: 57-102.
Johnson, Zackary I., Erik R. Zinser, Allison Coe, Nathan P. McNulty, E. Malcolm S. Woodward, and Sallie W. Chisholm. 2006. 'Niche Partitioning Among *Prochlorococcus* Ecotypes Along Ocean-Scale Environmental Gradients', *Science*, 311: 1737-40.
Kachel, V., and J. Wietzorrek. 2000. 'Flow cytometry and integrated imaging', *Scientia Marina; Vol 64, No 2 (2000)*.
Karl, David M., and Roger Lukas. 1996. 'The Hawaii Ocean Time-series (HOT) program: Background, rationale and field implementation', *Deep Sea Research Part II: Topical Studies in Oceanography*, 43: 129-56.
Karp-Boss, L., E. Boss, and P. A. Jumars. 1996. 'Nutrient fluxes to planktonic osmotrophs in the presence of fluid motion', *Oceanography and Marine Biology, Vol 34*, 34: 71-107.
Kashtan, Nadav, Sara E. Roggensack, Sébastien Rodrigue, Jessie W. Thompson, Steven J. Biller, Allison Coe, Huiming Ding, Pekka Marttinen, Rex R. Malmstrom, Roman Stocker, Michael J. Follows, Ramunas Stepanauskas, and Sallie W. Chisholm. 2014. 'Single-cell genomics reveals hundreds of coexisting subpopulations in wild *Prochlorococcus*', *Science*, 344: 416.
Kato, Chiaki, Lina Li, Yuichi Nogi, Yuka Nakamura, Jin Tamaoka, and Koki Horikoshi. 1998. 'Extremely Barophilic Bacteria Isolated from the Mariana Trench, Challenger Deep, at a Depth of 11,000 Meters', *Applied and Environmental Microbiology*, 64: 1510-13.
Kelly, Jason R., Adam J. Rubin, Joseph H. Davis, Caroline M. Ajo-Franklin, John Cumbers, Michael J. Czar, Kim de Mora, Aaron L. Glieberman, Dileep D. Monie, and Drew Endy. 2009. 'Measuring the activity of BioBrick promoters using an in vivo reference standard', *Journal of Biological Engineering*, 3: 4.
Kiene, R. P., L. J. Linn, and J. A. Bruton. 2000. 'New and important roles for DMSP in marine microbial communities', *Journal of Sea Research*, 43: 209-24.
Kim, Byung-Hyuk, Rishiram Ramanan, Dae-Hyun Cho, Gang-Guk Choi, Hyun-Joon La, Chi-Yong Ahn, Hee-Mock Oh, and Hee-Sik Kim. 2012. 'Simple, Rapid and Cost-Effective Method for High Quality Nucleic Acids Extraction from Different Strains of *Botryococcus braunii*', *PLOS ONE*, 7: e37770.
Kiørboe, Thomas. 2008. *A mechanistic approach to plankton ecology* (Princeton University Press: Princeton).
Kiørboe, Thomas, Hans-Peter Grossart, Helle Ploug, and Kam Tang. 2002. 'Mechanisms and Rates of Bacterial Colonization of Sinking Aggregates', *Applied and Environmental Microbiology*, 68: 3996-4006.
Kiørboe, Thomas, and George A. Jackson. 2001. 'Marine snow, organic solute plumes, and optimal chemosensory behavior of bacteria', *Limnology and Oceanography*, 46: 1309-18.
Klank, Henning, Jorg P. Kutter, and Oliver Geschke. 2002. 'CO2-laser micromachining and back-end processing for rapid production of PMMA-based microfluidic systems', *Lab on a Chip*, 2: 242-46.

Koester, Julie A., Jarred E. Swalwell, Peter von Dassow, and E. Virginia Armbrust. 2010. 'Genome size differentiates co-occurring populations of the planktonic diatom *Ditylum brightwelli*i (Bacillariophyta)', *BMC Evolutionary Biology*, 10: 1.

Kooistra, Wiebe H. C. F., Diana Sarno, David U. Hernández-Becerril, Philipp Assmy, Carmen Di Prisco, and Marina Montresor. 2010. 'Comparative molecular and morphological phylogenetic analyses of taxa in the Chaetocerotaceae (Bacillariophyta)', *Phycologia*, 49: 471-500.

Kostadinov, T. S., D. A. Siegel, and S. Maritorena. 2009. 'Retrieval of the particle size distribution from satellite ocean color observations', *Journal of Geophysical Research: Oceans*, 114: n/a-n/a.

Lambert, Bennett S., Robert J. Olson, and Heidi M. Sosik. 2017. 'A fluorescence-activated cell sorting subsystem for the Imaging FlowCytobot', *Limnology and Oceanography: Methods*, 15: 94-102.

Lambert, Bennett S., Jean-Baptiste Raina, Vicente I. Fernandez, Christian Rinke, Nachshon Siboni, Francesco Rubino, Philip Hugenholtz, Gene W. Tyson, Justin R. Seymour, and Roman Stocker. 2017. 'A microfluidics-based in situ chemotaxis assay to study the behaviour of aquatic microbial communities', *Nature Microbiology*, 2: 1344-49.

Langmead, Ben, and Steven L. Salzberg. 2012. 'Fast gapped-read alignment with Bowtie 2', *Nat Meth*, 9: 357-59.

Lauro, F. M., and D. H. Bartlett. 2008. 'Prokaryotic lifestyles in deep sea habitats', *Extremophiles*, 12: 15-25.

Lauro, Federico M., Diane McDougald, Torsten Thomas, Timothy J. Williams, Suhelen Egan, Scott Rice, Matthew Z. DeMaere, Lily Ting, Haluk Ertan, Justin Johnson, Steven Ferriera, Alla Lapidus, Iain Anderson, Nikos Kyrpides, A. Christine Munk, Chris Detter, Cliff S. Han, Mark V. Brown, Frank T. Robb, Staffan Kjelleberg, and Ricardo Cavicchioli. 2009. 'The genomic basis of trophic strategy in marine bacteria', *Proceedings of the National Academy of Sciences*, 106: 15527-33.

Lavin, Daniel P., A. G. Fredrickson, and Freidrich Srienc. 1990. 'Flow cytometric measurement of rates of particle uptake from dilute suspensions by a ciliated protozoan', *Cytometry*, 11: 875-82.

Lee, Cindy, Stuart Wakeham, and Carol Arnosti. 2004. 'Particulate Organic Matter in the Sea: The Composition Conundrum', *AMBIO: A Journal of the Human Environment*, 33: 565-75.

Legendre, Louis, Claude Courties, and Marc Troussellier. 2001. 'Flow cytometry in oceanography 1989–1999: Environmental challenges and research trends', *Cytometry*, 44: 164-72.

Levine, Naomi Marcil, Vanessa A. Varaljay, Dierdre A. Toole, John W. H. Dacey, Scott C. Doney, and Mary Ann Moran. 2012. 'Environmental, biochemical and genetic drivers of DMSP degradation and DMS production in the Sargasso Sea', *Environmental Microbiology*, 14: 1210-23.

Lewus, Paul, and Roseanne M. Ford. 2001. 'Quantification of random motility and chemotaxis bacterial transport coefficients using individual-cell and population-scale assays', *Biotechnology and Bioengineering*, 75: 292-304.

Lindquist, S., and E. A. Craig. 1988. 'The Heat-Shock Proteins', *Annual Review of Genetics*, 22: 631-77.

Lomas, Michael W., Deborah A. Bronk, and Ger van den Engh. 2011. 'Use of Flow Cytometry to Measure Biogeochemical Rates and Processes in the Ocean', *Annual Review of Marine Science*, 3: 537-66.
Lovelock, J. E., R. J. Maggs, and R. A. Rasmussen. 1972. 'Atmospheric Dimethyl Sulphide and the Natural Sulphur Cycle', *Nature*, 237: 452.
Luo, Haiwei, Bradley B. Tolar, Brandon K. Swan, Chuanlun L. Zhang, Ramunas Stepanauskas, Mary Ann Moran, and James T. Hollibaugh. 2013. 'Single-cell genomics shedding light on marine Thaumarchaeota diversification', *The Isme Journal*, 8: 732.
Malmcrona-Friberg, Karin, Amanda Goodman, and Staffan Kjelleberg. 1990. 'Chemotactic responses of marine *Vibrio* sp. strain s14 (CCUG 15956) to low-molecular-weight substances under starvation and recovery conditions', *Applied and Environmental Microbiology*, 56: 3699-704.
Mandel, Mark J., Amy L. Schaefer, Caitlin A. Brennan, Elizabeth A. C. Heath-Heckman, Cindy R. DeLoney-Marino, Margaret J. McFall-Ngai, and Edward G. Ruby. 2012. 'Squid-derived chitin oligosaccharides are a chemotactic signal during colonization by *Vibrio fischeri*', *Applied and Environmental Microbiology*.
Marie, D, F Partensky, S Jacquet, and D Vaulot. 1997. 'Enumeration and Cell Cycle Analysis of Natural Populations of Marine Picoplankton by Flow Cytometry Using the Nucleic Acid Stain SYBR Green I', *Applied and Environmental Microbiology*, 63: 186-93.
Massalha, Hassan, Elisa Korenblum, Sergey Malitsky, Orr H. Shapiro, and Asaph Aharoni. 2017. 'Live imaging of root–bacteria interactions in a microfluidics setup', *Proceedings of the National Academy of Sciences*, 114: 4549.
Mende, Daniel R., Jessica A. Bryant, Frank O. Aylward, John M. Eppley, Torben Nielsen, David M. Karl, and Edward F. DeLong. 2017. 'Environmental drivers of a microbial genomic transition zone in the ocean's interior', *Nature Microbiology*, 2: 1367-73.
Menolascina, Filippo, Roberto Rusconi, Vicente I. Fernandez, Steven Smriga, Zahra Aminzare, Eduardo D. Sontag, and Roman Stocker. 2017. 'Logarithmic sensing in *Bacillus subtilis* aerotaxis', *Npj Systems Biology And Applications*, 3: 16036.
Mesibov, Robert, and Julius Adler. 1972. 'Chemotaxis toward amino acids in *Escherichia coli*', *Journal of Bacteriology*, 112: 315-26.
Mojica, Kristina D. A., Willem H. van de Poll, Michael Kehoe, Jef Huisman, Klaas R. Timmermans, Anita G. J. Buma, Hans J. van der Woerd, Lisa Hahn-Woernle, Henk A. Dijkstra, and Corina P. D. Brussaard. 2015. 'Phytoplankton community structure in relation to vertical stratification along a north-south gradient in the Northeast Atlantic Ocean', *Limnology and Oceanography*, 60: 1498-521.
Montresor, Marina, Silvia Sgrosso, Gabriele Procaccini, and Wiebe H. C. F. Kooistra. 2003. 'Intraspecific diversity in *Scrippsiella trochoidea* (Dinophyceae): evidence for cryptic species', *Phycologia*, 42: 56-70.
Moran, Mary Ann, Chris R. Reisch, Ronald P. Kiene, and William B. Whitman. 2011. 'Genomic Insights into Bacterial DMSP Transformations', *Annual Review of Marine Science*, 4: 523-42.
Morán, Xosé Anxelu G., Ángel López-Urrutia, Alejandra Calvo-Díaz, and William K. W. Li. 2010. 'Increasing importance of small phytoplankton in a warmer ocean', *Global Change Biology*, 16: 1137-44.
Morimoto, R. I. 1993. 'Cells in stress: transcriptional activation of heat shock genes', *Science*, 259: 1409.

Muller-Karger, Frank E., Ramon Varela, Robert Thunell, Remy Luerssen, Chuanmin Hu, and John J. Walsh. 2005. 'The importance of continental margins in the global carbon cycle', *Geophysical Research Letters*, 32.

Newell, R. C., M. I. Lucas, and E. A. S. Linley. 1981. 'Rate of Degradation and Efficiency of Conversion of Phytoplankton Debris by Marine Micro-Organisms', *Marine Ecology Progress Series*, 6: 123-36.

Oliveira, Nuno M., Kevin R. Foster, and William M. Durham. 2016. 'Single-cell twitching chemotaxis in developing biofilms', *Proceedings of the National Academy of Sciences*, 113: 6532.

Olson, R. J., S. W. Chisholm, E. R. Zettler, and E. V. Armbrust. 1988. 'Analysis of *Synechococcus* pigment types in the sea using single and dual beam flow cytometry', *Deep Sea Research Part A. Oceanographic Research Papers*, 35: 425-40.

Olson, R. J., D. Vaulot, and S. W. Chisholm. 1985. 'Marine phytoplankton distributions measured using shipboard flow cytometry', *Deep Sea Research Part A. Oceanographic Research Papers*, 32: 1273-80.

Olson Robert, J., W. Chisholm Sallie, R. Zettler Erik, and E. Virginia Armbrust. 2003. 'Pigments, size, and distributions of *Synechococcus* in the North Atlantic and Pacific Oceans', *Limnology and Oceanography*, 35: 45-58.

Olson, Robert J., Alexi Shalapyonok, and Heidi M. Sosik. 2003. 'An automated submersible flow cytometer for analyzing pico- and nanophytoplankton: FlowCytobot', *Deep Sea Research Part I: Oceanographic Research Papers*, 50: 301-15.

Olson, Robert J., and Heidi M. Sosik. 2007. 'A submersible imaging-in-flow instrument to analyze nano-and microplankton: Imaging FlowCytobot', *Limnology and Oceanography: Methods*, 5: 195-203.

Olson Robert, J., R. Zettler Erik, and DuRand Michele D. 1993. 'Phytoplankton Analysis Using Flow Cytometry.' in P.F. Kemp, J.J. Cole, B.F. Sherr and E.B. Sherr (eds.), *Handbook of Methods in Aquatic Microbial Ecology* (Taylor & Francis).

Parks, Donovan H., Gene W. Tyson, Philip Hugenholtz, and Robert G. Beiko. 2014. 'STAMP: statistical analysis of taxonomic and functional profiles', *Bioinformatics*, 30: 3123-24.

Peacock, E. E., R. J. Olson, and H. M. Sosik. 2014. 'Parasitic infection of the diatom *Guinardia delicatula*, a recurrent and ecologically important phenomenon on the New England Shelf', *Marine Ecology Progress Series*, 503: 1-10.

Pedler, Byron E., Lihini I. Aluwihare, and Farooq Azam. 2014. 'Single bacterial strain capable of significant contribution to carbon cycling in the surface ocean', *Proceedings of the National Academy of Sciences*, 111: 7202-07.

Pfannschmidt, Thomas, Anders Nilsson, and John F. Allen. 1999. 'Photosynthetic control of chloroplast gene expression', *Nature*, 397: 625.

Pilskaln, C. H., T. A. Villareal, M. Dennett, C. Darkangelo-Wood, and G. Meadows. 2005. 'High concentrations of marine snow and diatom algal mats in the North Pacific Subtropical Gyre: Implications for carbon and nitrogen cycles in the oligotrophic ocean', *Deep Sea Research Part I: Oceanographic Research Papers*, 52: 2315-32.

Pohnert, Georg, Michael Steinke, and Ralph Tollrian. 2007. 'Chemical cues, defence metabolites and the shaping of pelagic interspecific interactions', *Trends in Ecology & Evolution*, 22: 198-204.

Poretsky Rachel, S., Shulei Sun, Xiaozhen Mou, and Ann Moran Mary. 2009. 'Transporter genes expressed by coastal bacterioplankton in response to dissolved organic carbon', *Environmental Microbiology*, 12: 616-27.
Poulson, Kelsey L., R. Drew Sieg, and Julia Kubanek. 2009. 'Chemical ecology of the marine plankton', *Natural Product Reports*, 26: 729-45.
Prindle, Arthur, Jintao Liu, Munehiro Asally, San Ly, Jordi Garcia-Ojalvo, and Gürol M. Süel. 2015. 'Ion channels enable electrical communication in bacterial communities', *Nature*, 527: 59.
Purcell, E. M. 1977. 'Life at low Reynolds number', *American Journal of Physics*, 45: 3-11.
Richardson, T. L., and G. A. Jackson. 2007. 'Small phytoplankton and carbon export from the surface ocean', *Science*, 315: 838-40.
Rinke, Christian, Serene Low, Ben J. Woodcroft, Jean-Baptiste Raina, Adam Skarshewski, Xuyen H. Le, Margaret K. Butler, Roman Stocker, Justin Seymour, Gene W. Tyson, and Philip Hugenholtz. 2016. 'Validation of picogram- and femtogram-input DNA libraries for microscale metagenomics', *PeerJ*, 4: e2486.
Rivkin, Richard B., David A. Phinney, and Clarice M. Yentsch. 1986. 'Effects of Flow Cytometric Analysis and Cell Sorting on Photosynthetic Carbon Uptake by Phytoplankton in Cultures and from Natural Populations', *Applied and Environmental Microbiology*, 52: 935-38.
Roller, Benjamin R. K., and Thomas M. Schmidt. 2015. 'The physiology and ecological implications of efficient growth', *The Isme Journal*, 9: 1481.
Rusconi, Roberto, Melissa Garren, and Roman Stocker. 2014. 'Microfluidics expanding the frontiers of microbial ecology', *Annual Review of Biophysics*, 43: 65-91.
Rusconi, Roberto, Jeffrey S. Guasto, and Roman Stocker. 2014. 'Bacterial transport suppressed by fluid shear', *Nature Physics*, 10: 212.
Rusconi, Roberto, Sigolene Lecuyer, Nicolas Autrusson, Laura Guglielmini, and Howard A Stone. 2011. 'Secondary Flow as a Mechanism for the Formation of Biofilm Streamers', *Biophysical Journal*, 100: 1392-99.
Sandgren Craig, D., A. Hall Shirley, and B. Barlow Steven. 1996. 'Siliceous scale production in chrysophyte and synurophyte algae. I. Effects of silica-limited growth on cell silica content, scale morphology, and the construction of the scale layer or *Synura petersenii*', *Journal of Phycology*, 32: 675-92.
Schultz, Mary E. 1971. 'Salinity-related polymorphism in the brackish-water diatom *Cyclotella cryptica*', *Canadian Journal of Botany*, 49: 1285-89.
Seymour, J. R., T. Ahmed, W. M. Durham, and R. Stocker. 2010. 'Chemotactic response of marine bacteria to the extracellular products of *Synechococcus* and *Prochlorococcus*', *Aquatic Microbial Ecology*, 59: 161-68.
Seymour, Justin R., Shady A. Amin, Jean-Baptiste Raina, and Roman Stocker. 2017. 'Zooming in on the phycosphere: the ecological interface for phytoplankton–bacteria relationships', *Nature Microbiology*, 2: 17065.
Seymour, Justin R., Rafel Simó, Tanvir Ahmed, and Roman Stocker. 2010. 'Chemoattraction to Dimethylsulfoniopropionate Throughout the Marine Microbial Food Web', *Science*, 329: 342.
Shapiro, H.M. 2005. *Practical Flow Cytometry* (Wiley).

Shapiro, Orr H., Esti Kramarsky-Winter, Assaf R. Gavish, Roman Stocker, and Assaf Vardi. 2016. 'A coral-on-a-chip microfluidic platform enabling live-imaging microscopy of reef-building corals', *Nature Communications*, 7: 10860.

Sieracki, Christian K., Michael E. Sieracki, and Charles S. Yentsch. 1998. 'An imaging-in-flow system for automated analysis of marine microplankton', *Marine Ecology Progress Series*, 168: 285-96.

Sieracki, Michael, N. J. Poulton, and Nicholas Crosbie. 2005. 'Automated Isolation Techniques for Microalgae.' in R.A. Andersen (ed.), *Algal Culturing Techniques* (Elsevier Science).

Sinigalliano, C. D., J. Winshell, M. A. Guerrero, G. Scorzetti, J. W. Fell, R. W. Eaton, L. Brand, and K. S. Rein. 2009. 'Viable cell sorting of dinoflagellates by multiparametric flow cytometry', *Phycologia*, 48: 249-57.

Smriga, Steven, Vicente I. Fernandez, James G. Mitchell, and Roman Stocker. 2016. 'Chemotaxis toward phytoplankton drives organic matter partitioning among marine bacteria', *Proceedings of the National Academy of Sciences*, 113: 1576-81.

Snoeyenbos-West, O. L., T. Salcedo, G. B. McManus, and L. A. Katz. 2002. 'Insights into the diversity of choreotrich and oligotrich ciliates (Class: Spirotrichea) based on genealogical analyses of multiple loci', *Int J Syst Evol Microbiol*, 52: 1901-13.

Sonnenschein, Eva C., Astrid Gärdes, Shalin Seebah, Ingrid Torres-Monroy, Hans-Peter Grossart, and Matthias S. Ullrich. 2011. 'Development of a genetic system for Marinobacter adhaerens HP15 involved in marine aggregate formation by interacting with diatom cells', *Journal of Microbiological Methods*, 87: 176-83.

Sosik, Heidi M., and Robert J. Olson. 2007. 'Automated taxonomic classification of phytoplankton sampled with imaging-in-flow cytometry', *Limnology and Oceanography: Methods*, 5: 204-16.

Sosik, Heidi M., Robert J. Olson, and E. Virginia Armbrust. 2010. 'Flow Cytometry in Phytoplankton Research.' in David J. Suggett, Ondrej Prášil and Michael A. Borowitzka (eds.), *Chlorophyll a Fluorescence in Aquatic Sciences: Methods and Applications* (Springer Netherlands: Dordrecht).

Squires, Todd M., and Stephen R. Quake. 2005. 'Microfluidics: Fluid physics at the nanoliter scale', *Reviews of Modern Physics*, 77: 977-1026.

Stemmann, L., D. Eloire, A. Sciandra, G. A. Jackson, L. Guidi, M. Picheral, and G. Gorsky. 2008. 'Volume distribution for particles between 3.5 to 2000 µm in the upper 200 m region of the South Pacific Gyre', *Biogeosciences*, 5: 299-310.

Stocker, R. 2012. 'Marine microbes see a sea of gradients', *Science*, 338: 628-33.

Stocker, R., and J. R. Seymour. 2012. 'Ecology and physics of bacterial chemotaxis in the ocean', *Microbiol Mol Biol Rev*, 76: 792-812.

Stocker, R., J. R. Seymour, A. Samadani, D. E. Hunt, and M. F. Polz. 2008. 'Rapid chemotactic response enables marine bacteria to exploit ephemeral microscale nutrient patches', *Proc Natl Acad Sci U S A*, 105: 4209-14.

Sun, Jing, Jonathan D. Todd, J. Cameron Thrash, Yanping Qian, Michael C. Qian, Ben Temperton, Jiazhen Guo, Emily K. Fowler, Joshua T. Aldrich, Carrie D. Nicora, Mary S. Lipton, Richard D. Smith, Patrick De Leenheer, Samuel H. Payne, Andrew W. B. Johnston, Cleo L. Davie-Martin, Kimberly H. Halsey, and Stephen J. Giovannoni. 2016. 'The abundant marine bacterium Pelagibacter simultaneously catabolizes dimethylsulfoniopropionate to the gases dimethyl sulfide and methanethiol', *Nature Microbiology*, 1: 16065.

Sunkara, Vijaya, Dong-Kyu Park, Hyundoo Hwang, Rattikan Chantiwas, Steven A. Soper, and Yoon-Kyoung Cho. 2011. 'Simple room temperature bonding of thermoplastics and poly(dimethylsiloxane)', *Lab on a Chip*, 11: 962-65.

Sykes, PJ, SH Neoh, MJ Brisco, E Hughes, J Condon, and AA Morley. 1992. 'Quantitation of targets for PCR by use of limiting dilution', *BioTechniques*, 13: 444.

Taira, Keisuke, Shoji Kitagawa, Toru Yamashiro, and Daigo Yanagimoto. 2004. 'Deep and Bottom Currents in the Challenger Deep, Mariana Trench, Measured with Super-Deep Current Meters', *Journal of Oceanography*, 60: 919-26.

Taniguchi, D. A. A., M. R. Landry, P. J. S. Franks, and K. E. Selph. 2014. 'Size-specific growth and grazing rates for picophytoplankton in coastal and oceanic regions of the eastern Pacific', *Marine Ecology Progress Series*, 509: 87-101.

Taylor, John R., and Roman Stocker. 2012. 'Trade-Offs of Chemotactic Foraging in Turbulent Water', *Science*, 338: 675.

Taylor, Sean C., Julie Carbonneau, Dawne N. Shelton, and Guy Boivin. 2015. 'Optimization of Droplet Digital PCR from RNA and DNA extracts with direct comparison to RT-qPCR: Clinical implications for quantification of Oseltamivir-resistant subpopulations', *Journal of Virological Methods*, 224: 58-66.

Temme, Karsten, Rena Hill, Thomas H. Segall-Shapiro, Felix Moser, and Christopher A. Voigt. 2012. 'Modular control of multiple pathways using engineered orthogonal T7 polymerases', *Nucleic Acids Research*, 40: 8773-81.

Thompson, A. W., R. A. Foster, A. Krupke, B. J. Carter, N. Musat, D. Vaulot, M. M. Kuypers, and J. P. Zehr. 2012. 'Unicellular cyanobacterium symbiotic with a single-celled eukaryotic alga', *Science*, 337: 1546-50.

Thrash, J. C., B. Temperton, B. K. Swan, Z. C. Landry, T. Woyke, E. F. DeLong, R. Stepanauskas, and S. J. Giovannoni. 2014. 'Single-cell enabled comparative genomics of a deep ocean SAR11 bathytype', *ISME J*, 8: 1440-51.

Todd, Jonathan D., Mark Kirkwood, Simone Newton-Payne, and Andrew W. B. Johnston. 2011. 'DddW, a third DMSP lyase in a model Roseobacter marine bacterium, Ruegeria pomeroyi DSS-3', *The Isme Journal*, 6: 223.

Urrios, Arturo, Cesar Parra-Cabrera, Nirveek Bhattacharjee, Alan M. Gonzalez-Suarez, Luis G. Rigat-Brugarolas, Umashree Nallapatti, Josep Samitier, Cole A. DeForest, Francesc Posas, Jose L. Garcia-Cordero, and Albert Folch. 2016. '3D-printing of transparent bio-microfluidic devices in PEG-DA', *Lab on a Chip*, 16: 2287-94.

Varaljay, Vanessa A., Julie Robidart, Christina M. Preston, Scott M. Gifford, Bryndan P. Durham, Andrew S. Burns, John P. Ryan, Roman Marin Iii, Ronald P. Kiene, Jonathan P. Zehr, Christopher A. Scholin, and Mary Ann Moran. 2015. 'Single-taxon field measurements of bacterial gene regulation controlling DMSP fate', *The Isme Journal*, 9: 1677-86.

Veldhuis, MJW, and GW Kraay. 1990. 'Vertical distribution and pigment composition of a picoplanktonic prochlorophyte in the subtropical North Atlantic:a combined study of HPLC-analysis of pigments and flow cytometry', *Marine Ecology Progress Series*, 68: 121-27.

Vergin, K. L., B. Done, C. A. Carlson, and S. J. Giovannoni. 2013. 'Spatiotemporal distributions of rare bacterioplankton populations indicate adaptive strategies in the oligotrophic ocean', *Aquatic Microbial Ecology*, 71: 1-13.

Vidoudez, Charles, and Georg Pohnert. 2012. 'Comparative metabolomics of the diatom *Skeletonema marinoi* in different growth phases', *Metabolomics*, 8: 654-69.
Vila-Costa, Maria, Johanna M. Rinta-Kanto, Shulei Sun, Shalabh Sharma, Rachel Poretsky, and Mary Ann Moran. 2010. 'Transcriptomic analysis of a marine bacterial community enriched with dimethylsulfoniopropionate', *The Isme Journal*, 4: 1410.
Yawata, Yutaka, Otto X. Cordero, Filippo Menolascina, Jan-Hendrik Hehemann, Martin F. Polz, and Roman Stocker. 2014. 'Competition–dispersal tradeoff ecologically differentiates recently speciated marine bacterioplankton populations', *Proceedings of the National Academy of Sciences*, 111: 5622.
Zehr, J. P., J. S. Weitz, and I. Joint. 2017. 'How microbes survive in the open ocean', *Science*, 357: 646-47.